DEVELOPMENT OF A MACHINE VISION SYSTEM FOR STRAWBERRY POWDERY MILDEW DISEASE DETECTION

by

Md. Sultan Mahmud

Submitted in partial fulfilment of the requirements
for the degree of Master of Science

at

Dalhousie University
Halifax, Nova Scotia
March 2019

DEDICATION

I would like to dedicate my Master of Science dissertation to my loving parents (Md. Azizul Haque and Nilufa Yasmin) for whom my education meant everything

Author

Md. Sultan Mahmud

TABLE OF CONTENTS

LIST OF TABLES

CHAPTER 3

CHAPTER 4

CHAPTER 5

LIST OF FIGURES

CHAPTER 3

CHAPTER 4

CHAPTER 5

ABSTRACT

Strawberry powdery mildew (*Sphaerotheca macularis)* has been a devastating foliar disease of both nursery and fruit production strawberry crops causing significant yield loss up to 70%. Traditionally, visual observations are made to monitor strawberry powdery mildew disease each week by human experts which is a laborious and time consuming endeavour. The main objective of this study was to detect powdery mildew disease in real-time field condition by developing an image processing-based machine vision system. The machine vision system consisted of a graphical user interface based powdery mildew detection program, two μeye cameras, a real-time kinematic global positioning system, and a ruggedized laptop computer. A colour co-occurrence matrices based image texture analysis program was generated by using C# programming language. Factors affecting machine vision parameters were optimised by evaluating performance upon 12,000 collected images from healthy and diseases affected strawberry leaves. Results suggested artificial cloud lighting system improved real-time powdery mildew detection accuracy as compared to natural lighting conditions. Results also suggested that feature model formed by green ratio, hue, saturation and intensity images including 23 features, image acquisition speed 1.5 km h^{-1} and camera working depth of 300 mm were outperformed for disease detection. Results of the classifier selection revealed that artificial neural network performed better than support vector machines and k-nearest neighbor based supervised learning classifiers to detect powdery mildew disease in strawberry leaves. Real-time performance of developed vision system was tested in 36 randomly selected rows in three commercial strawberry fields. Visual observations were compared with developed automatic detection system. Real-time test evaluation results demonstrated that the machine vision system was capable to detect powdery mildew disease with mean absolute error of 4.00, 3.42 and 2.83 per row and root mean square error of 4.12, 3.71 and 3.00 per row. The overall study reported the developed strawberry powdery mildew detection system can be used to help strawberry growers by reducing expenses associated with field scouts for manual monitoring.

LIST OF ABBREVIATIONS USED

ABBREVIATIONS

AAFC- Agriculture and Agri-Food Canada

ACC- Artificial Cloud lighting Conditions

AES- Auto Exposure Shutter

AGC- Auto Gain Control

An- Angular 2nd Moment

ANN- Artificial Neural Networks

AOI- Area of Interest

AST- Atlantic Standard Time

Av- Average

AWB- Auto White Balance

B- Blue

BGR- Blue-Green-Red

BMP- Windows Bitmap

BP-ANN- Back-Propagation Artificial Neural Network

CCM- Colour Co-occurrence Matrix

CCMs- Colour Co-occurrence Matrices

CIE- International Commission on Illumination

Co- Contrast

COM- Computer

CPU- Central Processing Unit

Cr- Correlation

CRD- Complete Randomized Design

CSV- Comma Separated Value

DBE- Doug Bragg Enterprises

DCNN- Deep Convolution Neural Network

Ds- Dissimilarity

En- Entropy

FN- False Negative

FP- False Positive

FPS- Frame Per Second

G- Green

G- Green Ratio

GB- Gigabyte

GDI- Graphics Device Interface

GHS- Green ratio, Hue and Saturation

GHSI- Green Ratio, Hue, Saturation and Intensity

GHSI- Green ratio, Hue, Saturation and Intensity

GHSIL- Green ratio, Hue, Saturation, Intensity and Luminance

GHz- Gigahertz

GIS- Geographical Information Systems

GLCM- Gray Level Co-occurrence Matrix

GPS- Global Positioning System

GUI- Graphical User Interface

H- Hue

Hm- Homogeneity

HSI- Hue, Saturation and Intensity

I- Saturation

kNN- K Nearest Neighbors

L- Luminance

Lm- Luminance Image

MAE- Mean Absolute Error

mm- Millimetre

ms- Millisecond

NIR- Near-Infrared

NLC- Natural Lighting Conditions

nm- Nanometer

NMEA- National Marine Electronics Association

NSERC- Natural Sciences and Engineering Research Council

NSGS- Nova Scotia Graduate Scholarship

NTSC- National Television System Committee

PM- Powdery Mildew

Pm- Product Moment

R- Red

R^2- Coefficient of Determination

RAM- Random Access Memory

RGB- Red, Green and Blue

R_H- Relative Humidity

RMSE- Root Mean Square Error

RTK-GPS- Real-Time Kinematic Global Positioning System

S- Saturation

SGDMs- Spatial Gray-texture Dependence Matrices

SIL- Saturation Intensity and Luminance

SVM- Support Vector Machines

TP- True Positive

TSWV- Tomato Spotted Wilt Virus

USB- Universal Serial Bus

YUV- Luminance, Chrominance and Chroma

ACKNOWLEDGEMENTS

First and foremost, all praise is to Almighty ALLAH, the greatest of all, who blessed me to successfully complete my master's study and for continuous grace and mercy throughout my life and ever more during the tenure of my research, and humblest and deepest gratitude to the greatest educator of mankind, the Holy Prophet MUHAMMAD (S.A.W) (Peace be Upon Him).

In the first place I would like to express my earnest and heartfelt gratitude to my supervisor, Prof. Dr. Qamar Zaman for his benevolent guidance, meticulous supervision, invaluable suggestions, freedom of work and critical appreciation in the execution of my work. I am also deeply grateful to my co-supervisor, Dr. Travis Esau for his encouragement, constructive comments, constant guidance and support throughout this study. I also want to express my profound gratitude to my committee members, Dr. Gordon Price and Dr. Balakrishnan Prithiviraj for their moral support, useful suggestions and continuous encouragement throughout the journey.

I am extremely grateful to all the funding partners, Doug Bragg Enterprises (DBE) Limited, the Natural Science and Engineering Research Council (NSERC) of Canada, Government of Nova Scotia and Dalhousie University, for supporting this research project. I would also like to give special thanks to Dalhousie University Graduate Studies Office for my selection in Nova Scotia Research and Innovation Graduate Scholarship (NSGS). Many thanks to Curtis Millen (Owner of Millen Farms Ltd) and Balamore Farm Limited for providing their field access to conduct this study. I am very much thankful to Dr. Peter Havard (Head of Engineering Department), Dr. Christopher Cutler (Associate Dean Research) and Mrs. Pamela Sutherland (Graduate Secretary) for believing and supporting me during the time when I wanted to give up from my study. I also want to thank precision agriculture research team, Scott Read (Senior Instructor), Negar Sharifi Mood (Research Assistant), Derrick Ouma, Jack Lynds and Justin Throne (Summer Students) for

their help/assistance during field experiments and data collection. I also like to thank Dr. Young Ki Chang for his initial training and help at the beginning of this program.

I also would like to express my sincere gratitude to Mr. Hassan Nabi, Mrs. Irin Arju, Dr. Nasif Sarowar, Mr. Mahboob Rahman, Dr. Zahidul Alam and their family for providing unconditional help, extreme care and mental support during my stay at Dalhousie University, which never let me feel home sick. Endless help from Hassan Nabi and his family during my entire master's study, is highly acknowledged.

Last but not least, I take this opportunity to record my deep sense of appreciation for my parents and family members who helped me a lot unconditionally throughout my life. I would like to thank my parents Md. Azizul Haque and Nilufa Yasmin, my elder brothers Md. Ahsan Habib and Md. Mahbub Jaman, my family members, and teachers for encouraging me and believing in me in every single step. Without my family support, none of this and where I stand in life would have been possible. Special thanks to my friends for their support and encouragement over the years.

CHAPTER 1: INTRODUCTION

Dating back to1990's, the application of machine vision in detecting plant diseases has increased rapidly. Machine vision aims to duplicate the effect of human vision by electronically perceiving and understanding an image, and preparing a suitably rapid, consistent, cost effective/economic and objective assessment of objects (Sun, 2000; Sonka et al., 2014). Several successful machine vision applications have been studied to detect plant diseases in different cropping systems (Giacomelli et al., 1996; Chaerle & Van Der Straeten, 2000; Moya et al., 2005; Pydipati et al., 2005; Huang, 2007; Boissard et al., 2008; Story et al., 2010; Kai et al., 2011; Arivazhagan et al., 2013; Pineda et al., 2018). However, most of machine vision based plant disease detection studies have largely been conducted indoors under controlled illumination and an adequate setup for the image acquisition of high quality images. Machine vision experiments are highly affected by uncontrolled imaging environments which provides imperfections of input images and results in poor accuracy and precision (Romeo et al., 2013). Conditions affecting image quality in the field includes: variable illumination conditions, image acquisition speed, wind speed, leaf canopy overlapping etc. The leaf canopy generates different illumination conditions outdoors resulting in variations in the image quality, and for many applications, such as disease detection this is not acceptable. Tian (1995) studied the feasibility of using a machine vision system in natural outdoor conditions to identify individual plants with images and reported problems associated with non-uniform illumination. Inappropriate image acquisition speed is another important parameter causing significant image blurring. Therefore, parameter optimization under outdoor conditions is a critical consideration for real-time machine vision system development. Machine vision systems integrated with machine learning have shown promising potential in a variety of domains (Ropodi et al., 2016). Traditional classification or regression systems require considerable domain

knowledge and careful engineering to extract features from image raw data (Cai et al., 2018). Machine learning techniques have been utilized in a variety of data-driven applications including image processing in agriculture and food industry (Chen et al., 2010; Savakar & Anami, 2015; Rojas-Moraleda et al., 2017). Variability of performance in different machine vision systems is largely affected by machine learning classifiers. Therefore, proper machine learning classifiers also must be accounted for in the development of a real-time machine vision system.

Strawberry (*Fragaria* × *ananassa* Duch.) is one of the most economically important cultivated fruit crops in the world (Wei et al., 2018). Strawberry powdery mildew (*Sphaerotheca macularis*) disease has become a major problem influenced by fluctuating humidity conditions in the late summer and fall months throughout the world (Dodgson, 2007). The disease can reduce strawberry yield from 20 to 70% (Dodgson, 2007) by decreasing fruit set, inducing cracks and decreasing flavor and storage time (Pertot et al., 2008). The disease identification based on visual symptoms has predominantly remained a manual exercise performed by trained pathologists, primarily due to the occurrence of confounding symptoms. Manual disease rating is tedious, time-consuming, and suffers from inter- and intra-rater variabilities. An automated powdery mildew disease detection system would facilitate disease management by strawberry growers. There have been few attempts to detect powdery mildew disease in different cropping systems by machine vision, (Velázquez-López et al., 2011; Wspanialy & Moussa, 2016) and fewer in disease detection for strawberry cropping systems. The problem addressed in this study is how to detect strawberry powdery mildew early enough to reduce its impact on crop yield and reduce management costs.

Therefore, the aim of this study is to develop a graphical user interface based real-time machine vision system incorporating machine learning classifiers for strawberry powdery mildew detection on strawberry plant leaves.

1.1 Objectives

- Development of an artificial cloud lighting condition system using machine vision for strawberry powdery mildew disease detection;
- Comparison of supervised learning classifiers for strawberry powdery mildew disease detection using machine vision;
- Development of on-the go prescription map for strawberry powdery mildew disease using a machine vision system.

CHAPTER 2: REVIEW OF LITERATURE

2.1 Machine Vision Applications in Agriculture

Machine vision is a science that tries to replicate human vision using computer software and hardware. The approach involves development of studies and algorithms to analyze and automatically extract useful details about an object or set of objects perceived (Gunasekaran, 1996; Sun, 2016). Machine vision also involves in taking decisions of physical objects with the help of their images. Different types of images including RGB (Wang et al., 2017), hyperspectral (Lu & Chen, 1999), multispectral (Mehl et al., 2002), thermal (Stajnko et al., 2004) etc. have already been applied in agricultural crop cultivation.

2.1.1 Colour or RGB Imaging

An RGB image is also called a true colour image which is stored by three data arrays defined as red, green and blue colour components for each individual pixel. Colour images are carried out by using prism construction with bandpass filters and a dichroic coating on selected surfaces of the prisms that distinct broadband light into RGB channels (Chen et al., 2002).

Colour imaging techniques are utilized in many sectors of agricultural crop production. Camargo and Smith (2009) used the colour images for automatically identifying plant disease visual symptoms by image pattern classification. Colour images also used by Polder et al. (2007) for early prediction of cabbage leaf disease which can handle the leaf warping and silt overlapping problem during leaf growth processes. Colour imaging is not only applied on plant diseases detection but also applied on product quality assessments (Daley et al., 1993; Daley et al., 1995;

Mahendran et al., 2012), yield prediction (Aggelopoulou et al., 2011; Wang et al., 2013; Zhou et al., 2012) and weed sensing (Tang et al., 2000). A classification of apple bruise damage was experimented by Throop et al. (1993) where a colour difference between bruised and unbruised regions on golden delicious apple images were undertaken. The study resulted colour differences were more effective for discriminating bruised from undamaged tissue. Daley et al. (1993) implemented colour imaging approach for grading and inspection of poultry and was successful to detect tumor regions on whole body. Dorj et al. (2017) developed citrus recognition and counting algorithm using colour images for estimating citrus yield. Payne et al. (2013) segmented colour images to establish an algorithm for mango fruit yield estimation from daytime images of individual trees. Colour images have also been used in cucumber (Zhang et al., 2007), Kiwifruit (Wijethunga et al., 2008), apple (Li et al., 2017a) and grape (Font et al., 2014) recognition algorithms for counting. Huang et al. (2017) applied colour imaging to account for variability of weed infestation and herbicide damage using unmanned aerial vehicles. Their system was developed using RGB imaging to identify weed species and determine crop injury over crop fields. Another weed detection system developed by Barrero et al. (2016) was conducted on rice fields with a final detection accuracy of 99%. The colour images were analysed by using gray-level co-occurrence matrix (GLCM) with Haralicks descriptor for texture classification.

2.1.2 Hyperspectral Imaging

Hyperspectral imaging is an emerging modality for present agricultural crop productions with the spectrum of sufficient resolution (Mohan & Porwal, 2015). Ochoa et al. (2016) tested a hyper-spectral imaging system for detecting black sigatoka pre-symptomatic responses which is caused by the fungus in banana leaves using a high-sensitivity vis-near-infrared camera and an optical

spectrograph. Kumar et al. (2016) used a 3D spectroscopy for yield prediction, disease forecasting, fungal pathogens identification and macronutrient analysis for fertilizer application and monitoring crop infestation in oilseed brassica crop. Monitoring is an essential factor for increasing the production of crops and much research has been done on applying hue-saturation-intensity (HSI) with sensing techniques in agricultural field. Rodriguez et al. (2006) and Haboudane et al. (2002) monitored fungal diseases, water stress and nitrogen status and observed that the presence of chlorophyll pigments in leaf tissues strongly affects the electromagnetic spectrum in the visible region, especially in the red (670 nm) bands and blue (450 nm). They realized that the strong absorption of the wavelengths increased the chlorophyll pigments concentration, which indicated a higher amount of nitrogen in crop leaves. Likewise, maturity identification and yield prediction are important for managing or increasing crop production. Fruits from the same cluster, i.e., young fruit, intermediate fruit and mature fruit have different maturation times. Yang et al. (2014) studied the feasibility of HSI for classifying blueberry growth stages for detecting different fruit maturity with the spectral range of 398-1010 nm and a spatial resolution of 1mm. Rajkumar et al. (2012) determined the maturation period considering parameters such as moisture content, firmness and total soluble solids in the visible and near infrared (400-1000 nm) regions. However, hyperspectral imaging technology is a very costly approach.

2.1.3 Multispectral Imaging

Multispectral imaging is composed of a series of several images, each gained at a narrow band of wavelengths. Images are obtained at a discrete spectral region by positioning a bandpass filter in front of a monochrome camera lens (Chen et al., 2002). Multispectral imaging systems have been

successfully used for identifying pest infestations (Backoulou et al., 2011), defect detection (Mehl et al., 2002; Unay et al., 2006) and other agricultural applications.

Most of the multispectral imaging frameworks can give 8 to 16-bit picture information with sub meter resolutions at 3-12 narrow spectral bands in the distinctive to near-infrared (NIR) regions of the electromagnetic spectrum (Yang et al., 2012; Gorsevski et al., 2009). Zarco-Tejada et al. (2009) observed that multispectral airborne data was acquired at 15 cm spatial resolution at 150 m above ground level in the visible, thermal and near infrared regions yielding imagery. Berni et al. (2009) utilized multispectral imaging techniques for vegetation monitoring having RMSE of 1.17% in ground reflectance. Multispectral imaging also applied with visible and near-visible infrared reflectance imaging by Kim et al. (2002) for fecal contamination of apple to monitor food safety issues. Peng and Lu (2007) secured the fruit firmness and soluble solid content using the characteristics of multispectral scattering images to build a better multispectral imaging system. Lleó et al. (2009) observed the maturity and firmness for peach by analysing multispectral images. However, multispectral images need more post-processing steps compared to others imaging, such as co-registration, that increases the cost of image analysis (Huang et al., 2010).

2.1.4 Thermal Imaging

Thermal imaging is a technique that converts the invisible radiation pattern of an object into visible images. Potential applications of thermal imaging in agricultural fields are possible, such as water stress prediction in crops, fruit yield prediction, plant diseases and pathogen detection, irrigation scheduling, fruit bruise detection and fruits maturity evaluation (Vadivambal & Jayas, 2011).

Identifying plant stress, investigating canopy temperature and measuring stomatal conductance have been studied by many researchers (Jones 1999a; Jones 1999b; Jones et al., 2002; Leinonen & Jones, 2004). Sela et al. (2007) considered leaf water potential for monitoring water status in corn crops using thermal visible images. Stoll and Jones (2007) investigated the feasibility of thermal imaging application in grapevines stress monitoring, concluded this technique can give reliable and sensitive indications of leaf temperature and hence to calculate stomatal conductance. Oerke et al. (2006) applied thermal imaging on cucumber crop leaves to monitor downy mildew and found the maximum temperature difference within the infected leaves was significantly larger than the maximum temperature difference within the non-inoculated plants. Hellebrand et al. (2000) experimented with the same camera system for detection of powdery mildew (*Blumeria graminis*) in wheat. Their experimental results showed the temperature of the infested plants to be lower than healthy plants and concluded that the infested plants could be identified under laboratory conditions using thermal imaging. However, a major drawback of this technique is that the results will vary as external lighting conditions and temperatures change (Jones, 2004).

2.2 Digital Image Processing

Over the last couple of decades, digital image processing has played a major role in agricultural automation, remote sensing, human diseases analysis and traffic control for identification of different objects (Gonzalez & Woods, 2018). Generally, images are processed to help gain insight and extract information regarding the dynamics of the system. According to Kebapci et al. (2010), plant digital images may contain information related to object's colour, shape and texture that can be analysed for disease/stress monitoring.

2.2.1 Colour based Image Processing

Colour is a visual attribute of radiation incident on the retina of the human eye by an object of producing different sensations. It is counted as a measure by which radiation of homogeneous spectral contents are grouped together and the objects are labelled as red, green, blue or yellow (Julesz, 1962). Colour image processing, which deals with colour features, have been utilized by Ohta et al. (1980) for region segmentation with more than hundred colour features. Behroozi-Khazaei and Maleki (2017) explored the colour features based algorithm for segmenting grape clusters from leaves and background. Colour features have been utilized by Zhou et al. (2012) for red and green apple recognition. Their study suggested the colour difference features had good potential for segmentation of apple fruits from the background. Li et al. (2017b) suggested that cucumber fruit identification was a very difficult task because of colour similarity and the complexity of colour discrimination in a similar background. Meyer et al. (2004) stated that various effects from different lighting sources may be induced upon a digital image resulting in poor identification of plants, as well as increased background noise.

2.2.2 Shape based Image Processing

The shape of an object is a vital and basic visual feature, for human visual form perception systems, that is described within the image content (Loncaric, 1998; Zhang & Lu, 2004). It can be thought of as a silhouette of the object (Loncaric, 1998), invariant to rotation, scale and translation (Dryden & Mardia, 1998). Shape features have been used to perceive between plant species found on leaf or plant canopy geometry.

Neto et al. (2006) utilized the shape features based on leaf boundary to identify young soybean, sunflower, redroot pigweed and velvetleaf plants. Four classical shape features were experimented by Guyer et al. (1986) for species identification from eight species of plants grown in containers using leaves. In a follow up study, Guyer et al. (1993) observed 17 quantitative shape features to identify soybean, jimsonweed, milkwood, velvetleaf, dandelion, ragweed, giant morning glory and foxtail plant species. Remagnino et al. (2017) argued that automated analysis of shape feature is a key challenge because of variation presented by a species and even by a single plant. They also stated that the natural variation could be expected from leaves as well as any organic object. Woebbecke et al. (1995) remarked that any particular shape feature did not work successfully as a plant classifier as the size of the plant increases, because of large phenological variation among plants of the same species.

2.2.3 Texture based Image Processing

Texture is perceived as visual and physical properties of three-dimensional shape in objects that have patterns of variations on the object's surface. Image texture is known as a set of matrices that provides information about the spatial arrangement of colour or intensities in an image or selected portion of an image (Shapiro & Stockman, 2001). The image textures are a complex of visual patterns, having characteristics including brightness, slope, colour and size and can be regarded as similarity of grouping in an image (Rosenfeld & Kak, 1982). According to Levine (1985), image texture has sub-pattern properties comprising density, uniformity, lightness, linearity, regularity, smoothness, randomness and granulation.

Haralick et al. (1973) were the first to describe tonal details of texture by quantification of co-occurrence of tonal pairs. Wavelet transformation based image texture analysis method has been applied as a frequency based textural analysis for plant disease detection (Meunkaewjinda et al., 2008) in agriculture. Kim et al. (2009) used textural analysis to detect grape fruit peel diseases like canker, copper burn, greasy spot, melanose and wind scar. Al Bashish et al. (2010) established a fast and accurate method using texture-based discrimination for leaf disease detection.

2.3 Texture Analysis Methods

Over the last few decades, many textural analysis algorithms have been implemented to extract different levels of information from corresponding images. Textural analysis methods have been widely utilized and studied in depth but there is no concurrence between the methods to provide the best information (Haralick, 1979). There are many different methods for textural analysis, which can be categorized into four general groups: Structure-based methods, Filter-based methods, Model-based methods and Statistical-based methods.

2.3.1 Structure-based Methods

The structure-based approach assigned that textures are composed of some elements called primitives or texels. The primitives and their spatial arrangements are used to characterize textures. The major reason for using structural information, or data, is that the human eye can perceive the structural information of some textures easily (Brodatz, 1966).

Different approaches have already been established to find primitives and their invariant features. Few methods define a primitive as a maximally connected set of pixels with the same attributes (Goyal et al., 1994; Jafari-Khouzani et al., 2006). A pixel's characteristics (e.g., intensity or

gradient) are used to represent the attribute. Then, numerous invariant properties of the primitives, such as the average element intensity (Goyal et al., 1994) and the compactness of primitives, are calculated. Zhang and Tan (2002a) used morphological operations to remove small holes in primitive regions to extract primitives where a texture image was segmented into regions with uniform intensity. Zucker (1976) exploited the isomorphic graph theory of usual collocation to represent the primitive placement rule from ideal texture, where real texture was conceived as a distortion of an underlying ideal texture. Structure-based methods provide a decent symbolic depiction of the image. However, the main difficulty of using structure-based approach is how to define primitives that represent numerous texture structures especially when the texture has no structure. In another word, the structure-based descriptors are better suited for textures with macro-structures (large structures) and do not work well with micro-textures and non-textures (Zhang and Tan, 2002b).

2.3.2 Filter based Methods

These methods decompose textures by applying filters to images in the spatial or the frequency domains. A basic frequency domain analysis is generally executed by utilizing Fourier transformations, which has some advantages making it very popular for image processing. Filter based methods can be implemented in the log-polar coordinate system to provide scale and rotation invariant features (Alapati & Sanderson, 1985). But, it cannot capture local texture features when it is applied to the whole domain of an image. Weszka et al. (1976) classified aerial photographs into five land use classes by applying a Fourier transform and reported lower accuracy around 74%. Haralick et al. (1973) made a comparison between second order statistics and Fourier transform for textural features extraction. They noticed the Fourier transform features performed

poorly due to a lack of spatial localization. As a result, localized spatial filters were suggested by Bovik et al. (1990). These filters used a windowed signal processing approach. The frequency information is calculated in a window rather than for whole image resulting in joint frequency information to the local spatial data. Windowed Fourier filters (Azencott et al., 1997) and multichannel Gabor filters (Bovik et al., 1990) are popular texture methods using joint frequency information. However, according to Teuner et al. (1995) Gabor filters were unfavorable because of their non-orthogonality which results in unnecessary features at different scale and orientation of filter window. The wavelet transform is also a very popular method for texture analysis that treats any image variability as a small wave having a specific frequency for a limited duration (Gonzalez & Woods, 2018). However, Brady and Xie (1996) suggested wavelet transforms are not resistant to variation in image created by the motion of object pixels as a problem.

2.3.3 Model based Methods

In model-based methods, textures can be computed by probabilistic models that include the Random Field models such as the Markov Random Fields (Cohen et al., 1991; Yousefi & Kehtarnavaz, 2011) and Gibbs Random Fields (Elfadel & Picard, 1994). Recognition properties of texture are accounted by capturing the model parameters. McCormick and Jayaramamurthy (1974) synthesized texture by assuming linear dependency of an image pixel on its neighboring pixels and allocated a weighted average texture value based on linear associativity using an autoregressive model. According to Zhang and Tan (2002b), selection of the correct model to effectively map a texture into the selected probability model is a critical issue. In addition, these models require many parameters to be calculated which is not trivial when the neighborhood size is large. Bennett and Khotanzad (1998) suggested that a large set of parameters originating

between and within numerous colour bands that rapidly increases the computational complexity and cost leading it to non-adaptable approach. Haralick (1979) noticed the model-based approach changing scale and direction of an image resulted in significantly different model parameters leading towards mismatched to image segments. Therefore, the computational complexity in measuring model parameters is of primary concern.

2.3.4 Statistical-based Methods

The statistical-based approaches are the most successful and popular method for texture analysis. Julesz (1975) and Julesz & Caelli (1979) stated that describing texture of an image by using statistical measures is initially perceived from experiments on human visual pattern discrimination. Darling and Joseph (1968) expanded the concept by extracting a set of features based on classical statistical measures of mean and variance of image gray texture for the statistical method. However, the results found the same scene for computation of texture features without performing texture normalization. After that, a textural coarseness measurement procedure was proposed by Rosenfeld and Troy (1970) by computing gray texture differences of adjacent image elements. In subsequent work, they detected the boundary by checking variability in textural coarseness (Rosenfeld & Thurston, 1971).

Haralick et al. (1973) expressed the gray level co-occurrence matrix (GLCM) is one of the first well-known methods using this approach. The authors developed Spatial Gray-texture Dependence Matrices (SGDMs) using probability measures of the spatial distribution of neighboring textural dissimilarity at different orientations. They extracted fourteen features from these matrices having accuracies of 82% and 83%, respectively, for aerial photographs and satellite

imagery classification. Shearer and Holmes (1990) invented the colour co-occurrence matrices (CCMs) using hue-saturation-intensity (HSI) colour features to SGDMs. They extracted features from three planes of HSI colour space and generated CCMs followed by Haralick et al. (1973). Their experiments have found higher accuracy around 91% for classifying the different types of nursery stocks using CCMs. Pydipati et al. (2006) identified greasy spot, melanose and scab disease of citrus having the accuracy over 95% using CCMs textural analysis.

2.4 Machine Learning Techniques in Agriculture

Machine learning is the study of algorithms and mathematical models that machine vision systems use to progressively improve their performance on a specific task. Machine learning methods are being applied to identify, detect and predict crop diseases and plant stress phenotyping in agricultural research fields. Based on the problem, machine learning has been applied in: classification, prediction, detection and quantification. Machine learning is partitioned into two classes: supervised learning and unsupervised learning, which are briefly discussed in the following sections.

2.4.1 Supervised Learning

Supervised machine learning is known as the most frequent tasks which are carried out by intelligent systems. If responses are given with known labels the learning is called supervised, in contrast to unsupervised learning, where responses are unlabeled (Jain et al., 1999). A couple of supervised learning approaches are frequently used in research, such as artificial neural networks (ANN), support vector machines (SVM), K nearest neighbors (kNN), decision tree etc.

Zhang (2000) provided an overview of multi-layer ANN that consists of large number of neurons joined together in a pattern of connections. An ANN based plant disease detection system was proposed by Kulkarni and Patil (2012) with diverse image processing techniques having better recognition rate of up to 91%. They also suggested that ANN based classifiers detect numerous plant diseases with combination of texture and colour features to recognize those diseases. Ramakrishnan (2015) reported much higher accuracy around 97.41% for classifying four different plant diseases including alternia leaf blight, cercospora affected, Cercosporidium personatum and phaeoisariopsis personata. The experiments were done by using CCMs textural analysis with back propagation ANN algorithm for detection of leaf disease. The SVM is one of the major supervised learning techniques that revolves around the notion of a margin on either side of a hyperplane of two distinct data classes. The expected generalization error is reduced by maximizing the margin and thereby creating the largest possible distance between the separating hyperplane and the instances or responses on either side. Islam et al. (2017) integrated an image processing technique along with SVM to allow diagnosing diseases from potato leaf images. The proposed techniques proved a path toward automated plant diseases diagnosis on a massive scale having an accuracy of 95% with utilization of SVM. An image pattern classification was experimented by Camargo and Smith (2009) for detection of the visual symptoms of cotton crop diseases using SVM. The CCMs having five features were extracted from their research. Their study suggested that the texture-related features and SVM as machine learning systems might lead to successful discrimination of plant diseases. Plant diseases also detected/classified by several researchers using another machine learning classifier named kNN. The kNN is based on the conception that responses within a dataset will generally exist in close proximity to other responses that have similar properties. If the responses are marked with a classification label, then the value of the

label of an unclassified response can be determined by observing the class of its nearest neighbors. kNN places the k nearest responses to the query response and decides its class by recognizing the single most frequent class label. Several algorithms utilize weighting schemes that adjust the distance measurements and voting influence of each response for more accurate results. Wettschereck et al. (1997) have observed the weighting schemes. The kNN experimented by Xu et al. (2011) with colour and textural features for developing a tomato diagnosis system that showed less accuracy around 82.5% because of less number of features. Murthy (1998) provided the description of working procedure in decision trees classifier. This classifier is based on features values to categorize responses. Responses are classified starting at the root node and are sorted based on their feature values. However, the problem with decision tree construction is that finding features that best divides the training data is a major step for classification. Murthy (1998) also demonstrated that there are different approaches for finding the feature, but most of studies have concluded that there is no single best method.

2.4.2 Unsupervised Learning

In unsupervised learning, the training data consists of only inputs and there are no target outputs. Unlike supervised machine learning, unsupervised machine learning does not have explicit task-specific goals. Unsupervised learning has very limited numbers of applications in agriculture till to date. The latest generation of deep convolution neural network (CNN) is one of the unsupervised machine learning technique used in image processing application which has achieved a top-five error of 16.4% by Krizhevsky et al. (2012). The authors used CNN for classification of images into 1000 possible categories. In the following three years, advances in CNNs have lowered the error rate to 3.57% (Krizhevsky et al., 2012; Zeiler & Fergus, 2014; Simonyan & Zisserman, 2014;

Szegedy et al., 2015; He et al., 2016). About 30,000 leaf images of various crop plants including pear (leaf spot), apple (powdery mildew and rust) and grapevine (powdery mildew, downey mildew, wilt and mites) were experimented for plant diseases recognition (Sladojevic et al., 2016). However, the major problem of this learning is that the model requires large datasets for training and that increases the time for validation (Sladojevic et al., 2016). Mohanty et al. (2016) also suggested that CNN model's accuracy is reduced substantially when tested on a set of images taken under conditions different from the images used for training. They found this reduction ranged from 31.00% to 99.35%. The authors also noted that this technique is not intended to replace existing solutions for diseases diagnosis.

2.5 Strawberry Powdery Mildew Severity and Management

Strawberry powdery mildew disease is caused by *Sphaerotheca macularis* that mainly causes foliar damage, but can also infect fruits especially on susceptible cultivars. It occurs everywhere strawberries are grown (Jordan & Hunter, 1972). Maas (1998) reported that reduction of photosynthesis occurs due to dense mycelium coverage resulting in serious damage of foliage, which can lead to necrosis and eventual defoliation. According to Liu (2017), the severity of powdery mildew disease can cause the yield losses up to 70% in strawberry crop. He also stated that this disease is accounted as the major fungal disease affecting production of strawberries, particularly in polyethylene tunnels. The fungal pathogen affects leaves, flowers, petioles, stolons and fruits, and appears to be specific in strawberry crop (Amsalem et al., 2006). Powdery mildew infected leaves are cup upward, become reddish on the underside and, in severe instances, develop areas that appear badly burned at the margins. Reddening of infected fruit is delayed and, in severe instances, fruit shows a white powdery surface film (Wilhelm, 1961). Affected flowers can be

deformed resulting in low levels of pollen, wilting or death, while contaminated green fruits fail to ripen and infected ripe fruit remain soft having a shortened shelf life and possess small seeds (Spencer, 1978).

The automatic disease detection in plants plays an important role in agriculture to reduce the scouting related expenses and fungicide/herbicide/pesticide cost, as having disease in plants are quite natural. Improper management practice results serious effects on plants and due to which respective product quality, quantity or productivity is affected. Diseases including powdery mildew is also a major problem for strawberry growers. Monitoring of strawberry powdery mildew is mainly conducted by manual inspection and is controlled using biocontrol agents and other chemical applications. Velázquez-López et al. (2011) developed a powdery mildew disease detection system using image processing techniques for rose. Wspanialy (2013) explored a detection system for powdery mildew disease in a greenhouse environment using machine vision having an accuracy of 85%. The experiment was conducted with tomato plant leaves. However, still there is no automatic detection system has been developed for strawberry powdery mildew disease detection using machine vision.

2.6 Conclusion

The above literature study concluded that machine vision based textural analysis of images with supervised learning classifiers has great potential to replace the tradition manual plant diseases detection techniques. There are many studies that have already been proved the usefulness of machine vision for plant diseases classification of different crops. However, strawberry plant disease identification is still primarily human dependent. This present study accepted the

challenges of developing an automated system for strawberry diseases especially powdery mildew disease detection by using machine vision based on machine learning with color co-occurrence matrix and supervised learning.

CHAPTER 3: DEVELOPMENT OF AN ARTIFICIAL CLOUD LIGHTING CONDITION SYSTEM USING MACHINE VISION FOR STRAWBERRY POWDERY MILDEW DISEASE DETECTION

Abstract

Strawberry plants have been facing a significant proportion of diseases during cultivation, scattered throughout the field, emphasizing the need for proper diseases management. Powdery mildew is one of the major fungal strawberry disease which is typically responsible for approximately 30-70% loss of yields. Disease inspection is limited by the human visual capabilities because of the microscopic preliminary symptoms. As powdery mildew disease scrutiny is still determined by human naked eyes due to lack of technological development for plant disease detection task, machine vision systems seem to be well adapted. The aim of this study was to develop a machine vision based artificial cloud lighting condition system for detecting strawberry powdery mildew leaf disease. The artificial cloud lighting condition system was developed consisting of custom software, two µEye colour cameras, a black cloth cover, real time kinematics-global positioning system and a ruggedized laptop computer and mounted on a mobile platform. The custom software was developed in C# programming language. The colour co-occurrence matrix based texture analysis was used to extract image features and discriminant analysis (quadratic) for classification. The study proposed mobile platform of artificial cloud lighting condition for image acquisition is beneficial. It showed higher detection accuracies of 95.26%, 95.45% and 95.37% for recall, precision and F-measure, respectively compared to 81.54%, 72% and 75.95% of recall, precision and F-measure, respectively with acquired images at natural cloud lighting condition. The feature selection results suggested the PM_GHSI feature model was best fit for this study. This study also revealed that the image acquisition speed (1.5 km

h^{-1}) and working depth (300 mm) are suitable for strawberry powdery mildew disease detection in real-time field condition.

Keywords: Machine Vision; Powdery Mildew; Lighting Condition; Acquisition Speed; Working Depth

3.0 Introduction

Strawberry powdery mildew (*Sphaerotheca macularis*) is a polycyclic disease, caused by a fungal pathogen, which affects petioles, leaves, runners, flowers, and fruits that appears to be specific to strawberry plants (Spencer, 1978; Maas, 1998). The disease also impacts the plant's photosynthetic ability influencing fruit quality, growth potential, and productivity (Amsalem et al., 2006) that can cause 30 to 70% yield loss (Liu, 2017). Plant fruit quality and yield are closely tied to appropriate disease management and control of the disease. The ability to detect the powdery mildew (PM) disease is essential to be able to apply suitable controls in order to decrease impacts on fruit quality. Plant diseases have unique developmental characteristics and behaviours that can aid in their detection (Meunkaewjinda et al., 2008). The optimal environmental condition for powdery mildew disease conidial germination ranged between 15 and 25 ˚C with relative humidity (R_H) higher than 75%, but less than 98% (Amsalem et al., 2006). The powdery mildew symptoms primarily appear on young leaves and conidial germination is significantly higher on young leaves compared to older leaves (Amsalem et al., 2006; Bolda & Koike, 2015). The young leaves of strawberry are presented from late July to frost (Carisse & Bouchard, 2010). The initial symptoms of PM are white patches of mycelium on the upper or lower leaf surfaces and leaf edges may roll upward and reddish irregular spots appear on the upper surface on the leaf as the disease progresses (Nelson et al., 1995, 1996). Generally, plant diseases are manually identified by growers, which is a laborious

and time consuming task that makes accurate estimates of total infected areas and prediction of severity in large scale farming systems very challenging (Kobayashi et al., 2001). Development of accurate and rapid techniques to detect plant diseases is of critical importance to the fruit industry.

The vast majority of machine vision based plant disease detection methods proposed so far rely on digital images, which allows the use of very fast, rapid and accurate techniques in different cropping systems (Sena Jr et al., 2003; Weizheng et al., 2008; Al-Hiary et al., 2011; Wspanialy & Moussa, 2016; Schor et al., 2017). Wspanialy and Moussa (2016) used a machine vision system to detect PM disease in greenhouse and achieved 85% of detection rate during test among tomato plants. Schor et al. (2017) applied machine vision technique as an automated diseases detection tool capable of ensuring timely control of PM and spotted wilt virus diseases in tomato. Velázquez-López et al. (2011) developed a machine vision based PM disease detection system for rose and reported the matching average rate was 77.6 ± 14.1%. However, several intrinsic and extrinsic factors may influence the characteristics of images resulting the machine vision technique remain too error prone. Light illumination problems are highly important for machine vision where aspects including time of day, overcast condition and position of sun respecting to the leaf, can greatly affect image quality and characteristics. Researchers revealed the light illumination variations during image acquisition as a major problem in the context of citrus diseases detection (Pydipati et al., 2006), citrus canker severity measurement (Bock et al., 2009) and analysis of *Zostera marina* leaf injuries (Boese et al., 2008). Some of attempts has been made to avoid the illumination variations toward the development of illumination invariant techniques (Guo et al., 2013; Ye et al., 2015), but their success has been modest so far. Researchers also chose to tackle light illumination problem by capturing images under the controlled environments of laboratories

(Peressotti et al., 2011; Clément et al., 2015), but were unsuccessful to eliminate the illumination variations completely. Conversely, a study by Tian et al. (1997) revealed the machine vision systems designed for agricultural crop cultivation sector must be capable of operating in uncontrolled environments. There are many factors affecting the performance of machine vision applications under outdoor conditions, including variable illumination (Tian & Slaughter, 1998; Steward & Tian, 1999; Chandler, 2003), image inappropriate features (Chang et al., 2012; Rehman et al., 2018), and image acquisition speed (Esau et al., 2018). This study limited to few major factors affecting machine vision performance due to its overwhelmed effects on accuracies reported in several studies in image processing. Therefore, the aim of this study was to develop a machine vision based artificial cloud lighting condition system for improving the performance in strawberry powdery mildew detection at a field scale.

3.1 Materials and Methods

3.1.1 Software Development

A graphical user interface (GUI) based image acquisition program was developed during this study using C# programming language (Microsoft Corp, Redmond, WA, USA). The GUI had the functionality of two cameras and continuously acquired, stored and displayed the images. The software acquires 24-bits blue-green-red (BGR) 640 × 256 pixel images corresponding to a 0.6096 m × 0.2438 m (length × width) area of interest (AOI) from each of the two cameras (full frame 1280 × 1024 pixel) was defined inside the software by setting the required width, height and location of the images. The BGR channel arrangement for image acquisition was selected to match the Windows graphics device interface (GDI) for image processing along with proper on-screen display. The AOI was extracted from the centre of the full frame images to minimize the barrel

effect caused by the wide-angle lens. The software used automatic camera control parameters including auto white balance (AWB), auto gain control (AGC) and auto exposure shutter (AES) to minimise the effects caused by varying outdoor illumination conditions and to ensure the high-quality images. The image GUI development process is shown in Fig 3-1.

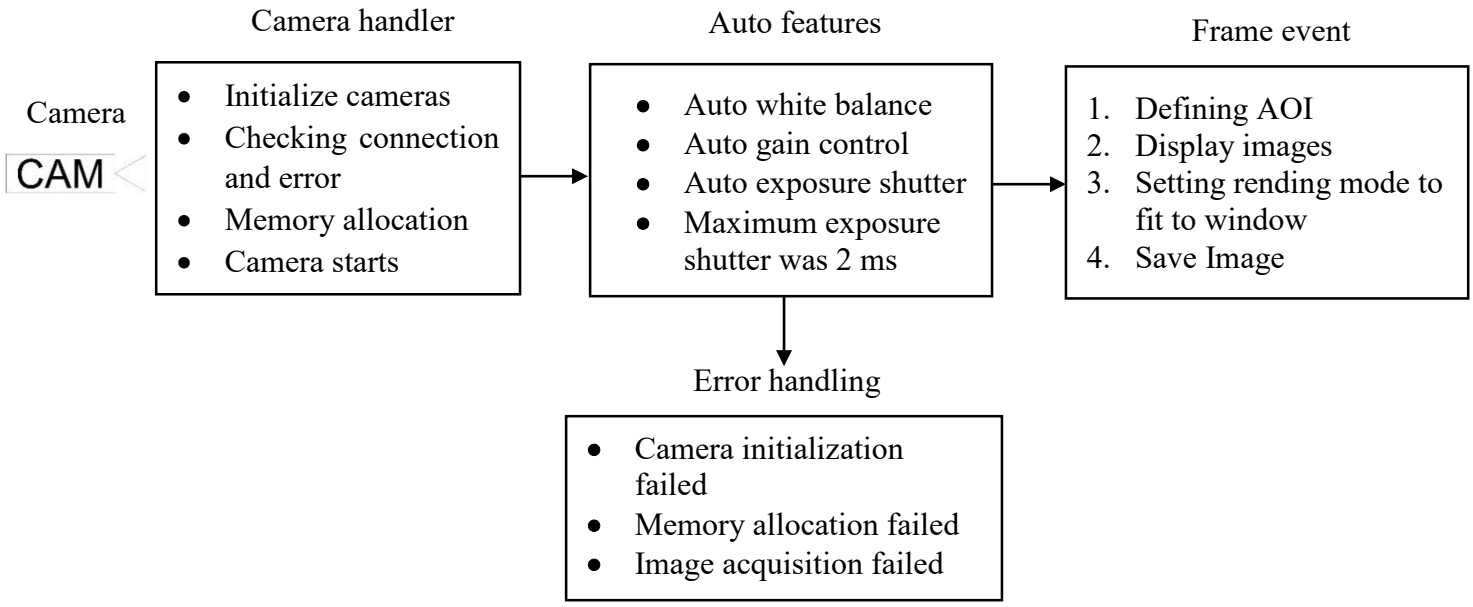

Figure 3-1. Image acquisition process for display and store images

3.1.2 Hardware Development

Strawberry powdery mildew disease detection hardware system consisted of two µEye cameras (IDS Imaging Development System Inc., Woburn, MA, USA) connected via 3 m length Universal Serial Bus (USB) 2.0 active extension cables (Sabrent CB-USBXT, Miami, Fla.) to a 2.40 GHz Intel® Core™ i5-4210U CPU and 4.00 GB random access memory (RAM) computer (Toshiba Corporation, Minato, Tokyo, Japan) installed with 64 bit Windows 7 operating system (Microsoft Corp, Redmond, WA, USA). The hardware system assembled like a four wheel cart system (Fig

3-2 and 3-3). The wide angle field of view lenses (LM4NCL, Kowa Optimed Inc., Torrance, Calif.) with a 3.5 mm focal length were set up to a fixed aperture (f/4.0) and infinity focus. Two types of setup were utilized for image acquisition during natural lighting conditions (NLC) and artificial cloud lighting conditions (ACC). The mobile platform of NLC and ACC are presented in Fig 3-2 and 3-3. The ACC was made outdoors with a black cloth cover using one flat sheet located over the object to avoid direct sunlight and reduce chromatic colour change, having a satisfied condition for image acquisition with less lighting effects and reflection problems in field. A lux meter (LX1010BS, V&A Instrument CO., LTD., Shanghai, China) was used to record the light illumination inside of ACC chamber and the readings were ranged between 800 to 900 lux during experiments.

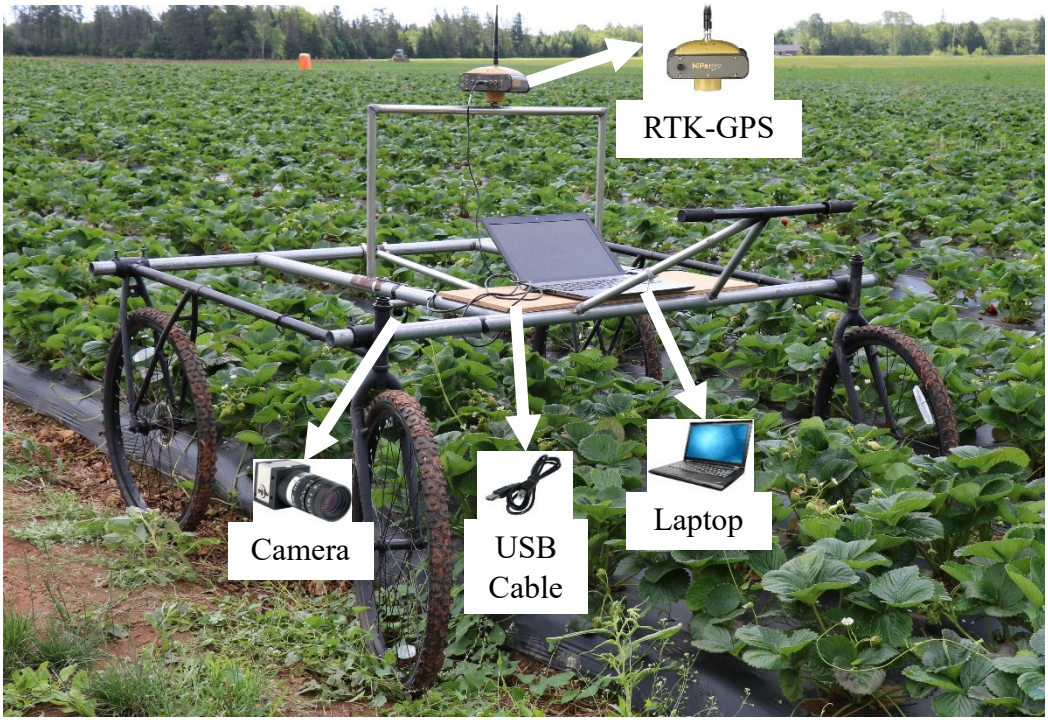

Figure 3-2. Mobile platform for image acquisition in natural lighting condition (NLC)

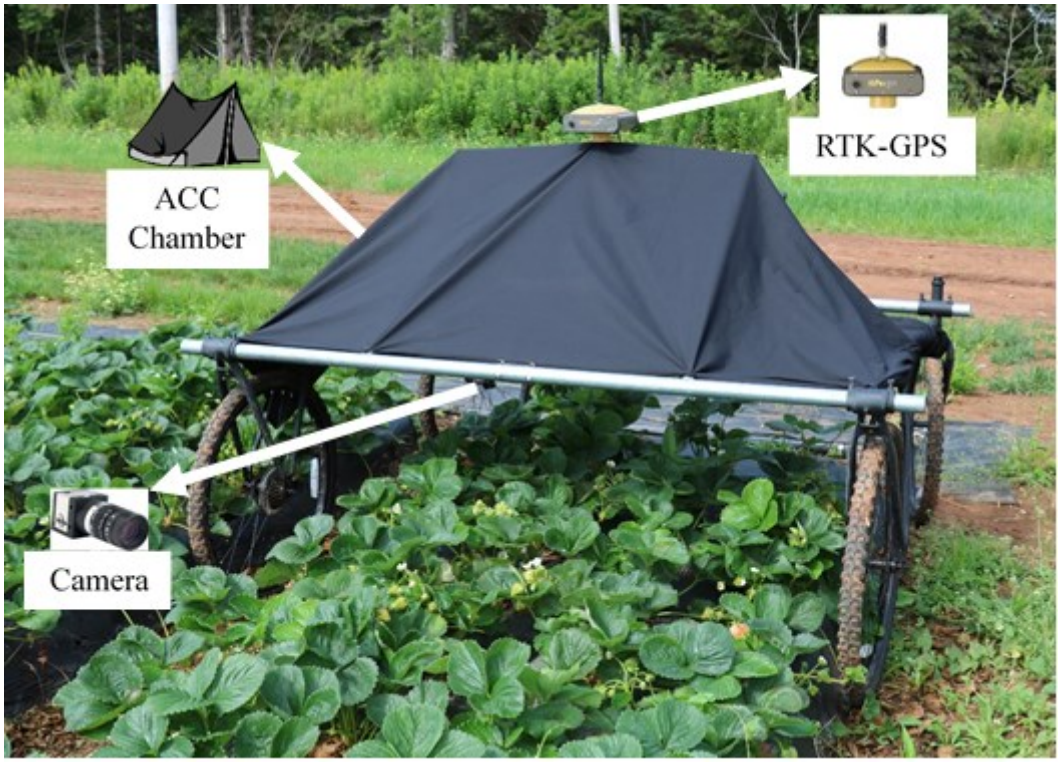

Figure 3-3. Mobile platform for image acquisition in artificial cloud lighting condition (ACC)

3.1.3 Image Processing

The first image processing step of this study was to convert the BGR images into green ratio, National Television System Committee (NTSC) standard for luminance and Hue, Saturation and Intensity (HSI) images. The following step embraced in textural features extraction from converted images. The ratio used was $(G \times 255)\,(B + G + R)^{-1}$ and a manually obtained threshold (>86). The 24-bit Bitmap (BMP) images were converted to 8-bit intensity images of NTSC standard for luminance during pre-processing. The blue (B), green (G) and red (R) intensity levels of individual pixel of an image was employed to calculate the luminance (Lm) in Eq. (3-1).

$$L_m = (0.1140\ B + 0.5870\ G + 0.2989\ R) \qquad (3\text{-}1)$$

A colour conversion was performed for this study from BGR to hue-saturation-intensity (HSI) colour plane on input images. Three 2-dimensional arrays were created from each input image. The pixel intensity of each array was applied for CCM construction from each colour plane. The HSI images were calculated by the following Eq's (3-2, 3-3, 3-4 & 3-5).

$$\theta_h = \cos^{-1}\{\frac{\frac{1}{2}[(R-G)+(R-B)]}{[(R-G)^2+(R-G)(G-B)]^{1/2}}\} \quad (3\text{-}2)$$

Where, θ_h is the angle and Hue (H) colour plane was calculated based on angle (0-360˚) of circle which was normalized in the range [0, 1]. This normalized angle was then linearly transformed to 256 different intensity levels for calculating the H of particular pixel depending upon it R, G and B components (Eq. 3-3).

$$H = \begin{Bmatrix} \frac{\theta_h}{360} * 255 \text{ if } B \leq G \\ \frac{360 - \theta_h}{360} * 255 \text{ if } B > G \end{Bmatrix} \quad (3\text{-}3)$$

$$S = 255 \times \{1 - \frac{3}{(R+G+B)}(\text{Min}(R, \text{Min}(G, B)))\} \quad (3\text{-}4)$$

Where, S is the saturation colour plane.

$$I = \frac{R+G+B}{3} \quad (3\text{-}5)$$

The CCMs, colour co-occurrence matrices (Shearer and Homes, 1990) are in essence a measure of relative frequencies where two neighboring pixels were separated by a distance, d occur in image, one with intensity level m, the other with intensity level n and assigning these frequencies to a new spatial location defined by tonal values (m, n). An image [I $(a, b), 0 \leq a \leq C_m - 1, 0 \leq b \leq C_n - 1$ with M intensity levels] can be used to generate a M × M co-occurrence matrix [P (m, n, d, α)] for a distance vector (d_a, d_b) (Eq. 3-6). The horizontal set of nearest neighbor pixel

pairs were generated by feed forward mechanism of image scanning with intensity levels m and n. The image also scanned with reverse feed mode mechanism for finding the pairs separated by distance (*– d)* and were added in the set (Eq. 3-6) to generate a symmetric CCM from input image (Fig. 3-5). The numbers of pairs with intensity level m and n in the set (M_c) were counted and placed in the matrix called CCM at a point whose geometric bounds were defined as (m, n) (Haralick et al., 1973).

$$P\ (m, n, d, \alpha) = freq\{\big((u, v), (w, z)\big) \in \mathrm{I}\ \big((C_m,\ C_n), (C_m,\ C_n)\big)\} \tag{3-6}$$

Where, (u, v) represents coordinate of image I with intensity level m, (w, z) represents coordinate of image I with intensity level n, C_m is horizontal spatial domain of image I, C_n is vertical spatial domain of image I, d is distance to consider two pixels as neighboring pixels, α is angular relationship between two neighboring pixels, and freq is frequency of elements in the set.

$$\begin{aligned} \mathrm{M_c} = \{&[(0)(0)], [(0)(0)], [(0)(1)], [(1)(0)], [(1)(1)], [(1)(1)], \\ &[(0)(0)], [(0), (0)], [(0)(1)], [(1)(0)], [(1)(1)], [(1)(1)], \\ &[(0)(2)], [(2)(0)], [(2)(2)], [(2)(2)], [(2)(2)], [(2)(2)], \\ &[(2)(2)], [(2)(2)], [(2)(3)], [(3)(2)], [(3)(3)], [(2)(2)]\} \end{aligned}$$

For example, the element at (1, 2) position of horizontal CCM with a displacement vector of 1 pixel was total number of times the two intensity levels with values 1 and 2 occurred horizontally. Extending this concept to additional orientations and summing the results over the entire image, four CCMs were developed from this imaginary image (Fig. 3-5).

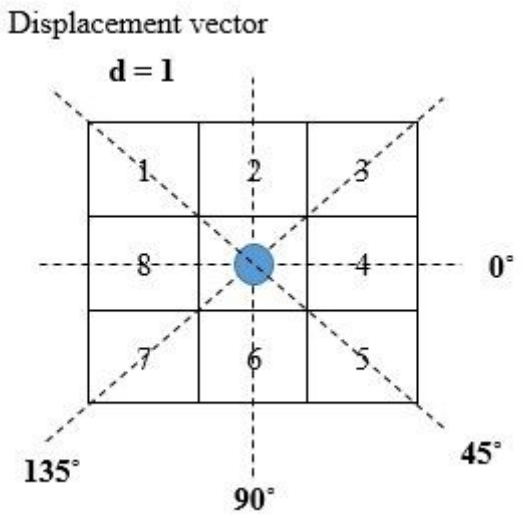

Figure 3-4. Directions of different orientation angles (0˚, 40˚, 90˚ and 135˚) used for CCM construction (circle showing nearest neighbor calculated from center)

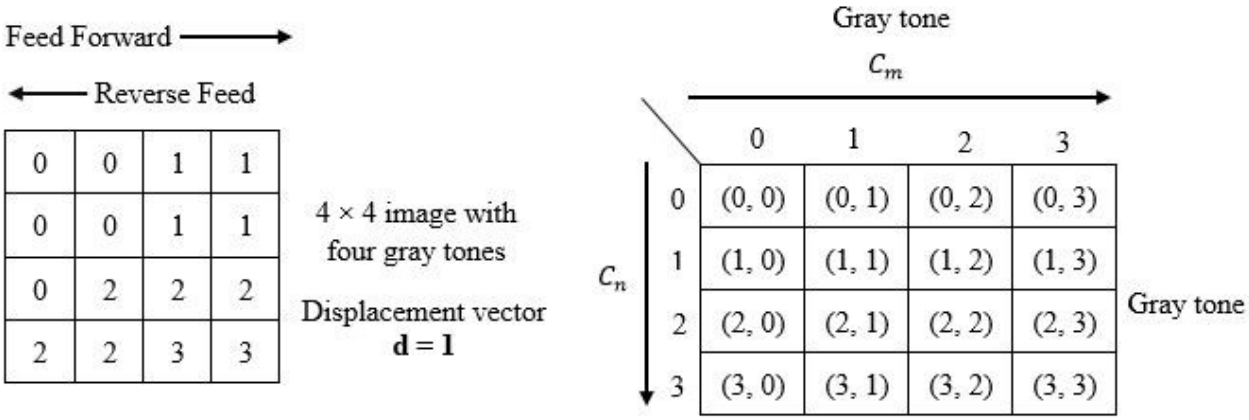

Figure 3-5. CCM construction from a 4 × 4 imaginary image

A 4 × 4 image matrix with an intensity level 4 (ranged from 0 to 3) was used to explain the concept of CCM construction in this study (Fig. 3-5), where 0 and 3 represented darkest and brightest pixels of image respectively. The dimensions of CCM was determined by the highest intensity value of input image matrix as it was proportional to M × M, M being the maximal gray tone value (highest intensity level). The reference pixel of CCM construction was marked with a blue circle

(Fig. 3-4) and surrounding nearest neighbors were labeled from 1 to 8 in a clockwise direction (Fig. 3-4). The displacement vector, d was 1 in this study which means all these neighbors were located at a distance equal to 1.

The CCM was calculated with a given offset(s) and relative orientation angle (α) in the image by collating a pixel's intensity level to another intensity. Thereafter, according to Haralick et al. (1973) these CCMs were normalized by dividing the individual entity in CCM matrix by the total number of pairs in each matrix. The resulting normalize value varies from 0 to 1 (Eq. 3-7).

Normalization,

$$p(m,n) = \frac{P(m,n)}{\sum_{m=0}^{N-1}\sum_{n=0}^{N-1} P(m,n)} \tag{3-7}$$

Where p (m, n) is a normalized CCM, P (m, n) is a marginal probability function, m is the intensity level at a certain pixel, n is another matching intensity level with an offset of s and an orientation angle α, and the denominator of the equation, sum of P (m, n), is the total number of pairs in the matrix with specific orientation and displacement vector.

0° (degree)

4	2	1	0
2	4	0	0
1	0	6	1
0	0	1	2

(A)

45° (degree)

4	1	0	0
1	2	2	0
0	2	4	1
0	0	1	0

(B)

90° (degree)

6	0	2	0
0	4	2	0
2	2	2	2
0	0	2	0

(C)

135° (degree)

2	1	3	0
1	2	1	0
3	1	0	2
0	0	2	0

(D)

Figure 3-6. Four CCMs construction from a 4 × 4 imaginary image at four different orientations with displacement vector, d = 1; (A) P (m, n, 1, 0), blue circle indicates the number of highlighted pairs from $\mathbf{M_c}$ (B) P (m, n, 1, 90) (C) (m, n, 1, 45) (D) (m, n, 1, 135)

After normalization of CCM,

0˚ (degree)

0.167	0.083	0.042	0.000
0.083	0.167	0.000	0.000
0.412	0.000	0.250	0.042
0.000	0.000	0.042	0.083

45˚ (degree)

0.222	0.056	0.000	0.000
0.056	0.111	0.111	0.000
0.000	0.111	0.222	0.056
0.000	0.000	0.056	0.000

90˚ (degree)

0.250	0.000	0.083	0.000
0.000	0.167	0.083	0.000
0.083	0.083	0.083	0.083
0.000	0.000	0.083	0.000

135˚ (degree)

0.111	0.056	0.167	0.000
0.056	0.111	0.056	0.000
0.167	0.056	0.000	0.111
0.000	0.000	0.111	0.000

Figure 3-7. Four CCMs construction after normalization from a 4 × 4 imaginary image at four different orientations with displacement vector, d = 1 for orientation angles 0˚, 40˚, 90˚ and 135˚

Normalization of CCMs from a 4 × 4 imaginary image is presented in Fig. 3-7 that were generated from four different orientation angles presented in Fig. 3-6. According to Chang et al. (2012), the offset value 1 with any orientation angle like 0˚, 90˚, 180˚ and 360˚ gave more accurate results out of five different offsets 1 to 5. Thus, offset 1 and orientation angle 0˚ were used in the study. Ten features were extracted from each luminance, hue, saturation and intensity CCM based on features applied by Shearer and Homes (1990) (Table 3-1).

Table 3-1. Textural feature equations (Shearer & Holmes, 1990)

Description	Textural Features	Equation[u]

Contrast	TF1	$\sum_{\lvert m-n\rvert=0}^{N-1}(m-n)^2\sum_{m=0}^{N-1}\sum_{n=0}^{N-1}p(m,n)$
Homogeneity	TF2	$\sum_{m=0}^{N-1}\sum_{n=0}^{N-1}p(m,n)\frac{1}{1+\lvert m-n\rvert}$
Entropy	TF3	$\sum_{m=0}^{N-1}\sum_{n=0}^{N-1}p(m,n)\ In\ p(m,n)$
Dissimilarity	TF4	$\sum_{m=0}^{N-1}\sum_{n=0}^{N-1}p(m,n)\lvert m-n\rvert$
Angular 2nd Moment	TF5	$\sum_{m=0}^{N-1}\sum_{n=0}^{N-1}p(m,n)^2$
Inverse Difference Moment	TF6	$\sum_{m=0}^{N-1}\sum_{n=0}^{N-1}\frac{p(m,n)}{1+(m-n)^2}$
Average	TF7	$\sum_{m=0}^{N-1}m\,p_x(m)$
Sum of Squares	TF8	$\sum_{m=0}^{N-1}(m-\mu)^2\,p_x(m)$
Product Moment	TF9	$\sum_{m=0}^{N-1}\sum_{n=0}^{N-1}p(m,n)(m-\mu)(n-\mu)$
Correlation	TF10	$\sum_{m=0}^{N-1}\sum_{n=0}^{N-1}p(m,n)\frac{(m-\mu_m)(n-\mu_n)}{\sigma_m\sigma_n}$

[u]N is the total number of intensity levels, *p(m, n)* is the *(m ,n)*th entry in a normalized CCM; and μ is the mean, μ_m is the mean of row, μ_n is the mean of column, σ_m and σ_n are the standard deviation along the m^{th} row and n^{th} column of *p(m, n)* and $p_x(m)$ was obtained by summation of CCM values in m^{th} row.

3.1.4 Factor Affecting Parameters

3.1.4.1 Feature Selection

The stepwise discriminant analysis procedure was applied by using SAS (SAS Institute Inc., Cary, NC, USA) to select subsets of most suitable texture features considering all features used in this study. A total of 50 features (extracted from five converted images including g-ratio, hue, saturation, intensity and luminance) were used to fine-tune the selected feature model by moving the selected features in /out to build a more suitable model. Total of 25 combinations of feature model were evaluated by forward selection and backward elimination during feature selection. The feature selection procedure was continued until all possible features had been added to make an optimum discriminant model. The feature addition and removal were supported by defining the significance level to enter (F to enter) and the significance level to remove (F to remove) thresholds using SAS statistical software. The thresholding level was set based on Chang et al. (2012) as F to enter and F to remove were 0.0015 and 0.0010, respectively. A multivariate statistic Wilk's lambda was calculated to measure the class centroid's differences over the selected features at the end of each step. Total of 27 features were selected to develop a final optimal discriminant model by using G-ratio, luminance, hue, saturation and intensity images that have the strongest relationship in output formation. A feature model with 23 features using G-ratio, hue, saturation and intensity images achieved highest accuracy during PM disease classification and chosen for further analysis of image data.

3.1.4.2 Lighting Conditions

The experimental image data under ACC and NLC were collected between the 09 to 13th July, 2018 in central Nova Scotia, Canada. The temperature ranged from 15 to 25 $^{\circ}$C, average humidity was 80-85% and wind speed were 4-6 km h^{-1} from the West (National Climate Data and Information, 2018). Three strawberry fields were selected to collect image data. The three categories of leaves selected for image acquisition were powdery mildew affected, other disease

affected, and healthy. The selected fields were located on two farms in Debert and Grate Village: the Millen farm site I (Field I: 45.429˚N, 63.484˚W), Millen farm site II (Field II: 45.429˚N, 63.481˚W), and the Balamore farm site III (Field III: 45.413˚N, 63.567˚W). Two strawberry varieties, Albion and Ruby June were cultivated in Field I, Field II and Field III, respectively. In total, 12,000 images were collected by extracting the AOI from each camera image. The images were taken from 10 AM to 4:00 PM (AST). The 60% of the image data used for training and remaining 40% for validation. The performance of NLC and ACC were evaluated with precision, recall and F-measure. The precision indicated the PM disease detection results that are true positives. While recall indicates the ratio of correctly detected PM disease image to all the ground truth PM images. The F-measure is the weighted harmonic mean of recall and precision. The equations of recall, precision and F-measures were presented in Eq. 3-8, 3-9 and 3-10, respectively.

$$\text{Recall} = \frac{\text{TP}}{\text{TP} + \text{FN}} \times 100\% \tag{3-8}$$

$$\text{Precision} = \frac{\text{TP}}{\text{TP} + \text{FP}} \times 100\% \tag{3-9}$$

$$\text{F}_{\partial} = \frac{(1 + \partial) \times \text{Recall} \times \text{Precision}}{\partial \times \text{Precision} + \text{Recall}} \tag{3-10}$$

Where, TP is the number of correctly classifier PM disease image, FN is the number of healthy and other diseases image that are falsely classified as PM disease, FP is the number of PM disease image that are falsely classified as healthy or other disease. ∂ is a nonnegative real value, representing the weighted coefficient between recall and precision, which we set $\partial = 0.8$ in our study to weigh recall more than precision.

3.1.4.3 Image Acquisition Speed

The effect of image acquisition speed on detection accuracy was analysed by processing different acquired images with different speeds. Five different speeds (1.0, 1.5, 2.0, 2.5 and 3.0 km h^{-1}) were applied to select an effective speed for real-time image acquisition. The speed was measured, monitored and maintained by using a HiPer® lite + RTK-GPS (Topcon positioning systems Inc., Livermore, CA, USA) from GUI display.

3.1.4.4 Working Depths

Five working depths (100 mm, 200 mm, 300 mm, 400 mm, and 500 mm) were used in this experiment to examine the effects of depth of field in strawberry powdery mildew detection accuracy. The working depths were adjusted by setting the adjustable camera mount holder. The working depth was measured from leaf canopy to the camera sensor by using a steel ruler scale (Global Industrial, Richmond Hill, ON, Canada). Images at different working depths were collected in ACC condition.

3.1.5 Statistical Analysis

A complete randomized design (CRD) was used for the image acquisition. The classification accuracies of each feature models, ACC and NLC data were calculated by SAS discriminant analysis using selected features. The performance of different acquisition speed and working depth used in this study were compared with ACC images by discriminant analysis. The level of significance used for both tests was 5%. The analysis was performed by using IBM SPSS Statistics 24 (SPSS Inc., Armonk, NY, USA) statistical software.

3.2 Results and Discussion

3.2.1 Effects of Features Selection

The stepwise discriminant analysis resulted in development of optimum feature model along with twenty-five different feature models by using 50 features extracted from CCMs. The optimal ten feature models are presented in Table 3-2. The models were developed by adding or removing the feature data from all possible combinations of colour spaces used in this study. The optimum model (PM_GHSI; PM means Powdery Mildew and each of GHSI means Green Ratio, Hue, Saturation and Intensity colour plane, respectively) was generated by reducing the features of all five colour planes (green ratio, hue, saturation, intensity and luminance) in order to get the list of features having the highest possible classification accuracy.

The classification results of optimal ten feature models resulted in Figure 3-8 by using discriminant analysis. The highest classification accuracy was obtained 95.57% for healthy leaves from PM_GHSIL model whereas the lowest overall classification accuracy achieved was 77.28% model for other disease classification from PM_SIL. When hue and saturation colour space were incorporated to model generation the accuracy was higher. The PM_GHS, PM_HSI, PM_GHSI and PM_GHSIL models achieved higher accuracies compared with other models. The PM_GHSI and PM_GHSIL models showed slight variations of their accuracy whereas PM_GHSI model showed higher accuracy (95.45%) in powdery mildew disease detection. There was no improvement reported by incorporating luminance feature in model development. Similar results were obtained by Chang et al. (2012) with luminance, hue, saturation and intensity colour space for weed detection in wild blueberry. The features extraction procedure suggested the hue and saturation (HS) features influenced the accuracy more than another colour space features. Rehman et al. (2018) reported the overall accuracy (>90%) in both training and test set of goldenrod

detection in wild blueberry fields by using hue and saturation features. Chang et al. (2012) achieved 91.77% of classification accuracy with the combination of hue and saturation features for weed detection.

Table 3-2. Selection of optimal features by stepwise discriminant analysis

Colour Spaces Used	Feature Model	Selected Features[V]
Green Ratio, Hue and Saturation	PM_GHS	G_Co, G_Hm, G_Ds, G_Pm, G_Cr, H_Co, H_Hm, H_En, H_Ds, H_Av, H_Cr, S_Co, S_Hm, S_Ds, S_Av, S_Pm, S_Cr
Green Ratio, Hue and Intensity	PM_GHI	G_Co, G_Hm, G_Ds, G_Pm, G_Cr, H_Co, H_Hm, H_En, H_Ds, H_Av, H_Cr, I_Co, I_Hm, I_Ds, I_Av, I_Pm, I_Cr
Green Ratio, Hue and Luminance	PM_GHL	G_Co, G_Hm, G_Ds, G_Pm, G_Cr, H_Co, H_Hm, H_En, H_Ds, H_Av, H_Cr, L_Ds, L_An, L_Pm, L_Cr
Hue, Saturation and Intensity	PM_HSI	H_Co, H_Hm, H_En, H_Ds, H_Av, H_Cr, S_Co, S_Hm, S_Ds, S_Av, S_Pm, S_Cr, I_Co, I_Hm, I_Ds, I_Av, I_Pm, I_Cr
Hue, Saturation and Luminance	PM_HSL	H_Co, H_Hm, H_En, H_Ds, H_Av, H_Cr, S_Co, S_Hm, S_Ds, S_Av, S_Pm, S_Cr, L_Ds, L_An, L_Pm, L_Cr
Saturation, Intensity and Luminance	PM_SIL	S_Co, S_Hm, S_Ds, S_Av, S_Pm, S_Cr, I_Co, I_Hm, I_Ds, I_Av, I_Pm, I_Cr, L_Ds, L_An, L_Pm, L_Cr
Green Ratio, Hue, Saturation and Intensity	PM_GHSI	G_Co, G_Hm, G_Ds, G_Pm, G_Cr, H_Co, H_Hm, H_En, H_Ds, H_Av, H_Cr, S_Co, S_Hm, S_Ds, S_Av, S_Pm, S_Cr, I_Co, I_Hm, I_Ds, I_Av, I_Pm, I_Cr
Green Ratio, Hue, Saturation and Luminance	PM_GHSL	G_Co, G_Hm, G_Ds, G_Pm, G_Cr, H_Co, H_Hm, H_En, H_Ds, H_Av, H_Cr, S_Co, S_Hm, S_Ds, S_Av, S_Pm, S_Cr, L_Ds, L_An, L_Pm, L_Cr
Hue, Saturation, Intensity and Luminance	PM_HSIL	H_Co, H_Hm, H_En, H_Ds, H_Av, H_Cr, S_Co, S_Hm, S_Ds, S_Av, S_Pm, S_Cr, I_Co, I_Hm, I_Ds, I_Av, I_Pm, I_Cr, L_Ds, L_An, L_Pm, L_Cr

Green Ratio, Hue, Saturation Intensity and Luminance	PM_GHSIL	G_Co, G_Hm, G_Ds, G_Pm, G_Cr, H_Co, H_Hm, H_En, H_Ds, H_Av, H_Cr, S_Co, S_Hm, S_Ds, S_Av, S_Pm, S_Cr, I_Co, I_Hm, I_Ds, I_Av, I_Pm, I_Cr, L_Ds, L_An, L_Pm, L_Cr

[V] G = Green Ratio; H = Hue; S = Saturation; I = Intensity; L = Luminance; Co = Contrast; Hm = Homogeneity; En = Entropy; Ds = Dissimilarity; Av = Average; An = Angular 2nd Moment; Pm = Product Moment; Cr = Correlation.

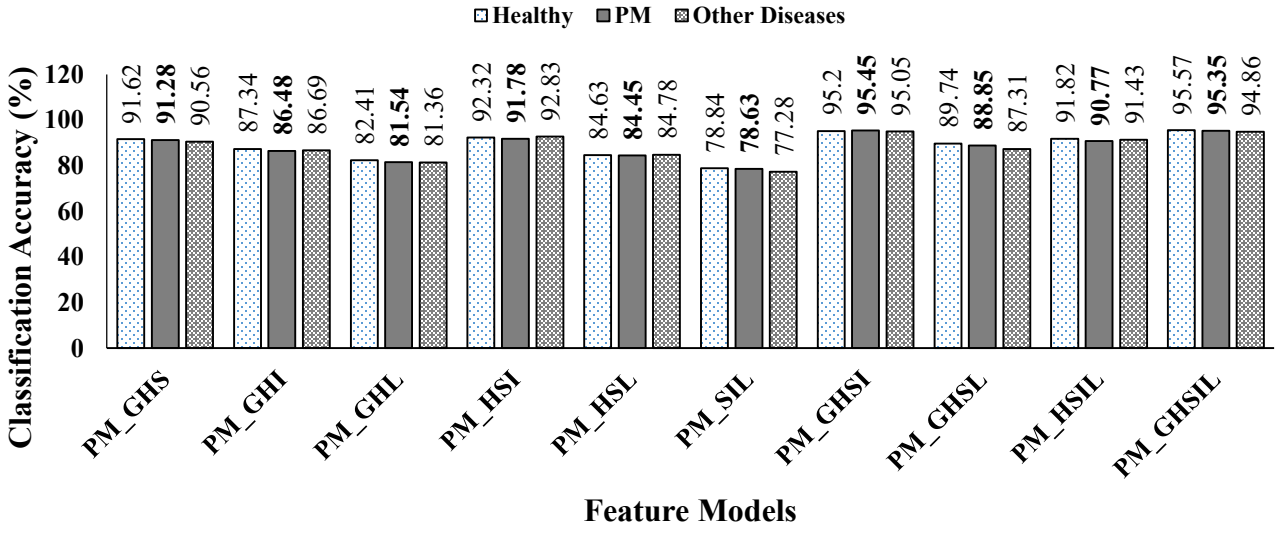

Figure 3-8. Classification results for different feature models using Discriminant analysis

3.2.2 Effects of Lighting Conditions

The results to evaluate the effect of lighting was done under NLC, natural lighting conditions and ACC, artificial cloud lighting conditions are resented in Table 3-3. The evaluation of lighting effects was done by discriminant analysis based classification. The highest classification accuracies were achieved in both of healthy and PM disease classifications with ACC. Conversely, the natural lighting condition images were classified with a lower rate of accuracy. The highest overall accuracy achieved was 95.45% to classify powdery mildew disease using ACC. The lowest

accuracy of 72% was achieved to classify PM disease in natural lighting condition. The highest recall, precision and F-measure of 95.26%, 95.45% and 95.37%, respectively, were reported from ACC and the lowest recall, precision and F-measure of 81.54%, 72% and 75.95% were reported by NLC. This study showed huge variation in accuracy using ACC that could help to solve the illumination problem in field condition. Many researchers have been struggling with illumination variation and reflection problems that are presented during image collection from agricultural fields. Kurtulmus et al. (2011) reported higher value of false negative rate (40.3%) from sunny canopies. There have been various attempts to reduce the effect of light reflecting from the canopy. Aggelopoulou et al. (2011) used black cloth to reduce reflection and Esau et al. (2017) used a light diffuser with artificial light. In this study, ACC showed promising potential in producing clear, informative images with less effort in the pre-processing of the images. The ACC increased the accuracy of the results because the effect of lighting condition was diminished, which was in accordance with Aggelopoulou et al. (2011). The ACC would also serve as a one of aiding options of lighting control for our upcoming real-time application.

Table 3-3. Effect of lighting conditions using natural lighting condition (NLC) and artificial could lighting condition (ACC)

			Predicted Group Membership			
		Response	**Healthy**	**PM**	**Others**	**Total**
Natural Lighting Condition (NLC)[a]	Count	Healthy	1502	129	369	2000
		PM	196	1440	364	2000
		Other Diseases	223	197	1580	2000
	Recall for PM (%)		1440/ (1440 + 129 + 197) = 81.54%			
	Precision for PM (%)		1440/ (1440 + 196 +364) = 72%			
	F-measure for PM (%)		**75.95%**			
	%	Healthy	75.10	6.45	18.45	100.00
		PM	9.80	72.00	18.20	100.00

		Other Diseases	11.15	9.85	79.00	100.00
Artificial Cloud Lighting Condition (ACC)[a]	Count	Healthy	1904	22	74	2000
		PM	28	1909	63	2000
		Other Diseases	26	73	1901	2000
	Recall for PM (%)		1909/ (1909 + 22 + 73) = 95.26%			
	Precision for PM (%)		1909/ (1909 + 28 + 63) = 95.45%			
	F-measure for PM (%)		**95.37%**			
	%	Healthy	95.20	1.10	3.70	100.00
		PM	1.40	95.45	3.15	100.00
		Other Diseases	1.30	3.65	95.05	100.00

[a]Cross validation is done only for those cases in the analysis. In cross validation, each case is classified by the functions derived from all cases other than that case.

3.2.3 Effects of Image Acquisition Speeds

Figure 3-9 shows the results of different image acquisition speeds in strawberry powdery mildew detection under ACC. The experimental results indicated that the increase of ground image acquisition speed could decrease the accuracy of the system. The highest recall (95.29%), precision (95.48%) and F-measure (95.40%) were achieved by running the system with 1 km h^{-1} and the recall, precision and F-measure were decreasing with increasing acquisition speed (Fig 3-9). The slight differences on performance were reported between 1 km h^{-1} and 1.5 km h^{-1} image acquisition speed. The image quality was blurry when the acquisition speed was increased above 1.5 km h^{-1}. In this study, the μEye camera model UI-1240LE with 25.8 frame per second (FPS) was used for image acquisition. The image acquisition speed could be increased with higher camera FPS (must be higher than 25.8 FPS). Therefore, this study revealed the recommended real-time image acquisition speed is 1.5 km h^{-1} for powdery mildew detection in strawberry field at 25.8 FPS. Chattha et al. (2015) suggested ground speeds of 1.6 and 3.2 km h^{-1} were suitable for real-time detection and fertilizer application in wild blueberry field using an 87.2 FPS camera.

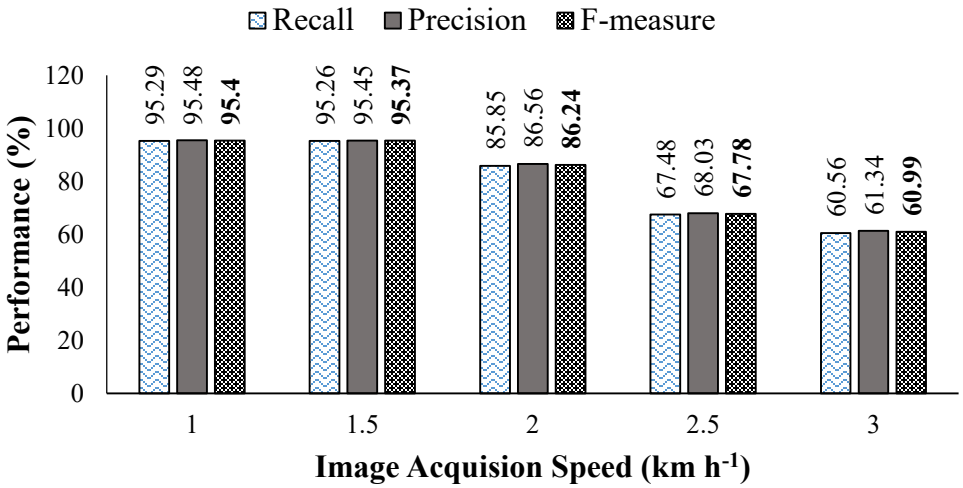

Figure 3-9. Results of different ground based image acquisition speeds for strawberry powdery mildew detection

3.2.4 Effects of Working Depths

Figure 3-10 presents the performance of different working depths used in these experiments. The suitable working depth for strawberry PM detection was 300 mm with highest recall (95.26%), precision (95.45%) and F-measure (95.37%). The lowest recall (43.25%), precision (45.83%) and F-measure (44.83%) were reported using a working depth of 500 mm in this study. The closeness of the camera sensor using a 100 mm and 200 mm working depth provided less detection accuracy 84.35%, 85.22% and 84.83%, and 90.47%, 91.48% and 90.03%, respectively for recall, precision and F-measure compared with a 300 mm depth. On the other hand, the accuracy decreased with increasing working depth above 300 mm (Fig 3-10).

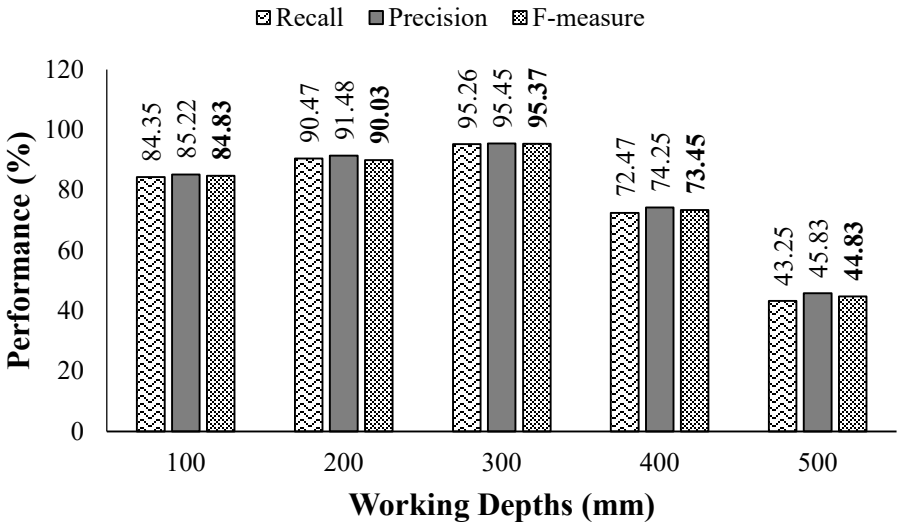

Figure 3-10. Results of different camera working depths for strawberry powdery mildew detection

3.4 Conclusion

The image texture based machine vision technique was applied for strawberry PM detection under two different lighting conditions (ACC and NLC) at different acquisition speeds and working depths. Five different colour spaces (Green Ratio, Hue, Saturation, Intensity, Luminance) were utilized and 50 texture features were extracted by using CCM, colour co-occurrence matrices. The 25 different features models were considered to select optimal feature model. The PM_GHSI model achieved highest accuracy of 95.45% for PM detection compared to other models. The results suggested the ACC was found to be suitable for PM detection at image acquisition speed (1.5 km h^{-1}) and working depth (300 mm). The poor performances were reported under NLC due to huge light illumination variability from the plant canopy during image acquisition. The higher acquisition speeds (2, 2.5 and 3 km h^{-1}) were resulted in the detection failure of PM disease due to blurred images with the 25 FPS cameras using CCM algorithm. The working depths of 400 and 500 mm were provided poor recall, precision and F measure scores due to unclear images and were

not fit for texture analysis. The study concluded that the mobile platform of ACC at 1.5 km h^{-1} acquisition speed and 300 mm working depth would be successful for operation in real-time detection of strawberry PM disease in field by using CCM based machine vision technique.

Acknowledgements

This work was supported by Nova Scotia Research and Innovation Graduate Scholarship Program, Natural Sciences and Engineering Research Council (NSERC), Dalhousie Entrance Scholarship Program and Doug Bragg Enterprises Ltd. The authors would like to give special thanks to Negar Sharifi Mood (Research Assistant) for her help during image acquisition and Scott Read (Senior Instructor) for fabrication of mobile platform. The authors would also like to thank Curtis Millen (Owner of Millen Farm Ltd.) for providing the field access to conduct this study.

CHAPTER 4: COMPARISON OF SUPERVISED CLASSIFIERS FOR POWDERY MILDEW DISEASE DETECTION IN STRAWBERRY USING MACHINE VISION

Abstract

Strawberry is one of the important fruits (ranked 4th among all fruits in term of farm gate value) in Canada, having farm gate income of 10% of total Canadian farm gate (AAFC, 2016). Powdery mildew of strawberry plants is a serious disease caused by an obligate fungal pathogen which is responsible for major yield loss during cultivation. This paper presents an image texture based disease detection algorithm using supervised classifiers. Three supervised classifiers, including artificial neural networks, support vector machines, and k-nearest neighbors were evaluated for disease detection. A total of fifty textural features were extracted using a colour co-occurrence matrix and 23 features were used for classification after reduction. The collected features data was normalized, and used for training and internal, external and cross validations of developed classifiers. Results of this study revealed that the highest recall, precision and F-measure were 98.75% for all cases of internal validation using the artificial neural networks classifier and lowest were 53.97%, 66.37% and 60.22%, respectively using the k-nearest neighbors classifier in external validations. Results identified the artificial neural network classifier disease detection having a lower mean absolute error = 0.0031 and root mean square error = 0.0037 values and 88.50%, 90.80% and 89.24% of F-measure scores during external validations with three different fields. Overall results suggested that an image texture based artificial neural network classifier performed better to classify powdery mildew disease compared to other classifiers in strawberry.

Keywords: Image processing, texture analysis, colour co-occurrence matrix, artificial neural network, support vector machine, k-nearest neighbor, powdery mildew.

4.0 Introduction

Strawberry (*Fragaria* × *ananassa* Duch.) is one of the major horticultural fruit crops with high economic value, grown in tropical, subtropical and temperate regions, in approximately 80 countries worldwide (FAO, 2016). In recent decades, the farm gate value of strawberries in Canada has rapidly increased each year generating almost 129 million CAD in 2017 (Statistics Canada, 2018a). However, strawberry cultivation is decreasing in Canada (Statistics Canada, 2018b). Major cultivation constraints to strawberry in Canada include both biotic (fungal diseases and insects) and abiotic (low temperature injury) stresses (Elmhirst, 2015). Strawberry powdery mildew (*Sphaerotheca macularis*) (PM) is a serious fungal polycyclic disease affecting strawberry production in warm and dry climates (Maas, 1998). The powdery spots develop on all parts of the plant except roots and reduce crop yields by causing decreased fruit set, inadequate ripening, fruit cracking and deformation, poor flavour development and reducing post-harvest storage time (Pertot et al., 2008). These obligate fungal pathogens are typically responsible for 30 to 70% loss of yield (Liu, 2017). The disease can also cause serious damage to foliage with reduction of photosynthesis that can lead to necrosis and eventual defoliation (Maas, 1998). Generally, the initial symptoms of PM are white patches of mycelium on the upper or lower leaf surfaces and leaf edges may roll upward and reddish irregular spots appear on the upper surface on the leaf as the disease progresses (Nelson et al., 1995 and 1996). Thus, recognition is the key factor to control the disease severity in strawberry fields. Farmer detect the presence of plant disease by visual and manual inspection, which is a time-consuming endeavour (Kobayashi et al., 2001). The visual inspection might also cause misjudgements and delay the scouting process, which might lead to lower crop quality and misapplied agrochemicals (Zhou et al., 2015).

Machine vision techniques (Al-Hiary et al., 2011; Arivazhagan et al., 2013; Al Bashish et al., 2011; Chaudhary et al., 2012) have been used to replicate human vision by combining different algorithms and hardware systems in plant disease detection of different cropping systems. Schor et al. (2017) applied machine vision techniques as an automated disease detection tool ensuring timely control of PM and TSWV diseases. Image texture analysis is widely used as a best image processing approach to extract key plant health information compared with colour and shape feature analysis. Li et al. (2017b) suggested cucumber fruit identification is difficult because of colour similarity and complex background with colour discrimination by using colour features. An automated analysis of shape feature is a key challenge because of variation presented by a species and even by a single plant (Remagnino et al., 2017). Conversely, texture analysis can achieve with higher accuracy to identify early and late scorch, as well as fungal diseases, with a software solution that extracted textural features from red-green-blue (RGB) images (Arivazhagan et al., 2013). The colour co-occurrence matrix (CCM) based textural analysis was introduced for plant identification (Shearer & Holmes, 1990) and leaf and stem disease classification (Al Bashish et al., 2010). Choudhary and Gulati (2015) detected scorch and spot diseases of different plant species by using CCM based texture analysis and achieved 100% accuracy. Although the features themselves are not enough for object identification, requiring classifiers for further plant disease recognition after extraction. Artificial neural networks (ANN), support vector machines (SVM), and k-nearest neighbors (kNN) based supervised machine learning classifiers are mostly applied in agricultural research (Mucherino et al., 2009). These approaches have successfully classified different plant diseases with a high success rate (Al Bashish et al., 2011; Sankaran et al., 2011; Omrani et al., 2014). However, variabilities in performance have been reported through different studies (Pydipati et al., 2005; Wang et al., 2008; Camargo & Smith, 2009; Xu et al., 2011;

VijayaLakshmi & Mohan, 2016; Yano et al., 2017). In particular, the application of inappropriate classifiers has been found to result in poor performance and higher misclassification rates (Miller et al., 1998). Therefore, selecting an appropriate classifier for PM detection is of critical importance.

To date, there has been very limited research conducted applying machine vision with different learning algorithms for powdery mildew disease detection in strawberry cropping systems. Yang et al. (2018) recognized the presence of PM disease on strawberry leaves using CNN. However, the experiment was conducted to detect PM disease on harvested single leaf that is not common in strawberry field. Therefore, the aim of this study was to evaluate a series of supervised classifiers for detection of strawberry powdery mildew disease from strawberry branch leaves.

4.1 Materials and Methods

4.1.1 Study Area and Experimental Overview

Three strawberry fields were selected in western Nova Scotia, Canada to collect strawberry leaf image samples. The selected fields were located on two farms in Debert: The Millen farm site I (Field I: 45.429˚N, 63.484˚W), Millen farm site II (Field II: 45.429˚N, 63.481˚W), and one in Great Village: The Balamore farm site I (Field III: 45.413˚N, 63.567˚W). The Albion strawberry variety was cultivated in two fields (Field I and Field II), and Ruby June variety cultivated in Field III. There was no difference in PM symptoms on leaves between both varieties. All image samples were taken between July 09 to July 27, 2018. The leaf samples used were collected based on experienced field scouts by monitoring white patches of mycelium on upper leaf surface. A total of 6,000 images (healthy, PM and other diseases affected) were collected from all fields to conduct

these experiments under artificial cloud lighting condition (ACC). A description of ACC was presented in Chapter 3. The experimented images of healthy and PM leaves were presented in Fig. 4-1 and 4-2. The images were manually divided into two sets containing of 3,600 images for training and 2,400 images for validation in three different classifiers. Internal, external and cross validations were experimented for performance evaluation of this study. The performances evaluated by recall, precision and F-measure were defined in Chapter 3 (Sec 3.1.4.2). Internal validations were conducted with a portion of the data (60% of total) collected from a certain field was used for training while the remaining data (40% of total) from that field was used to validate the results. Cross validation was done with 5-fold, splitting the total data from all fields in 5 different subsets and then 4 sets of data were utilized for training and separate one set for validation. Correspondingly, other 4 sets used for training and remaining one set used for validation and vice versa. The data set was divided into k subsets and a holdout method was repeated k times. At each time, k-1 subsets were utilized for training and k^{th} subsets was utilized for testing. Finally, the average error across all k trials was computed. Thereafter, every data point gets to be in a test set exactly once and gets to be in a training set k-1 times. In case of external validation, Field I and Field II images were used to train the classifiers and remaining Field III images were used for validation. Similarly, Field I and Field III were used for training and Field II for external II validation. Final external validation was done with Field II and Field III for training and Field I for validation.

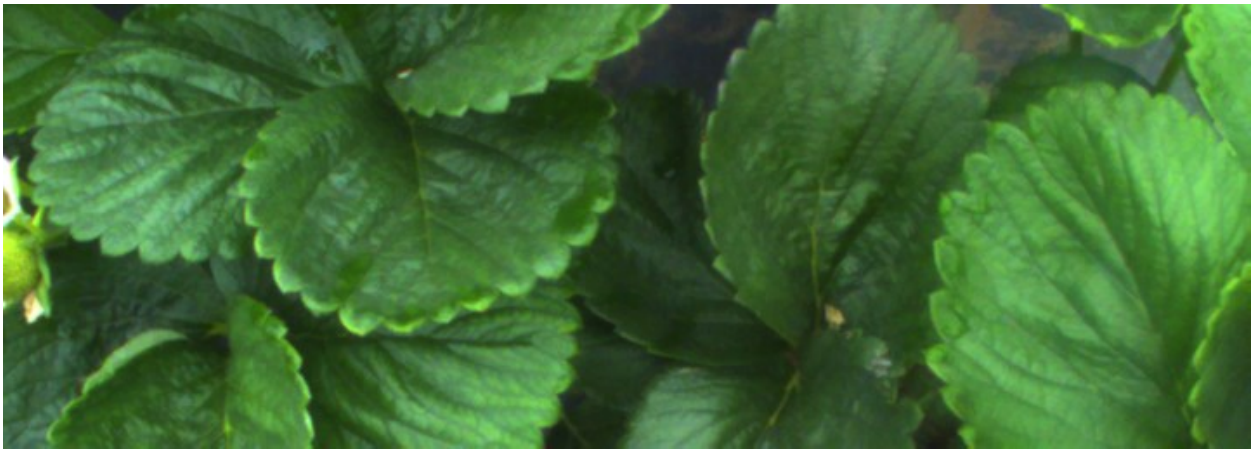

Figure 4-1. Experimented healthy leaves image sample

Figure 4-2. Experimented powdery mildew affected leaves image sample

4.1.2 Image Processing

The image acquisition system consisted of two major components: an ACC on a mobile platform and two digital colour μEye camera (model: UI-1240LE/C, IDS Imaging Development System Inc., Woburn, MA, USA) with a sensor resolution of 1280 × 1024 pixels and a complementary metal oxide semiconductor sensor for taking very detailed images. The two camera were best fit to cover 4 feet (1.2192 m) wide strawberry row and to avoid image overlapping. The images were

taken by two cameras having ACC system installed over a mobile platform and saved from the camera in the RAW format, were subsequently converted to Windows Bitmap (BMP) format to overcome loss related issues caused by image compression. The images were processed with a hardware system composed of an Intel® Core™ i5-4210U CPU @ 2.40 gigahertz and 4.00 gigabyte Random Access Memory laptop (Toshiba Corporation, Minato, Tokyo, Japan). A custom image acquisition program was developed during this study using C# programming language (Microsoft Corp., Redmond, WA, USA) for a 64-bit Windows 7 operating system. The details of image acquisition software and hardware system are briefly described in Chapter 3 (Sections 3.1.1 & 3.1.2).

The image processing steps began with conversion of blue, green and red (BGR) image into green ratio, luminance (Lm), HSI images. According to Meng et al. (2015), the HSI colour space works better than RGB (red, green and blue) and YUV (luminance, chrominance and chroma) for image processing in field conditions. HSI color space represents colors similarly how the human eye senses colors which help to get better information from an image. The HSI colour space represented the purity of colour such as pure blue (B), green (G), and red (R) in terms of degree, whereas saturation represented the measure 1 to 0 to which pure colour is diluted by neutral colour (Gonzalez & Woods, 2018). The B, G, and R intensity levels of individual pixel of an image were utilized to calculate the hue (H), saturation (S) and intensity (I) components of that pixel by using the geometrical transformation relationships. These relationships were defined by the International Commission on Illumination (CIE) chromaticity diagram (Gonzalez & Woods, 2018). The colour co-occurrence matrices (CCMs) were constructed from converted images, followed by feature extraction. The H, S, I and L images were converted using equations suggested by Gonzalez and Woods (2018).

The CCMs were implemented in C# programming language with five converted images from one image and extracting a set of 10 features from individual CCM. Since frequency in the CCMs is a function of angular relationship and distance between neighboring pixels, in this research an angular relationship of 0˚ and a displacement vector of 1 pixel were selected for CCMs construction. The displacement vector of 1 pixel was selected as it provided exceptional results when varied between 1 and 5 (Chang et al., 2012). The resulting normalization of each CCM value varied from 0 to 1.

A total of 50 textural features were extracted from an individual image after constructing the CCM. The texture features such as contrast, homogeneity, entropy, dissimilarity, angular second moment, inverse difference moment, average, sum of square, product moment and correlation were extracted to detect strawberry PM disease. Image feature extraction equations are given in Chapter 3 (Section 3.1.3).

4.1.3 Data Normalization

A total of 50 features were extracted from one image that were utilized as inputs for classifiers after feature reduction. Twenty-three features were selected for classification. The feature reduction procedure is presented in Chapter 3 (Section 3.1.4.1**)**. The non-normalized data was found to reduce the performance of the classifiers. In order to enhance the performance of classifiers, the input data was normalized (Lee et al., 2004) and hence outputs obtained were also normalized quantities. The following equation was used for the normalization of the data (Eq. 4-1).

$$u_i = \frac{(R_i - Min_i)}{(Max_i - Min_i)} \tag{4-1}$$

Where,

u_i = Normalized value of input

R_i = Actual value of input

Min_i = Minimum value of input

Max_i = Maximum value of input

4.1.4 Classifiers

In this study, different types of classifiers were evaluated to determine the most effective at classifying strawberry powdery mildew disease using CCM based textural features analysis. The three supervised learning classifiers evaluated were the ANN, SVM, and kNN by using ACC collected images.

4.1.4.1 ANN Classifier

The textural features of the CCMs were used to provide the input data for training the ANN classifier. Neural network models were found to incorporate all the selected textural features in the discrimination scheme. Peltarion Synapse (Peltarion Corp., Stockholm, Sweden) was used for classifying the textural features, as well as images of healthy and powdery mildew affected leaves. A back-propagation artificial neural network (BP-ANN) algorithm was applied for training of the proposed network. The 23-46-46-1 network structure was examined which represents twenty-three nodes for the input layer, forty-six nodes for two hidden layers each, and one node for the output layer for the data analysis (Figure 4-3). The extracted textural features were selected as inputs for

the input layer and corresponding healthy or disease labels (powdery mildew and other diseases) were established as an output in the output layer. All the settings of developed models were kept constant, the mathematical functions were changed and, finally MAE and RMSE were recorded to find optimal mathematical function for this study. Four different functions such as the tanh sigmoid, exponential, logistic sigmoid, and linear transfer were used to translate the input signals into output signals ranging from 0 to 2 (i.e., 0, 1 and 2). The predictor model used was the Mean Absolute Error (MAE) and Root Mean Square Error (RMSE) to find the best model structure. The MAE is a measure of absolute difference between actual and predicted observation and the RMSE is the square root of the average of squared differences between prediction and actual observation that measures the average magnitude of the error.

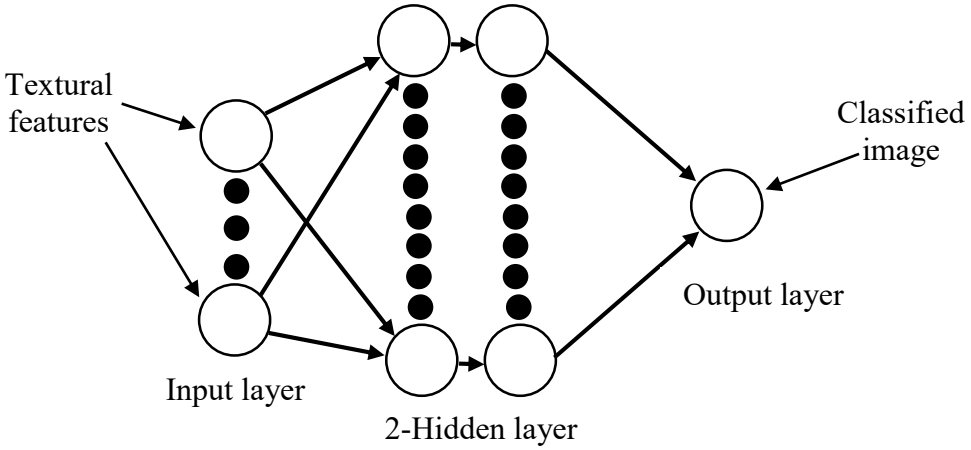

Figure 4-3. ANN Structure

The training process was initiated using randomly selected initial weights and biases. The experimental conditions involved a supervised training mechanism providing the network output by labelling. The MSE and RMSE values were used to determine the performance of the model structures. The activation or non-linear function was determined by the presence of particular

neural features that determined the optimal weights. The neural network performed a non-linear transformation on the input variables (N) to achieve an output (M) by Eq. (4-2).

$$\{M\} = f(\{N\}) \tag{4-2}$$

Where,

M = Output

f = Non-linear function

N = Input variables

Four ANN model structures were developed and tested to discover a satisfactory mathematical function to process image data. Seventeen simulations of the ANN model were conducted to select the optimal three model structures. The size of input layer and two hidden layers with corresponding neurons was considered enough to model the continuous non-linear functions. Additional hidden layers may cause over and under fitting of the model (Torrecilla et al., 2004). All the selected models were run at an epoch size (iterative steps) of 15,000 with learning rate of 0.1. To determine the optimal epoch size, the best selected ANN model was operated at different epoch sizes at an interval of 1,000 and the error values of MAE and RMSE were calculated at each interval. According to Madadlou et al. (2009), the epoch size has a major influence on error terms. The momentum term of 0.7 was used to develop ANN models. The best model structure and mathematical function were selected based on lower MAE and RMSE values and by comparing the actual and predicted values. Finally, the model developmental process was completed having acceptable errors (i.e., MAE <0.003 and RMSE <0.005) from predicted data set compared with actual data set. The MAE is more robust (less sensitive to outliers) compared to MSE. Thus, MSE

and RMSE were best fit for calculating error in our study. After training the model, the performance of the ANN model was tested by employing the internal, external, and cross validation separately (Fig. 4-4).

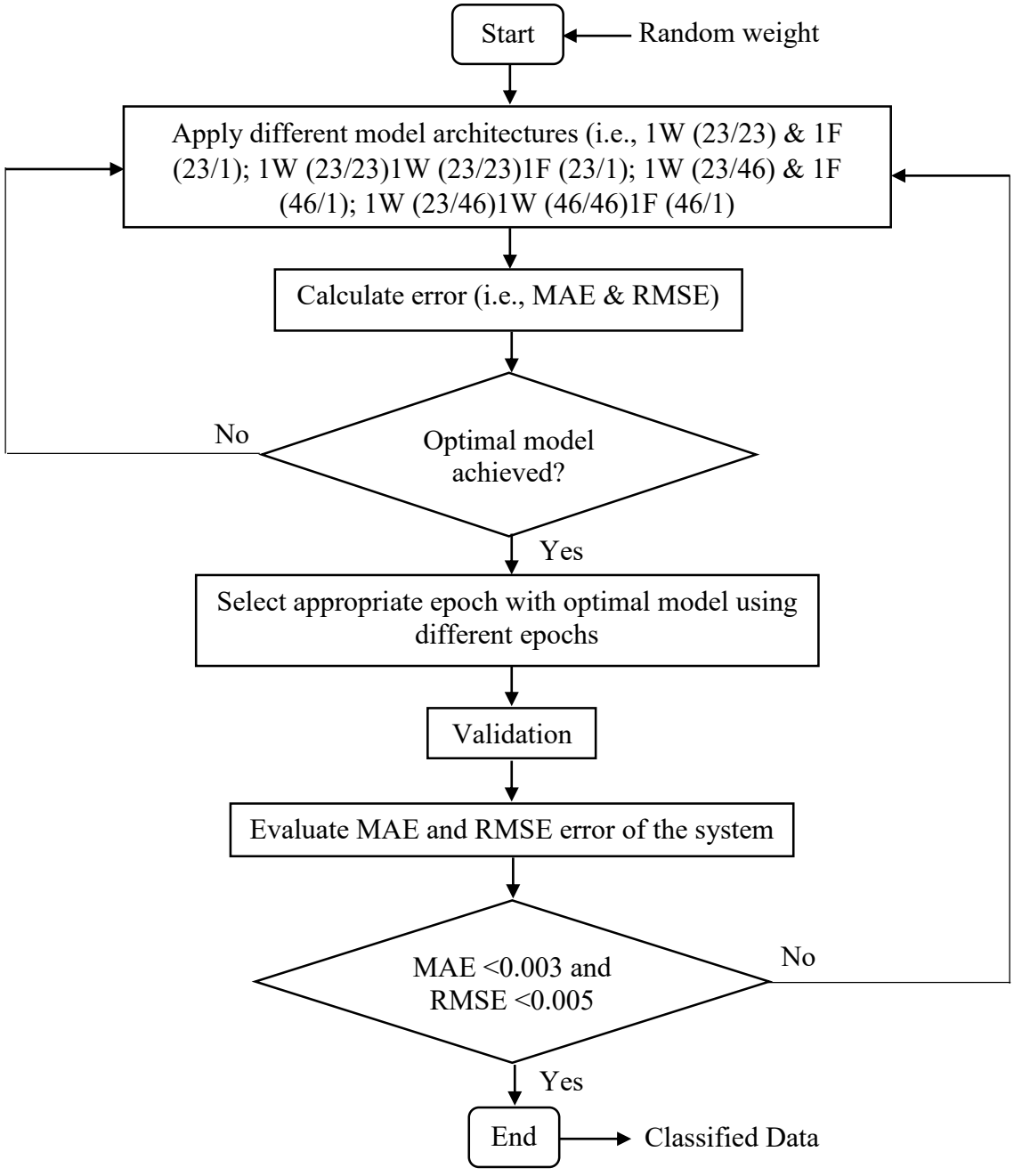

Figure 4-4. Flowchart of artificial neural network algorithm for model development

4.1.4.2 SVM Classifier

A SVM classifier was selected for these experiments based on previously established studies reporting efficient implementation and performance for high dimensional problems and small datasets. The classifier was tested to exemplify the effectiveness of powdery mildew disease leaf classification from healthy and other diseases leaves. The feature vectors were applied as the input to the SVM classifier after normalization. Training and testing were evaluated for measuring the performance of the classifier. MATLAB® Classification Toolbox version 2017a (MathWorks, Natick, MA, USA) was used for SVM performance evaluation. The general concept of SVM (Figure 4-5**)** is to provide a solution of classification problems by calculating the input vectors into a new high-dimensional space through some nonlinear mapping and constructing an optimal separating hyperplane that measures the maximum margin to separate positive and negative classes (Cristianini & Shawe-Taylor, 2000). The SVM constructs a hyperplane in the space to observe the training input vector in an n-dimensional space for classification that has the largest distance to the closest training data point of any class. A linear and separable sample set belonging to separate classes are separated by the hyperplane. The generalization ability of SVM model is better as the distance between the closest vectors to the hyperplane was maximized. The mathematical form of SVM classifier is as follow:

$$F : U^X \rightarrow Q \tag{4-3}$$

Where, specified data set mapping is made via a map function F from input space into higher dimension feature space Q (dot product space).

A linear learning algorithm was performed in Q which required the evaluation of dot products. If Q is of a higher dimensional value, then the right-hand side of Eq. 4-3 will be very costly to compute (Schölkopf & Smola, 2002). Hence, kernel functions are utilized using the input parameters to compute the dot product in the feature space for the non-linear data.

Five different kernels including linear, quadratic, cubic, fine Gaussian and RBF were utilized for experimentation. One promising kernel was selected based on internal and 5-fold cross validations performance for external validation. Internal, external, and cross validations were tested for performance evaluation of classifier. Two fields of data were used for training and one field of data was simultaneously utilized for testing. The external validation process began with exporting the model after development. The exported model was used in C# for testing experimental image data. The exported model tested the data from separate fields that were not used for training the model. Finally, the accuracy was determined based on correctly classified textural features from diseases and healthy strawberry leaves.

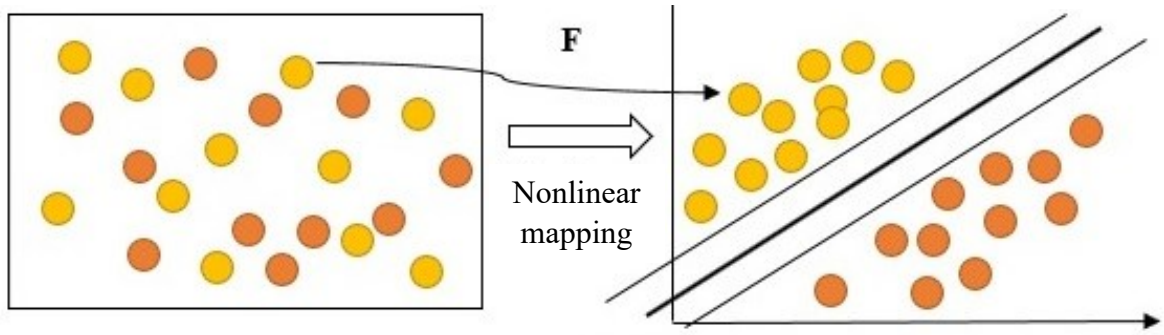

Figure 4-5. Working principle of SVM classifier

4.1.4.3 kNN Classifier

Another supervised learning classifier evaluated in this study was the kNN. The kNN classifier is a non-parametric method that separates a test object according to the class of majority of its k^{th}

nearest neighbour in the training set. It applies the Euclidean distance in the multidimensional space as a similarity measurement to separate the test objects. k represents the number of highly data-dependent tuning of neighbours and uses uniform weights meaning which is assigned the value to a query point is computed from a simple majority vote of the nearest neighbours. The unknown object in the query object is compared to every sample of objects which are previously being used to train the kNN classifier. The distance measurements of kNN classifier were conducted using Euclidean distance with the following equation:

$$\mathrm{E_{Dp}}(\mathrm{P},\mathrm{Q}) = \sqrt{\frac{\sum_{i=1}^{x}(m_i - n_i)^2}{m}} \tag{4-4}$$

Where P and Q are represented by feature vectors $\mathrm{P} = (\mathrm{m_{1,}m_{2,}m_{3\ldots\ldots,}m_x})$ and $\mathrm{Q} = (\mathrm{n_{1,}n_{2,}n_{3\ldots\ldots,}n_x})$ and x is the dimensionality of the feature space. The equation measures the Euclidean distance between two points P and Q.

The performance of kNN varies with different kernel functions. Fine, cosine, coarse, cubic and RBF kernels were used for performance evaluation in this study. MATLAB software was used for implementing the kNN classifier. After normalizing the textural features, data classification was done between the data of healthy, powdery mildew and other diseases affected leaf images using kNN classification method. The performance of kNN classifier was evaluated by using internal, external, and cross validations.

4.2 Results and Discussion

4.2.1 Classification Using ANN

The results from four network structures evaluated to obtain a suitable ANN network for data processing are listed in Table 4-1. The highest RMSE was derived from the exponential mathematical/transfer function (1.9732), compared to the other functions evaluated to classify healthy, powdery mildew and other diseases affected leaves. The tanh sigmoid function was able to process data with a reasonably low MAE (0.0031 to 0.0398) and RMSE (0.0037 to 0.0582) when compared to the other functions in the networks. Based on low error rates, tanh sigmoid was chosen for further processing. All the networks were operated at an epoch of 15,000, as there was no improvement in error even if the model was trained more than 15,000 epochs. The results corresponding to different epoch sizes are presented in Table 4-2. Farooque et al. (2016) also developed an optimal ANN model with an epoch size of 15,000 and reported the model was more suitable in capturing non-linearity of relationships between variables.

Table 4-1. Tested mathematical functions at an epoch size of 15,000 with normalized data

Model Structures	**Tanh Sigmoid**		**Logistic Sigmoid**		**Linear**		**Exponential**	
	MAE	**RMSE**	**MAE**	**RMSE**	**MAE**	**RMSE**	**MAE**	**RMSE**
1W (23/23) & 1F (23/1) 23 inputs 1 output	0.0398	0.0582	0.0727	0.0824	0.2645	0.3426	1.6386	1.9732
1W (23/23)1W (23/23)1F (23/1) 23 inputs 1 outputs	0.0083	0.0102	0.0536	0.0682	0.1463	0.2105	0.6826	0.7690
1W (23/46) & 1F (46/1) 23 inputs 1 output	0.0042	0.0048	0.0172	0.0206	0.1187	0.1925	0.6138	0.6872
1W (23/46)1W (46/46)1F (46/1) 23 inputs 1 output	0.0031	0.0037	0.0101	0.0228	0.1016	0.1789	0.5277	0.6924

Where: W = weight layer; F = function layer;

After determination of an optimal model, it was tested to select an appropriate epoch size testing with different numbers of epochs. In total, six different epoch sizes were analysed using the optimized model with a tanh sigmoid function (Table 4-2). The model (1W (23/46)1W(46/46)1F(46/1)) with an epoch size of 15,000 was selected as the best combination based on low MAE (0.0031) and RMSE (0.0037). The optimized model using epochs of 1,000, 2,000, 3,000 and 4,000 resulted in higher MAE and RMSE values suggesting inferior performance compared to 15,000 epochs (Table 4-2). Although the epoch size 5,000 showed lower MAE and RMSE values, the 15,000 epoch was determined to be more sufficient for the model structure to perform the classification rather than other epochs due to lowest error rates.

Table 4-2. Selection of approximate epoch

Sr. No	Model Structure	Epoch	Tanh Sigmoid	
			MAE	**RMSE**
1.	1W (23/46)1W (46/46) 1F (46/1) 23 inputs 1 output	1,000	0.0738	0.0963
2.		2,000	0.0384	0.0589
3.		3,000	0.0137	0.0195
4.		4,000	0.0093	0.0126
5.		5,000	0.0056	0.0072
6.		15,000	0.0031	0.0037

Where: W = weight layer; F=function layer;

Table 4-3 shows ANN classifier performances based on internal, external and cross validations with different datasets. The model classified healthy, powdery mildew and other diseases leaf images with higher accuracy in all the case of internal validations. The highest recall (98.75%), precision (98.75%) and F-measure (98.75%) were reported using healthy leaves during internal validation and the lowest recall, precision and F-measure of 80.82%, 86.04% and 83.64%,

respectively were measured with external-I validation for other diseases classification. Results suggested that the ANN classifier performed better at healthy and powdery mildew images classification with less numbers of misclassifications whereas comparatively higher misclassification rate was obtained by other diseases images.

Table 4-3. Performance of ANN classifier for strawberry leaf images classification

Validations	Response	Predicted				Performance		
		Healthy	PM	Other Diseases	Total	Recall (%)	Precision (%)	F-Measure (%)
Internal	Healthy	790	3	7	800	98.75	98.75	98.75
	PM	6	784	10	800	98.49	98.00	98.22
	Other Diseases	4	9	787	800	97.89	98.38	98.16
5-fold Cross	Healthy	394	2	4	400	98.25	98.50	98.39
	PM	4	388	8	400	97.98	97.00	97.43
	Other Diseases	3	6	391	400	97.02	97.75	97.42
External I[a]	Healthy	578	23	65	666	90.73	86.79	88.50
	PM	26	569	71	666	87.27	85.44	86.24
	Other Diseases	33	60	573	666	80.82	86.04	83.64
External II[b]	Healthy	587	24	55	666	94.37	88.14	90.80
	PM	16	579	71	666	86.81	86.94	86.88
	Other Diseases	19	64	583	666	82.23	87.54	85.10
External III[c]	Healthy	586	29	51	666	90.85	87.99	89.24
	PM	32	576	58	666	86.75	86.49	86.61
	Other Diseases	27	59	580	666	84.18	87.09	85.77

Where: [a]External-I: training with Field I + Field II and validated with Field III; [b]External-II: training with Field I + Field III and validated with Field II; [c]External-III: training with Field II + Field III and validated with Field I.

4.2.2 Classification Using SVM

Experimental results showed that the accuracy of the classifier varied with different kernel functions (Fig. 4-6). The highest overall performance (averaged values of internal and 5-fold cross

validations) was from the linear kernel (98.07%), whereas a 93.17% of accuracy was observed using the fine Gaussian kernel. The linear kernel also achieved the highest accuracy value of 98.38% across internal validation (Fig. 4-6). The best kernel was selected by evaluating the accuracy of internal and cross validation, having the highest overall accuracy of approximately 98.07% (Fig. 4-6). The accuracies were reported due to find out optimal kernel that used to analyse experimental image data for detection.

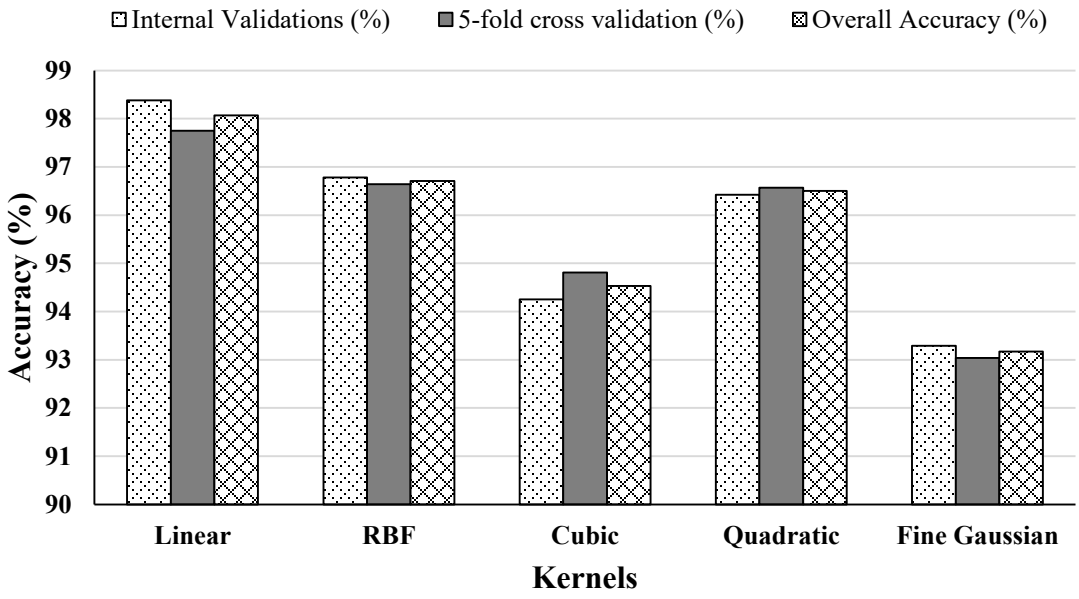

Figure 4-6. Selection of kernel for SVM classifier

Different assessments conducted for analysing the performance of the proposed SVM classifier with linear kernel and the test performances of SVM classifier are presented in Table 4-4. The SVM classifier predictions measured values at a high recall and precision rates. The highest recall, precision and F-measure were 96.75% for all cases during internal validation and the lowest recall, precision and F-measure values of 77.29%, 82.28% and 79.98%, respectively were calculated in external-I validation. The external validations (Table 4-4) results varied based on different field data used for validations. The highest external validation recall and precision were computed of

90.82% and 84.68% with Field II data and lowest with Field III data during validations. The higher recall, precision and F-measure rates of 96.73%, 96.25% and 96.46%, respectively also resulted with 5-fold cross validation through healthy leaf images (Table 4-4).

Table 4-4. Performance of SVM classifier for strawberry leaf images classification

Validations	Response	Predicted				Performance		
		Healthy	PM	Other Diseases	Total	Recall (%)	Precision (%)	F-Measure (%)
Internal Validations	Healthy	774	7	19	800	96.75	96.75	96.75
	PM	12	765	23	800	96.96	95.63	96.22
	Other Diseases	14	17	769	800	94.82	96.13	95.54
5-fold Cross Validation	Healthy	385	4	11	400	96.73	96.25	96.46
	PM	8	380	12	400	95.72	95.00	95.32
	Others Diseases	5	13	382	400	94.32	95.5	94.97
External I[a]	Healthy	556	31	79	666	88.96	83.48	85.83
	PM	32	552	82	666	83.13	82.88	82.99
	Others Diseases	37	81	548	666	77.29	82.28	79.98
External II[b]	Healthy	564	26	76	666	90.82	84.68	87.30
	PM	38	559	69	666	83.31	83.93	83.65
	Other Diseases	19	86	561	666	79.46	84.23	82.04
External III[c]	Healthy	558	35	73	666	88.15	83.78	85.67
	PM	36	561	69	666	83.73	84.23	84.01
	Others Diseases	39	74	553	666	79.57	83.03	81.46

Where: [a]External-I: training with Field I + Field II and validated with Field III; [b]External-II: training with Field I + Field III and validated with Field II; [c]External-III: training with Field II + Field III and validated with Field I.

4.2.3 Classification Using kNN

Fig. 4-7 shows the classification results using different kernels of kNN classifier model. The results from Fig. 4-7 show that the highest classification accuracy was obtained with fine kernel, approximately 88.84% during internal validation. The results also showed a fairly high

classification accuracy of 86.45% for RBF kernel at the time of internal validation, however the highest overall classification accuracy of 87.38% was achieved using the fine kernel. The fine kernel was selected as best for these experiments.

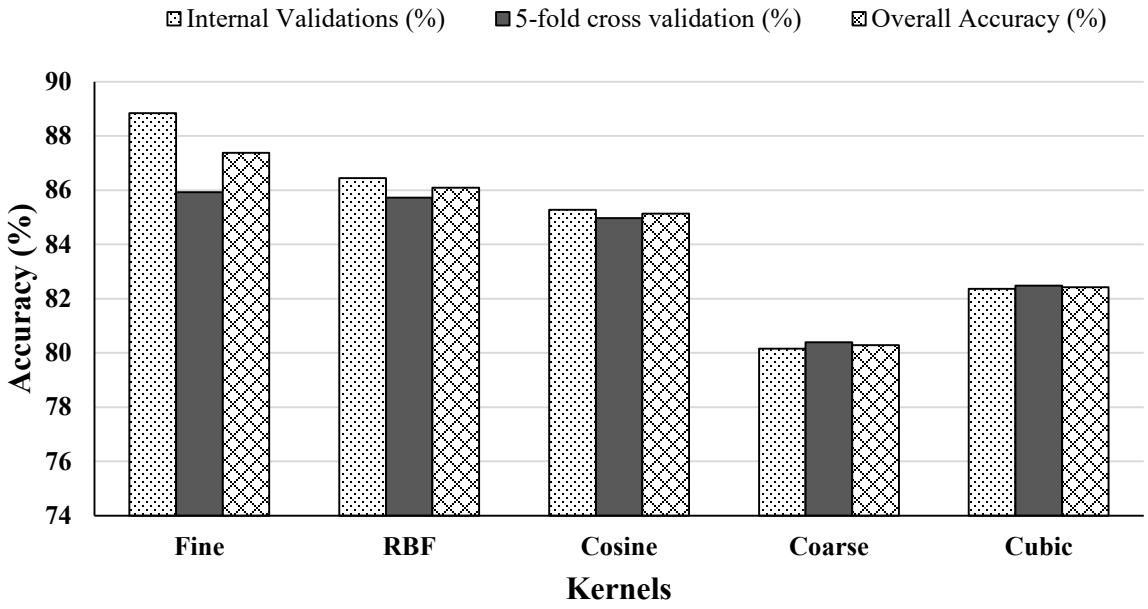

Figure 4-7. Selection of kernel for kNN classifier

Table 4-5 outlined the performance of kNN classifier in three different validations, e.g., internal, external and cross validation by using fine kernel. As shown in Table 4-5, the best performance achieved with internal validation having highest recall, precision and F-measure of 94.25%, 90.13% and 91.92%, respectively for healthy images. Likewise, ANN and SVM classifier, the kNN also reported poor performance at the time of external validations, having lower scores of 53.97%, 66.37% and 60.22% for recall, precision and F-measure, respectively using Field III data. The healthy and powdery mildew leaf images classified more correctly compared to other diseases images. The classifier performed better in internal and cross validations and achieved >80%

success rates in all cases. Xu et al. (2011) reported in their study that kNN could successfully classified 82.5% of tomato diseases which is matched closely with our results with strawberry PM.

Table 4-5. Performance of kNN classifier for strawberry leaf images classification

Validations	Response	Predicted				Performance		
		Healthy	PM	Other Diseases	Total	Recall (%)	Precision (%)	F-Measure (%)
Internal	Healthy	721	16	63	800	94.25	90.13	91.92
	PM	19	697	84	800	90.05	87.13	88.40
	Other Diseases	25	61	714	800	82.93	89.25	86.33
5-fold Cross	Healthy	348	9	43	400	94.05	87.00	90.00
	PM	9	339	52	400	86.70	84.75	85.61
	Other Diseases	13	43	344	400	78.36	86.00	82.43
External I[a]	Healthy	453	37	176	666	87.79	68.02	75.59
	PM	16	449	201	666	67.72	67.42	67.55
	Other Diseases	47	177	442	666	53.97	66.37	60.22
External II[b]	Healthy	479	52	135	666	90.55	71.92	79.16
	PM	27	466	173	666	67.63	69.97	68.91
	Other Diseases	23	171	472	666	60.51	70.87	65.86
External III[c]	Healthy	444	67	155	666	83.46	66.67	73.22
	PM	32	452	182	666	67.16	67.87	67.55
	Other Diseases	56	154	456	666	57.50	68.47	63.12

Where: [a]External-I: training with Field I + Field II and validated with Field III; [b]External-II: training with Field I + Field III and validated with Field II; [c]External-III: training with Field II + Field III and validated with Field I.

4.2.4 Discussion

In this study, accuracy scores varied during external validations compared to internal and cross validations. The accuracies were lower when the classifiers were trained with one variety of strawberry plant and validated with another variety of strawberry plant. The Field I and Field II were cultivated with Albion variety and Field III with Ruby June variety. The poorest

performances were reported when the classifier tested with Field III (Ruby June) data because the training was done using the Albion variety from Field I and Field II. The improvements were noticed when the Field I and Field II data used for validation. In that case both of Albion and Ruby June variety used for training corresponding to the Albion data for validation. The textural differences of leaves between two strawberry varieties may cause the variability of performance. Al-Saddik et al. (2018) detected yellowness and Esca in Chardonnay grapevine variety using texture analysis of leaf images and reported the detection results will be varied for other grapevine varieties. This study used a single classifier to classify healthy, powdery mildew and other diseases leaf image at the same time. In future studies, we may apply a layered classifier that first discerns variety of strawberry and is followed by leaf image classification (i.e., healthy, powdery mildew and other diseases) in the second stage by using a second classifier. Many researchers have also been struggling to detect powdery mildew disease in different cropping systems (Ei-Helly et al., 2004; Wspanialy & Moussa, 2016). Wspanialy and Moussa (2016) detected powdery mildew disease in tomato plants with a detection rates of 85% in a controlled greenhouse setting.

The CCMs based image texture analysis using 23 features was found to be effective for this specific problem. Stepwise discriminant analysis was performed that could successfully reduce the number of textural features to find an optimum features model. The reduction method may also be required for future real-time applications that would require fast calculation. An ANN based plant disease detection system previously proposed by Kulkarni and Patil (2012) with diverse image processing techniques scored high recognition rates of up to 91% in pomegranate crop. They suggested that ANN based classifiers detect numerous plant diseases with combination of colour and texture features to recognize Alternaria, Bacterial Blight Disease and Anthracnose diseases. Ramakrishnan (2015) obtained much higher accuracies of disease detection, around 97.41% for

Ground nut. Their experiments were done with CCM textural analysis and back propagation ANN algorithm for detection of leaf disease. Results from our study using the ANN classifier with strawberry leaves and powdery mildew appear to support previous assertions as to the accuracy of ANN. The best performance reported using ANN classifier with (1W(23/46)1W(46/46)1F(46/1)) model where the external validation results were also higher than the other two classifiers.

Islam et al. (2017) presented an approach that integrates machine learning (i.e., SVM) and image processing techniques to allow diagnosing diseases from potato leaf images. The proposed techniques provide a path toward automated plant disease diagnosis on a large, i.e. field, scale with potential accuracy of detection >95% using SVM classifiers. An image pattern classification was studied by Camargo and Smith (2009) for detection of the cotton crop diseases using SVM. The CCM, co-occurrence matrix having five features were extracted on their research and reached a classification accuracy of 90%. Their study suggested that texture-related features and SVM might lead to successful for classifying plant diseases but a study by VijayaLakshmi and Mohan (2016) reported some difficulty using SVM to understand the structure and size and speed limitations both in training and testing the data. Outcomes from our study resulted in similar limitations in speed of training but detection accuracies were also high in internal and cross validations. The speed of data processing was found to be slower in SVM model development (Fig 4-8).

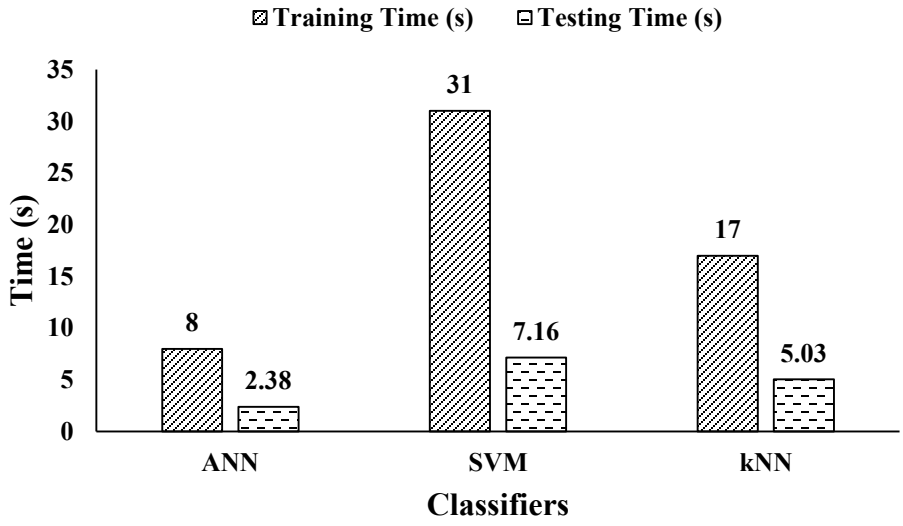

Figure 4-8. Averaged training and testing times of classifiers

In contrast, kNN had the lowest accuracy in plant disease classification. Sankaran et al. (2011) classified citrus disease in leaves resulting in overall accuracies of 83.3%, 86.8% and 86.8%, for 1st derivative, 2nd derivative, and combined spectral features using kNN, respectively. Similar results were obtained in our study using kNN. The inferior results reported by kNN having the lowest recall, precision and F-measures scores compared to ANN and SVM.

Therefore, despite having some misclassifications between healthy, powdery mildew and other diseases affected leaf images, the proposed study suggests the ANN classifier for classifying/detecting strawberry powdery mildew disease leaves using machine vision.

4.3 Conclusions

This study was completed to investigate the different supervised classifiers performance for classifying strawberry powdery mildew disease in leaf using machine vision. Three different classes of strawberry leaves (healthy and powdery mildew affected) were used for this study. Image texture based processing algorithms were developed for feature extraction by using colour

co-occurrence matrices (CCMs). A total of 50 features were extracted from single leaf image after conversion from RGB to g-ratio, Lm and HSI. Stepwise discriminant analysis was used to reduce the variable sets (features data) and to evaluate the potential classification accuracies. Three supervised classifiers (i.e., ANN, SVM and kNN) were studied to find the best model for strawberry powdery mildew disease classification. Overall results of this study reported ANN classifier achieved the highest recall (98.75%), precision (98.75%) and F-measure (98.75%) with less data processing time (average training time 8s and testing time 2.38s) compared to SVM and kNN. The SVM achieved the high accuracy of disease detection (recall: 96.75%, precision: 96.75%, F-measure: 96.75%) but limitations associated with speed of training and testing of data were found (average training time 17s and testing time 5.03s). The poor performance achieved by kNN classifier with accuracies (recall: 94.25%, precision: 90.13%, F-measure: 91.92%). Results suggested that ANN classifier emerged as the best classification model for the task of strawberry powdery mildew disease classification. Consequently, it is recommended that the ANN classifier be further considered when applying the texture based machine vision technique in an outdoor scene, which will be the focus of future studies.

Acknowledgements

This work was supported by Nova Scotia Research and Innovation Graduate Scholarship Program, Dalhousie Entrance Scholarship Program, Doug Bragg Enterprises Limited and Natural Science and Engineering Research Council of Canada. The authors would also like to thank Millen farm and Balamore farm as they provided field access for image collections and experiments.

CHAPTER 5: DEVELOPMENT OF ON-THE-GO PRESCRIPTION MAP FOR STRAWBERRY POWDERY MILDEW DISEASE USING MACHINE VISION

Abstract

An essential part of strawberry cropping system is proper disease management to reduce losses in crop yield. Powdery mildew is one of the major diseases in strawberry which can cause significant yield losses. The objective of this research was to develop an on-the-go prescription map using a real-time machine vision system for detecting powdery mildew disease in strawberry under field condition. A real-time kinematics global positioning system, two cameras, a custom program and a ruggedized laptop computer were utilized for development of disease detection system. A custom image processing program was developed using colour co-occurrence based texture analysis along with artificial neural network technique to process and classify continuously acquiring image data simultaneously. Three strawberry field sites were used to evaluate the performance of the developed system. A total of thirty-six strawberry rows were tested within three fields and powdery mildew detected points were measured manually followed by automatic detection system. The manually detected points were compared with automatically detected points to ensure the accuracy of the developed system. Results of regression and scatter plots revealed that the system was able to detect disease having mean absolute error values of 4.00, 3.42 and 2.83 per row and root mean square error values of 4.12, 3.71 and 3.00 per row in field site-I, field site-II and field site-III, respectively. The slight deviation in performance was caused by high wind speeds (<8 km h^{-1}) and presence of spider mite disease during test in strawberry fields were reported.

Keywords: Machine Vision, Powdery Mildew, Real-Time, Field Test Evaluation

5.0 Introduction

Machine vision is a promising technique usage has grown in last few decades to detect plant diseases in the open field (Sankaran et al., 2010) and, fast and accurate monitoring. Imaging in the open field is a challenge compared to imaging under laboratory conditions due to harsh and difficult to control environment. The highly variable and adverse operating environments offer random variations and imperfections of input images that can easily influence the accuracy and precision of machine vision specifically used in open agricultural fields (Romeo et al., 2013). Pajares et al. (2016) provided the guidelines for selection of appropriate agricultural machine vision systems considering the adverse conditions on outdoor environments with high variability on the illumination, irregular terrain conditions or different plant growth states for optimum performance. Lee et al. (1999) developed a real-time intelligent machine vision system which was only capable to detect 47.6% of weeds properly with 24.2% over-sprayed tomato plants in outdoor condition for commercial application. Sabzi et al. (2017) suggested a machine vision system based on hybrid artificial neural network-harmony search classifiers for automatic segmentation of plants under different illumination conditions and claimed to be applicable for all field applications with higher accuracies. However, the tests were not conducted using mixed canopy conditions that are common in agricultural fields. Therefore, a feasible real-time machine vision system needs to be developed to detect plant disease under mixed canopy field conditions.

A prescription map is a set of instructions that contains rate information so that variable rate controller can apply the appropriate application to the specific location. Prescription maps utilize geographical information systems (GIS) to evaluate variable rate technologies for different cropping systems (Carrara et al., 2004; Miller et al., 2004; O'Shaughnessy et al., 2015), spot

applications (Zaman et al., 2011; Esau et al., 2014), weed mapping (López-Granados et al., 2016; de Castro et al., 2018), crop disease map (Yang et al., 2016) and site specific managements (Brown et al., 1995; Fleming et al., 2000; Amaral et al., 2018). Saleem et al. (2013) used a prescription map with variable rate spreaders for site-specific fertilizer application in wild blueberry fields. Miller et al. (2004) applied granular fertilizer in citrus and observed GPS map based control were similar to those found for real-time control. Prescription maps also incorporate well with real-time machine vision systems in different cropping systems to detect weeds, bare spots and fruits (Tian, 2002; Zhang et al., 2010; Esau et al., 2014).

Strawberry powdery mildew is a serious disease affecting strawberry production during warm and dry climates (Mass, 1998) and reduce crop yields by causing decreased fruit set, inadequate ripening, poor flavour development, fruit cracking and deformation, and reducing post-harvest storage time (Pertot et al., 2008). Although the detection of powdery mildew is time consuming, inappropriate, labour intensive and human dependant, an automated detection system is crime needed for strawberry growers in real-time field condition. Many studies have been conducted for weed detection in real-time but a very limited numbers of studies have been conducted for real-time plant disease detection in agricultural fields. Therefore, the objective of this study is to detect strawberry powdery mildew disease in real-time field conditions and develop an on-the-go prescription map to support fungicide application decisions.

5.1 Materials and Methods

5.1.1 Machine Vision System Development

A machine vision system was developed with a mobile platform using locally available bicycle parts to minimize the cost. The picture of machine vision system was presented in Chapter 3 (Sec 3.1.2). The system was controlled by the rear wheels, similar to a shopping cart. An ACC, artificial cloud lighting condition system was mounted on the mobile platform to minimize the illumination variation during image acquisition. The description of ACC was presented in Chapter 3 (Sec 3.1.2). The system was run over single strawberry rows and slim bicycle wheels were used to minimize the damage of strawberry runners during the study. The system consisted of two μEye 1240 LE/C colour cameras (IDS Imaging Development System Inc., Woburn, MA, USA), a HiPer® lite + RTK-GPS (Topcon positioning systems Inc., Livermore, CA, USA) for geo-referencing and ruggedized laptop computer (Toshiba Corporation, Minato, Tokyo, Japan). Each of the cameras covered a 0.61 m (length) of section in strawberry row. Cameras were connected directly using universal serial bus (USB) cables to the laptop computer. The cameras had a 0.3 m working depth from the camera sensor to leaf canopy. The 0.3 m working depth performed better for strawberry powdery mildew detection based on work presented in Chapter 3 (Sec 3.2.4). The system speed was 1.5 ± 0.4 km h^{-1} and that was maintained constant during the study by continuous visually monitoring the GUI display. The system speed (in knots) was parsed from RTK-GPS string and converted into metric units (speed (ms^{-1}) = 0.51444 × speed (knots)). Digital gain and exposure time were automatically controlled by auto gain control and auto exposure shutter. Details of camera settings and hardware system were presented in Chapter 3 (Sec 3.1.1). The RTK-GPS antenna was mounted over the cameras to record the coordinates simultaneously. The RTK-GPS position of the images was continuously stored in laptop computer by using National Marine Electronics Association (NMEA-0183) standard code sentences. The program was designed to

only store the powdery mildew images location when it was detected into a comma-separated values (CSV) file.

A real-time strawberry powdery mildew disease detection algorithm was developed in C# using Visual Studio 2017 (Microsoft, Redmond, WA, USA). The algorithm was capable of processing images to differentiate powdery mildew affected leaf from healthy and other diseases leaves. Image pixel and area of interest dimensions were same as Chapter 3 image acquisition. The algorithm was built to acquire the image from the cameras and transfer onto the laptop for image processing. The image processing stage began with a conversion of red-green-blue (RGB) image into green ratio, hue, saturation and intensity images. The real-time algorithm did not account luminance image features for detection due to not having any improvement was made, presented in Chapter 3 (Sec 3.2.1). The details of image processing functioning were given in Chapter 3 (Sec 3.1.3) and 4 (Sec 4.1.2). Image processing works was conducted using a colour co-occurrence matrix (CCM) based texture analysis and a total of 23 features were extracted. The extracted features were analyzed to detect powdery mildew disease by using an artificial neural networks (ANN) classifier. The ANN was performed better than other classifiers presented in Chapter 4 (Sec 4.2.1 & 4.2.4). The detection results of geo-referenced coordinates location were imported into ArcGIS 10.5 computer software (ESRI, Redlands, CA, USA) for prescription mapping. The overview of real-time detection algorithm is presented in Fig. 5-1.

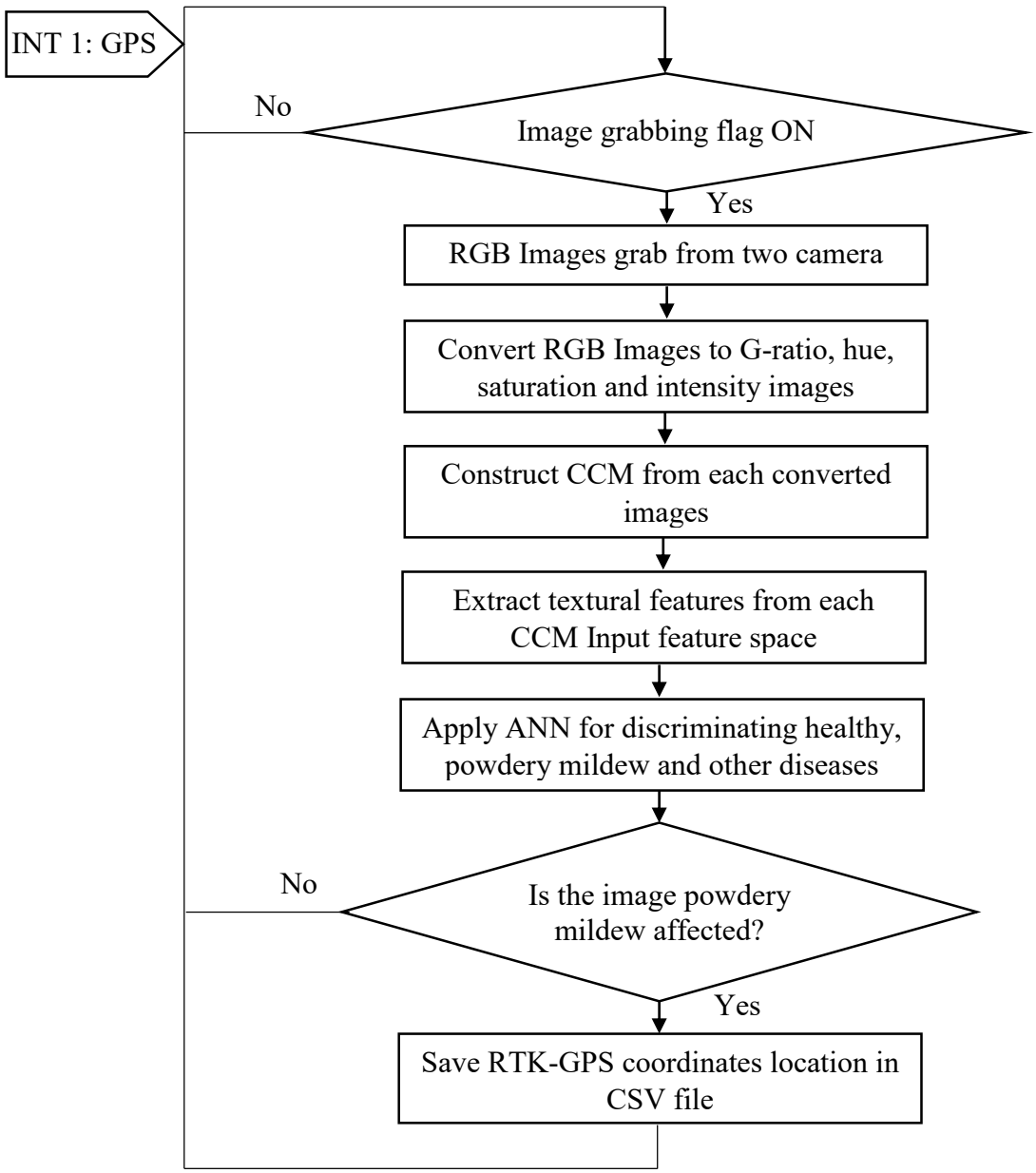

Figure 5-1. Flow chart of real-time strawberry powdery mildew disease detection algorithm

5.1.2 Testing of Machine Vision System in Strawberry Fields

The testing of real-time machine vision system performance to detect powdery mildew disease in strawberry fields were carried out on 6th, 7th and 13th August 2018 at sites in Debert, Nova Scotia.

The tests were conducted during sunny days, having the temperatures ranging from 20 to 32 °C with 50 to 82% R_H and wind speeds ranged from 3 to 14 km h^{-1} (National Climate Data and Information, 2018). The software interface of machine vision system is presented in Fig. 5-2. The communication between RTK-GPS and laptop computer was directed using setting (COM Port 1 (computer port 1), baud rate 9,600, stop bit none and parity bit 1). The speed of the system was calculated from NMEA-0183 standard code system directly from RTK-GPS data displayed in GUI (Fig. 5-2). The latitude and longitude were also recorded from standard code from RTK-GPS. The checkbox of camera selection added to control the two cameras used for image acquisition. Although the experiments used four processed images from one camera, two picture boxes (for one camera) were added in the real-time software due to a lack of space in the GUI display. The processed g-ratio and hue images were displayed from both cameras. The program was able to process the images to differentiate powdery mildew leaf images for the strawberry fields in real-time from both images taken by the two cameras. The system performance was evaluated by correlating the manual detection results with the automatic system detection results from both cameras in all the fields. Detection maps also called prescription maps were developed from the experimental data using ArcGIS 10.5 software.

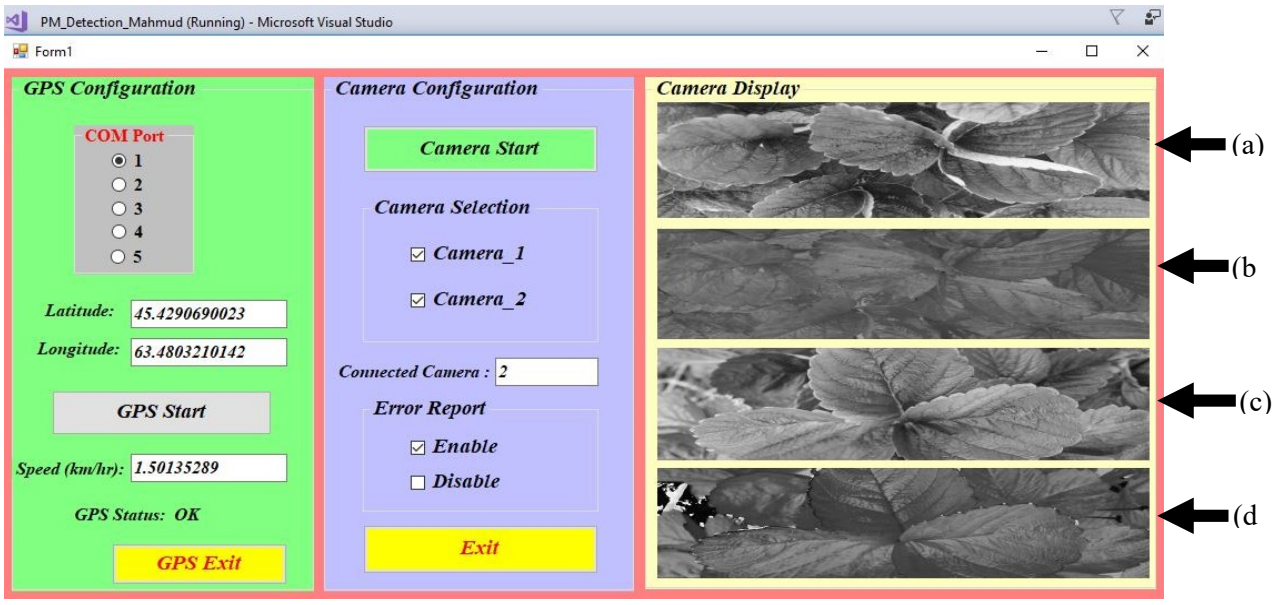

Figure 5-2. Machine vision based powdery mildew disease detection software interface. (a: g-ratio image from camera 1; b: hue image from camera 1; c: g-ratio image from camera 2; d: hue image from camera 2)

5.1.2.1 Experimental sites

Three strawberry field sites were selected in Debert, Nova Scotia to evaluate the performance of machine vision based powdery mildew disease detection system. The fields were Debert site I (field 1; 45.429318°N, 63.483843°W), Debert site II (field 2; 45.429611°N, 63.48114°W) and Debert site III (field 3; 45.429098°N, 63.480276°W). A commercial 12-hectare strawberry farm was used to conduct this study. All fields were cultivated with Albion strawberry variety. The fields were cultivated in strawberries over the past several years and were commercially managed. A total of 12 randomly selected strawberry rows were tested from one side of each field. The experimental field image is shown in Fig. 5-3. The strawberry rows evaluated had dimensions of 1.22 m × 220 m (wide × length) for field site-I and 1.22 m × 180 m for field site-II and field site-III with a 0.31 m buffer between rows.

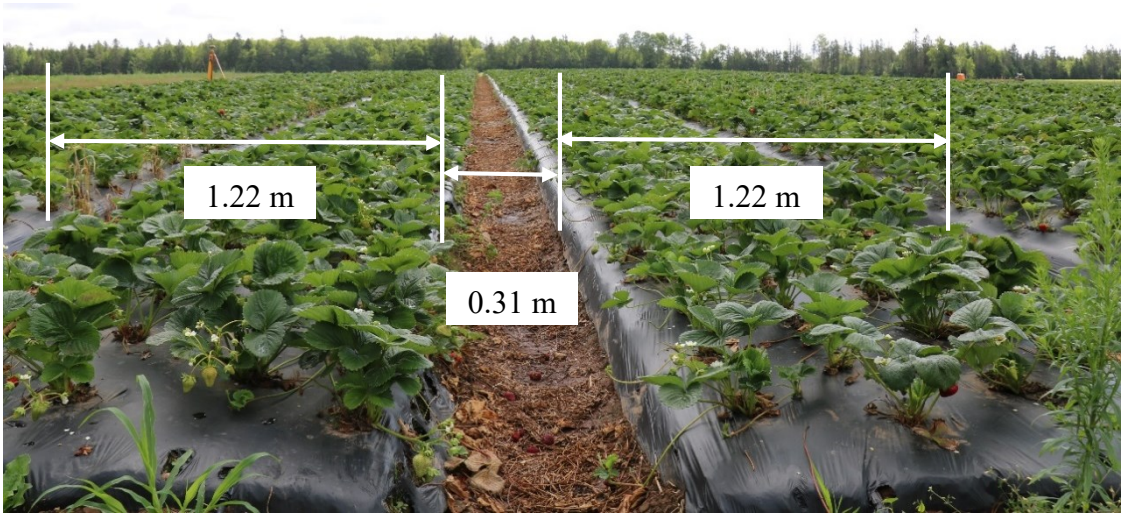

Figure 5-3. Experimental Strawberry Field

5.1.2.2 Manually Powdery Mildew Detection

The manual detection of powdery mildew disease was based on recommendations from two experienced field scouts who checked for symptoms including white patches of mycelium on the upper leaf surface, roll upward leaf edges and reddish irregular spots on leaf. The number of detected points of powdery mildew affected plants in a single row were logged in a paper notebook (Hilroy, Mississauga, ON, Canada) after counting. The locations of the detected points were recorded at the meantime using ProMark3 mobile mapper (Thales Navigation, Santa Clara, Ca). The mobile mapper was calibrated before using to detect the manually detected points. Calibration was made by logged about 50 points by mobile mapper that were used to compare with the same points measured by RTK-GPS to find out the errors of mobile mapper. The measures points were located 8-30 cm away from each point to another.

5.1.2.3 Automatically Powdery Mildew Detection

The machine vision system was deployed over individual rows of strawberry plants for continuous image acquisition by the two cameras. A total of 36 rows were covered over three strawberry fields (12 rows each) in this study. The images were processed through texture analysis by CCM and followed by detection using the ANN classifier. The powdery mildew detected leaf image locations (latitude and longitude) were saved automatically to a CSV file using a function in the custom software. Manually and automatically detected points were compared by manually counting points to evaluate the outcomes of the system. The detected points were mapped to create prescription map using the co-ordinates (longitude and latitude) collected from RTK-GPS and mobile mapper.

5.1.3 Statistical Analysis

Linear regression analysis was used to compare the results of manually measurements and automatically measurements separately in each field by using Minitab 18 statistical software (Minitab Inc., NY, USA). The coefficient of determination (R^2), mean absolute error (MAE) and root mean square error (RMSE) were calculated. A paired t-test was also used to compare the mean of two measurements in Minitab version 18.

5.2 Results and Discussion

The machine vision based powdery mildew disease detection system was tested on three strawberry field sites and corresponding testing results are presented in Fig. 5-4, Fig. 5-5 and Fig. 5-6 for field site-I, field site-II and field site-III, respectively. The linear regression model showed that automatically powdery mildew detection from the system to the strawberry plants was highly significantly correlated with manually detection for field site-I ($R^2 = 0.93$; $P< 0.001$; $N = 12$) (Fig. 5-4). The system also showed strong correlation significantly with the other two fields (field site-II: $R^2 = 0.88$; $P< 0.001$; $N=12$, field site-III: $R^2 = 0.92$; $P< 0.001$; $N=12$) (Fig. 5-5 & Fig. 5-6). The MAE and RMSE were also calculated from all field tests. The results showed that higher MAE and RMSE were obtained from field site-I test (4.00/row and 4.12/row). Lower MAE and RMSE were noted in validation with field site-III, having values of 2.83/row and 3.00/row, respectively. The MAE calculated values from three fields were lower than RMSE values because MAE does not give undue importance to large errors (Meade, 2000). The co-efficient of determination (R^2) was higher in field site-I test. However, the MAE and RMSE values were also higher compared to the other two fields. This was due to the number of powdery mildew affected plants being higher (more severe than others) in field site-I compared to the other field sites. The lowest R^2 value was

0.88 generating from testing in field site-II due to slight deviation can be seen in the Fig. 5-5 compared to others, where the detection points were comparatively more over or under estimated than other fields. The reason for over estimation might be the system accounted other diseases with white patch symptoms (i.e., spider mites) as powdery mildew disease. The under estimation was due to the higher density of plant leaves resulted in powdery mildew affected leaves being hidden under leaves. The variations in plant leaf density may have contributed to determine machine vision system accuracy. Palleja and Landers (2015) noted the plant density could be caused errors for image processing in describing the importance to plant density measurements. Ali et al. (2018) also encountered the problems of over and under predicted problems to examine the ripening of wild blueberries for appropriate harvesting time using image processing based blue-ratio algorithm, which were similar to present study problems.

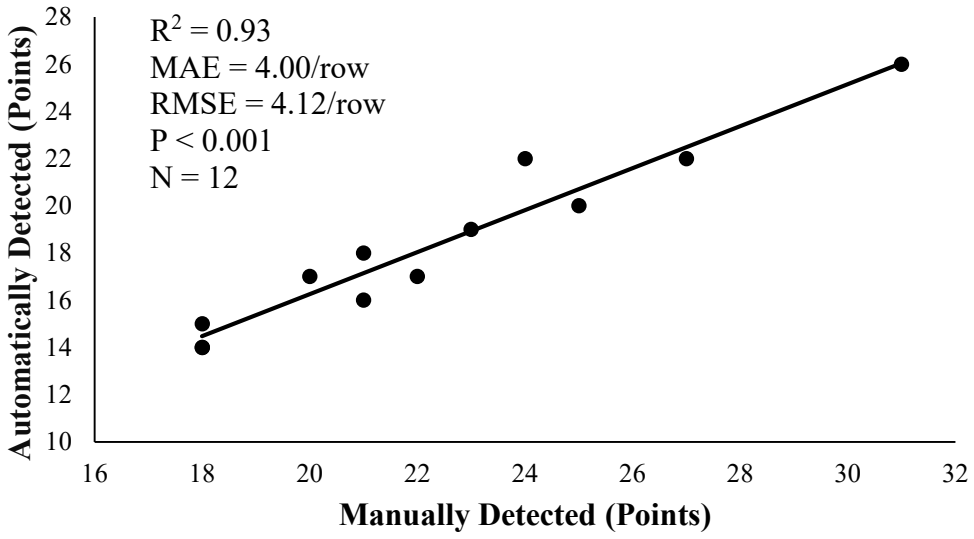

Figure 5-4. Manually and Automatically Detected Points Comparison for Field Site I

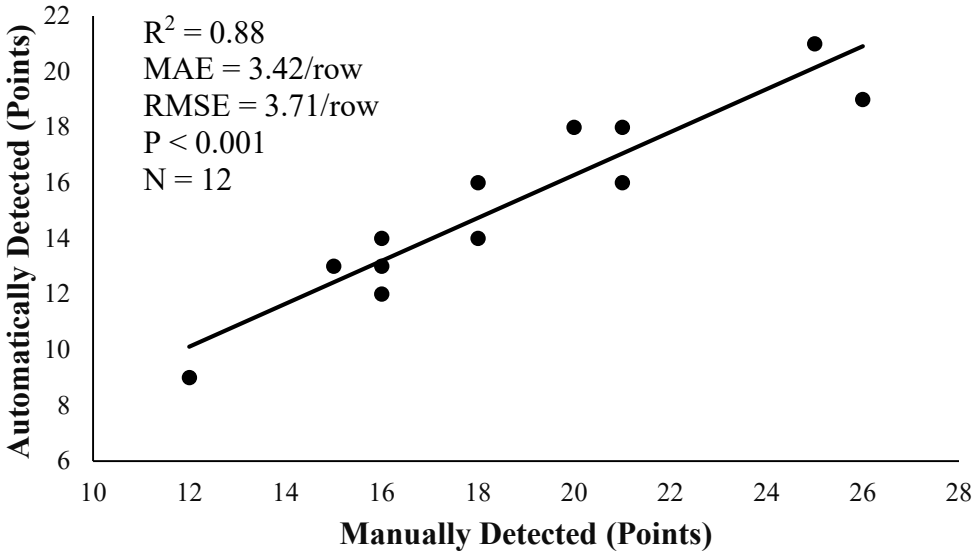

Figure 5-5. Manually and Automatically Detected Points Comparison for Field Site II

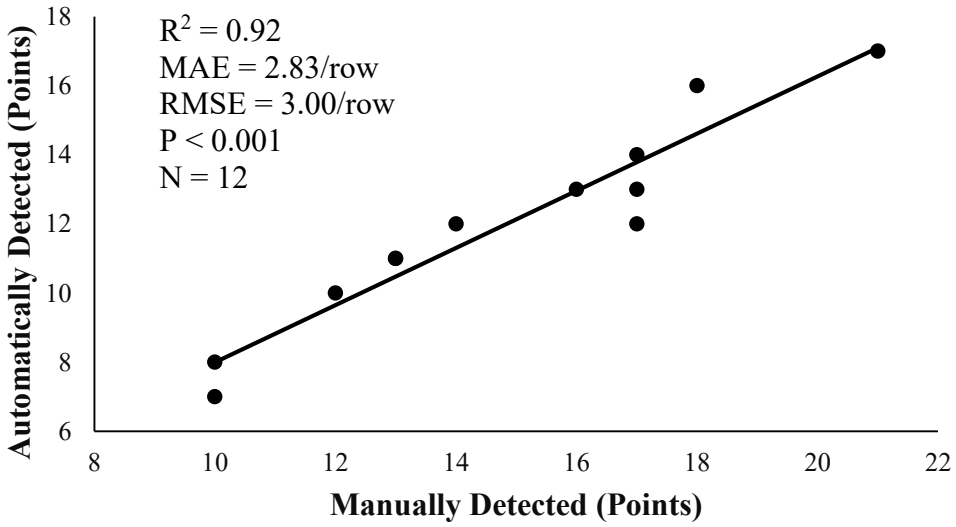

Figure 5-6. Manually and Automatically Detected Points Comparison for Field Site III

A direct comparison of manually and automatically detected powdery mildew disease in strawberry fields are presented in Fig. 5-7. The more pronounced fluctuations were observed in the field site-II testing the strawberry rows (12-24 rows) with high wind speed (7-14 km hr^{-1}) for powdery mildew detections. The comparatively lower fluctuations were reported in field site-I (1-12 rows) results where the wind speed was 4-10 km $hr^{-1}$and followed by field site-III (25-36 rows) was 3-8 km hr^{-1}. Although the wind speed was comparatively higher in field site-II test, the movement of the branches and the leaves during real-time testing was a bit faster. Another reason could be the position of a plant leaves changed from frame to frame due to the wind moving the leaves resulting in a false match, which was a similar observation reported by Shrestha and Steward (2003). The wind speed has direct effects upon real-time machine vision system performance under field conditions were also reported by previous studies. Zhang and Chaisattapagon (1995) developed a machine vision system for weed identification which was successful during laboratory experiments but they pointed out that it was not practical for real-time weed detection, especially when a wind effect is considered. The wind speed can be causing blurring boundaries in the images which becomes quite complicated for image analysis (Guyer et al., 1986). Safren et al., (2007) did not account the leaf images for their experiments when the wind speed was too high. The numbers of affected plants were higher in field site-I compared to other two field sites due to longer row (220 m each) compared to other fields (180 m each). The misclassification rates of some strawberry rows were also higher. A reasonable explanation of this higher misclassification rate might be the plants in rows with large number of spider mite containing white spider net over the leaves.

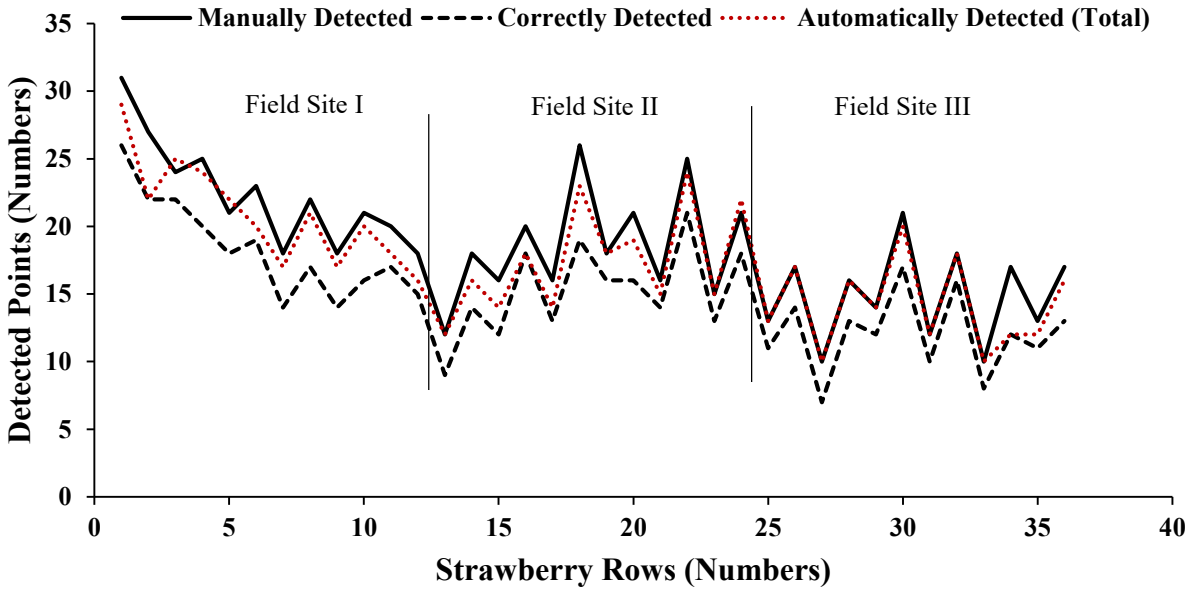

Figure 5-7. Strawberry powdery mildew disease detection comparison row by row between manually and automatically

The results of paired-sample t-test suggested that a statistically significant mean difference exist between two measurements (manual and automatic) for powdery mildew detection having a mean difference of 4.000 (95% CI, 3.336 to 4.664; P <0.001) for field site-I. The results also showed statistically significant results with a mean difference of 3.417 (95% CI, 2.460 to 4.373; P <0.001) and 2.833 (95% CI, 2.179 to 3.488; P <0.001) for field site II and field site III (Table 1), respectively.

Table 5-1. Pair-wise t-test for manually and automatically powdery mildew disease detection

Fields	Detections	Mean (points)	S.D. (points)	Mean diff. (points)	p-value
Field site-I	Manual	22.330	3.960	4.000	<0.001[a]
	Automatic	18.330	3.650		
Field site-II	Manual	18.670	4.120	3.417	<0.001[a]
	Automatic	15.250	3.390		
Field site-III	Manual	14.833	3.380	2.833	<0.001[a]

	Automatic	12.000	2.923

[a]Significant at a confidence level of $\alpha = 0.05$

Strawberry powdery mildew disease detection results from three field sites were mapped in ArcGIS 10.5 software are presented in Fig. 5-8, Fig 5-9, Fig. 5-10. The map of automatically detected points marked with red bullets were placed over manually detected points as a star signed bullets to examine the accuracy of the machine vision system. Subjective analysis of prescription maps indicated that the system could detect powdery mildew disease with 82.09%, 81.70% and 80.90% accuracies for field site-I, field site-II and field site-III, respectively. The accuracies were calculated using the ratio of total correctly detected points with the machine vision system relative to the total manual detected points. Figure 5-8 identified the presence of powdery mildew diseases were higher in western and eastern parts of field compared to the central part. Correspondingly, the figure 5-9 showed western and central western parts were more severe than remaining parts of field site II whereas figure 5-10 indicated field site III was severe powdery mildew affected in eastern part. The map revealed field site III (Fig. 5-10) strawberry plants were less affected by powdery mildew disease compared to field site I (Fig. 5-8) and field site II (Fig. 5-9). The misclassifications were presented in all fields. The red bullets without having star bullets suggested that the system mistakenly detected the points as powdery mildew affected presented in all field maps. Consequently, the star bullets without containing red bullets over it revealed the points originally affected in powdery mildew measured by manual detection but the system couldn't able to identify the points as powdery mildew affected. A total of 48 powdery mildew affected points were missed in field site I compared to 41 points and 34 points in field site II and field site III, respectively by the developed system. In contrast, the system inaccurately detected powdery mildew points were 31, 27 and 26 for field site-I, field site-II and field site-III, respectively (Fig. 5-8, Fig. 5-9, Fig. 5-10).

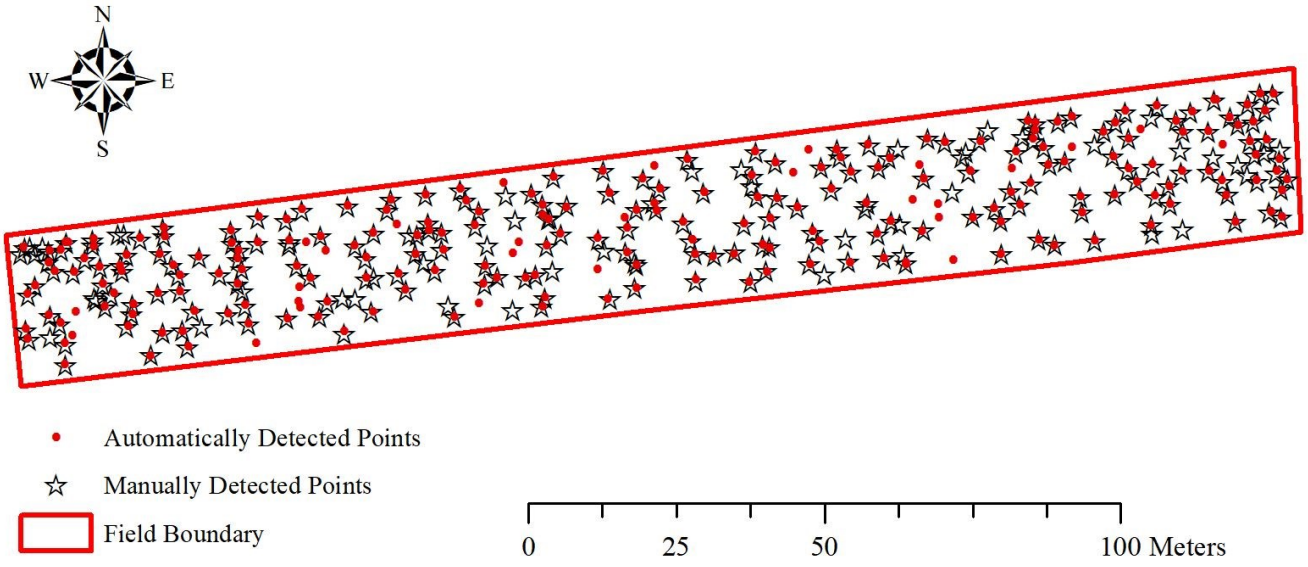

Figure 5-8. Field I (Powdery mildew disease detection map)

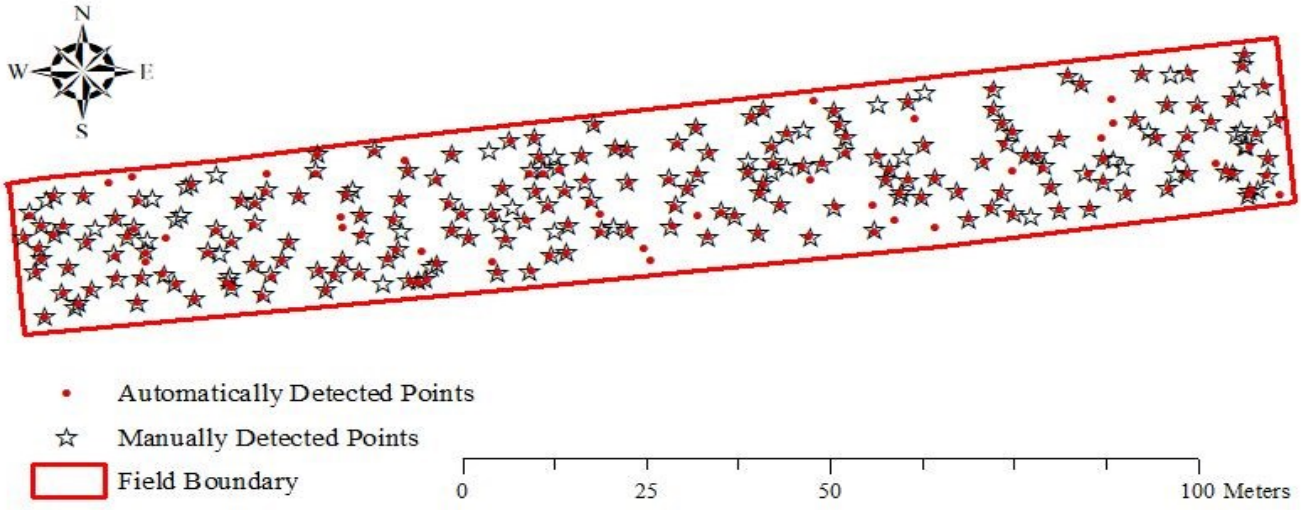

Figure 5-9. Field II (Powdery mildew disease detection map)

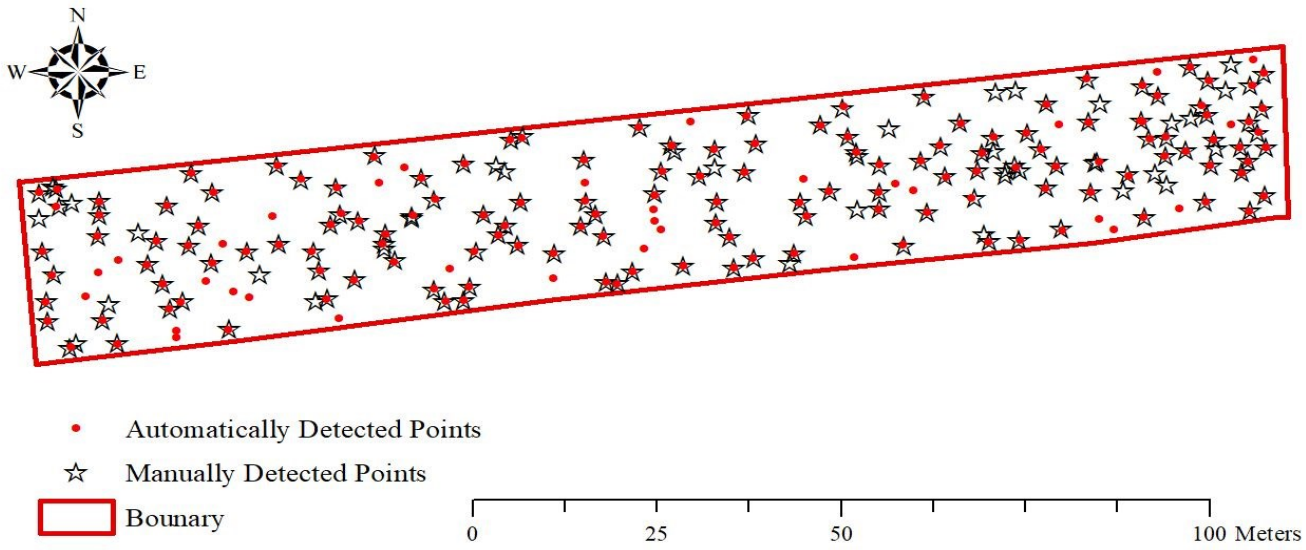

Figure 5-10. Field III (Powdery mildew disease detection map)

Overall, our study identified some challenges associated with real-time machine vision system applications under field conditions, as previously reported by various researchers (Tian & Slaughter, 1998; Jafari et al., 2006; Jeon et al., 2011). A real-time crop and weed segmentation algorithm was developed by Jeon et al. (2011) that was able to detect 72.6% of crop correctly using ANN. Tian and Slaughter (1998) attempted to overcome the problems raised from field conditions by developing an environmentally adaptive segmentation algorithm, however the algorithm only correctly identified 45 to 67% of tomato cotyledons. This study detected over 80% of powdery mildew disease correctly in the fields studied. The wind effects were a primary driver of misclassification in this study and that will always be a major challenge to overcome in real-time field conditions. However, a high frame per second (FPS) camera might be a possible option to reduce the effects of wind in field experiments.

5.3 Conclusions

Field based evaluation of developed machine vision based powdery mildew detection using image texture analysis was moderately successful. A total of 23 texture features along with ANN classifier were utilized for machine vision system development. Three strawberry field sites were selected for evaluating the performance of developed machine vision system. Manually measured powdery mildew detected points were compared with the real-time automatically detected points using the machine vision system. Results of linear regression plots showed significant correlations were presented between manually and automatically powdery mildew detected points. The MAE and RMSE of the detection results were 4.00, 3.42 and 2.83 per row, and 4.12, 3.71 and 3.00 per row for field site-I, field site-II and field site-III, respectively. The proposed machine vision system could detect disease with having 82.09%, 81.70% and 80.90% accuracies measured from field site-I, field site-II and field site-III, respectively. The misclassification rates were bit higher due to spatial variability of wind speeds, effects leaf overlapping or density and presence of spider mites in field tests which can have notably affected upon system performance that needs to be addressed. The advancement of detection system would be needed considering different environmental factors affecting performance in future studies. Although the impartially misclassifications were reported in this study, the developed system can be economically viable option to detect powder mildew disease in real-time as there is no real-time automatic detection technique available till to date for strawberry cropping system.

Acknowledgements

The authors would like to thank Carl Bragg (President, DBE), Doug Wyllie (Farm Manger, Bragg Lumber Company), Curtis Millen (Owner of Millen Farm Ltd.), Scott Read (Senior Instructor)

and the Precision Agriculture team (especially, Negar Sharifi Mood (Research Assistant) and Derrick Ouma (Summer Student)) of Dalhousie University for their support during experiments. Also, special thanks to Doug Bragg Enterprises, Natural Sciences and Engineering Research Council, and Nova Scotia Graduate Research and Innovation Scholarship for financial support during these study.

CHAPTER 6: OVERALL CONCLUSIONS AND RECOMMENDATIONS

Although agriculture has been a lot of technological advancements over the last couple of decades, detection of strawberry powdery mildew disease is still human dependent called manual scouting. In manual field scouting, human intellect can be harnessed in detecting disease to keep plant and fruit damage at a low level. However, the present trend of decreasing availability and increasing cost of field scouter has raised serious concerns on timely detection of strawberry powdery mildew disease especially in large scale farm. The strawberry growers are uniformly applying fungicides to control powdery mildew disease in three times of every two weeks. The powdery mildew diseases are not present uniformly in strawberry field that caused huge fungicide losses every year. The long-term goal of this study is to apply spot-application of fungicide by adding sprayer system into developed machine vision system, which can lead to wider adoption of automatic detection and spraying thus reducing dependency on field scouters. The task of automatic detection of powdery mildew disease in the strawberry field is a difficult problem due to several challenges and bottlenecks in sensing (machine vision based system for powdery mildew disease detection) technology. In this study, innovative image processing based machine vision concepts were investigated to address some of the bottlenecks in sensing technology, which would be incorporated into automatic spot application system development in the future study. The machine vision system composed of two cameras, an ACC chamber, a RTK-GPS, a custom made C# algorithm and a ruggedized laptop computer was developed. The developed system was mounted on a four-wheel cart based mobile platform for non-destructive detection of powdery mildew disease at leaves in strawberry fields. Performance of developed machine vision system was tested and evaluated in three selected strawberry field sites. Results of field evaluations using developed system and corresponding GIS maps revealed that machine vision system has potential to detect

powdery mildew disease in site-specific manner. Results of this study also revealed that the developed system preformed fairly accurate, rapidly, reliable and efficiently to detect powdery mildew disease in field scale with certain rates of misclassifications.

6.1 General Conclusions

The first objective of this study was to optimize the parameter influencing performance of machine vision system. The parameters including feature selection, illumination conditions, image acquisition speed and working depths were investigated and evaluated to select optimum conditions for developing a system. The RGB cameras were used during required image acquisition. No additional sensing camera and image features (accept texture features) were needed for successive powdery mildew detection, which significantly reduced the vision computation load and improved overall processing time. The illumination variations were the primary and major challenge, which can be lead to change the image contrast and colour completely. An ACC system was developed by this study could address the challenges come up with different illumination variations. In this study described in Chapter 3, the ACC achieved higher detection accuracies (95.26%, 95.45% and 95.37% for recall, precision and F-measure, respectively) collated with NLC (81.54%, 72% and 75.95% for recall, precision and F-measure, respectively). Unnecessary image features are not only increase the computational time but also decrease the accuracy in some cases. The present study noticed (described in Chapter 3) that the extracted 50 features from G-ratio, hue, saturation, intensity and luminance images were not needed to achieved optimum performance. The step-wise quadratic discriminant analysis suggested the combination of 23 features from extracted 50 features performed better to detect powdery mildew in leaves. The image acquisition speed is another parameter that inauspiciously effects on detection performance, which is needed to be adjusted. The study reported the acquisition speed with 1.0 km h^{-1} and 1.5 km h^{-1} provided

better performance among other designated speed values. Also, a working depth of 300 mm showed tremendous results among all working depths used for experimentations.

The second objective of this study was conducted to select an optimal supervised classifier for powdery mildew detection that was used for real-time disease detection in strawberry fields. The detection results were varied with different classifiers used for analysis in machine vision system described in Chapter 4. Three popular supervised classifiers including ANN, SVM and kNN were appraised/evaluated with a dataset of 6,000 images. The ANN model structure (1W(23/46)1W(46/46)1F(46/1)) was selected by assessing the performance of different combination of model structure (by adjusting number of hidden layers and nodes). Similarly, the kernels (Linear and Fine) for SVM and kNN were selected by analysing the performance of different kernels upon powdery mildew disease classification. The powdery mildew disease classification rates using ANN achieved recall, precision and F-measure level of 98.49%, 98.00% and 98.22% during internal validation, the SVM achieved 96.96%, 95.63% and 96.22%, while kNN was 90.05%, 87.13% and 88.40%. The highest recall, precision and F-measure were resulted by ANN classifier (98.75% for all cases of internal validation in healthy leaves classification), whereas lowest accuracies reported by kNN having recall, precision and F-measure of 53.97%, 66.37% and 60.22%, respectively during external-I validation. All classifiers performed poorly through external validation compared to internal and cross validations. The ANN achieved highest recall (88.96%), precision (83.48%) and F-measure (85.83%) for healthy leave images classification and kNN performed poorly having accuracies of 53.97%, 66.37% and 60.22%, respectively during other diseases leaves classification. The average training and testing times were lowest by ANN, having average training and testing times were 8 and 2.38 seconds. The

results prove the feasibility of real-time powdery mildew detection using ANN on strawberry leave images.

The final objective of this study was to evaluate the performance of real-time machine vision system for strawberry powdery mildew disease detection in field scale. The real-time machine vision system composed of two cameras, a ACC, a ruggedized laptop computer and a RTK-GPS system. A graphical user interface based CCM algorithm was developed by C# and an ANN classifier was used for classification after feature extraction. Three strawberry fields were experimented and a total of thirty-six (twelve from each field) rows were randomly selected to conduct these experiments. Performance of this study was evaluated by comparing manually detected points and automatically detected points. The manually detections were made using a mobile mapper and automatic detection by developed machine vision system incorporated with RTK-GPS. The speed of the system was maintained around 1.5 km hr^{-1} during all the experiments. However, the wind speeds were varying between 3-14 km hr^{-1} which showed significant impact on detection accuracies. The ACC performed tremendously to reduce the illumination variation and maintained the light intensity ranged 800-900 lux. Results revealed that the detection system performed highly significantly correlated with manually detection for field site-I ($R^2 = 0.93$; $P< 0.001$; $N = 12$), field site-II ($R^2 = 0.88$; $P< 0.001$; $N=12$) and field site-III ($R^2 = 0.92$; $P< 0.001$; $N=12$). The system preformed poorly in field site-II compared to field site-I and field site-III due to high wind speed during experiment. Overall study reported the developed system can be detected over 80% of powdery mildew disease in strawberry field. The accuracy is fairly less because of various environmental factors affecting the performance of machine vision system during experiments. These study have been facing the major problem associated with wind speed which may be overcome using high FPS camera.

6.2 Future Recommendations

Future work could install the smart spraying system along with machine vision based detection system to ensure spot application of fungicides into the strawberry fields. Results of this study emphasize the need to evaluate the performance of the developed machine vision system during spot spraying in different stages of powdery mildew disease development (early, mid and late). Higher leaf density presented a problem called occluded leaf by creating under fitting which needs to be evaluated in detail. Improvement would be to use multiple cameras in different angles to capture all leaves of strawberry plants. The higher wind speeds accounted as another major problem in real-time detection of powdery mildew disease which can be addressed by using high frame per second cameras. Additionally, severity/incidence of powdery mildew disease in field also need to evaluate in detail to help farmer in making decision about the control.

The developed machine vision system can be modified to detect other diseases presented in different cropping systems. It also can help to transfer the technology to other cropping systems for detecting in-season diseases and weeds, thereby allowing the farmers to increase farm gate value of their crops. Deep learning (DCNN, deep convolutional neural networks) and other advanced artificial intelligence technologies can also be used to modify in existing system for detecting real-time strawberry powdery mildew disease in field.

REFERENCES

AAFC (2016). Statistical Overview of the Canadian Fruit Industry. Retrieved on March 06, 2018, from http://www.agr.gc.ca/resources/prod/doc/pdf/fruit_report_2016_1-eng.pdf.

Aggelopoulou, A. D., Bochtis, D., Fountas, S., Swain, K. C., Gemtos, T. A., & Nanos, G. D. (2011). Yield prediction in apple orchards based on image processing. *Precision Agriculture*, *12*(3), 448-456.

Al Bashish, D., Braik, M., & Bani-Ahmad, S. (2010). A framework for detection and classification of plant leaf and stem diseases. In *Signal and Image Processing (ICSIP), 2010 International Conference on IEEE*, 113-118.

Al Bashish, D., Braik, M., & Bani-Ahmad, S. (2011). Detection and classification of leaf diseases using K-means-based segmentation and. *Information Technology Journal*, *10*(2), 267-275.

Alapati, N. K., & Sanderson, A. C. (1985). Texture classification using multi-resolution rotation--invariant operators. In *Intelligent Robots and Computer Vision IV*, *579*, 27-39.

Al-Hiary, H., Bani-Ahmad, S., Reyalat, M., Braik, M., & ALRahamneh, Z. (2011). Fast and accurate detection and classification of plant diseases. *Machine learning*, *14*(5).

Ali, S., Zaman, Q. U., Farooque, A. A., Schumann, A. W., Udenigwe, C. C., Esau, T., & Chang, Y. K. (2018). Potential use of digital photographic technique to examine wild blueberry ripening in relation to time of harvest. *Applied Engineering in Agriculture, 34*(2)*,* 299-308.

Al-Saddik, H., Laybros, A., Billiot, B., & Cointault, F. (2018). Using image texture and spectral reflectance analysis to detect yellowness and esca in grapevines at leaf-level. *Remote Sensing*, *10*(4), 618.

Amaral, L. R., Trevisan, R. G., & Molin, J. P. (2018). Canopy sensor placement for variable-rate nitrogen application in sugarcane fields. *Precision Agriculture*, *19*(1), 147-160.

Amsalem, L., Freeman, S., Rav-David, D., Nitzani, Y., Sztejnberg, A., Pertot, I., & Elad, Y. (2006). Effect of climatic factors on powdery mildew caused by *Sphaerotheca macularis* f. sp. fragaria*e* on strawberry. *European journal of plant pathology*, *114*(3), 283-292.

Arivazhagan, S., Shebiah, R. N., Ananthi, S., & Varthini, S. V. (2013). Detection of unhealthy region of plant leaves and classification of plant leaf diseases using texture features. *Agricultural Engineering International: CIGR Journal*, *15*(1), 211-217.

Azencott, R., Wang, J. P., & Younes, L. (1997). Texture classification using windowed Fourier filters. *IEEE Transactions on Pattern Analysis and Machine Intelligence*, *19*(2), 148-153.

Backoulou, G. F., Elliott, N. C., Giles, K., Phoofolo, M., & Catana, V. (2011). Development of a method using multispectral imagery and spatial pattern metrics to quantify stress to wheat fields caused by Diuraphis noxia. *Computers and Electronics in Agriculture*, *75*(1), 64-70.

Barrero, O., Rojas, D., Gonzalez, C., & Perdomo, S. (2016). Weed detection in rice fields using aerial images and neural networks. In *Signal Processing, Images and Artificial Vision (STSIVA), 2016 XXI Symposium on IEEE*, 1-4.

Behroozi-Khazaei, N., & Maleki, M. R. (2017). A robust algorithm based on color features for grape cluster segmentation. *Computers and Electronics in Agriculture*, *142*, 41-49.

Bennett, J., & Khotanzad, A. (1998). Multispectral random field models for synthesis and analysis of color images. *IEEE Transactions on Pattern Analysis and Machine Intelligence*, *20*(3), 327-332.

Berni, J. A., Zarco-Tejada, P. J., Suárez, L., & Fereres, E. (2009). Thermal and narrowband multispectral remote sensing for vegetation monitoring from an unmanned aerial vehicle. *IEEE Transactions on Geoscience and Remote Sensing*, *47*(3), 722-738.

Bock, C. H., Cook, A. Z., Parker, P. E., & Gottwald, T. R. (2009). Automated image analysis of the severity of foliar citrus canker symptoms. *Plant disease*, *93*(6), 660-665.

Boese, B. L., Clinton, P. J., Dennis, D., Golden, R. C., & Kim, B. (2008). Digital image analysis of Zostera marina leaf injury. *Aquatic Botany*, *88*(1), 87-90.

Boissard, P., Martin, V., & Moisan, S. (2008). A cognitive vision approach to early pest detection in greenhouse crops. *Computers and Electronics in Agriculture*, *62*(2), 81-93.

Bolda, M., & Koike, S. T. (2015). Powdery mildew of strawberry. Retrieved from http://www.calstrawberry.com/Portals/2/Reports/Research%20Reports/Production%20 Guidelines/English/Powdery%20Mildew%20of%20Strawberry%20-%202015.pdf?ver= 2018-01-12-155446-510.

Bovik, A. C., Clark, M., & Geisler, W. S. (1990). Multichannel texture analysis using localized spatial filters. *IEEE transactions on pattern analysis and machine intelligence*, 12(1), 55-73.

Brady, M., & Xie, Z. Y. (1996). Feature selection for texture segmentation. *Advances in Image Understanding*, 29-44.

Brodatz, P. (1966). Textures: a photographic album for artists and designers. *Dover Pubns.*

Brown, R. B., & Steckler, J. P. (1995). Prescription maps for spatially variable herbicide application in no-till corn. *Transactions of the ASAE*, *38*(6), 1659-1666.

Cai, Y., Guan, K., Peng, J., Wang, S., Seifert, C., Wardlow, B., & Li, Z. (2018). A high-performance and in-season classification system of field-level crop types using time-series Landsat data and a machine learning approach. *Remote Sensing of Environment*, *210*, 35-47.

Camargo, A., & Smith, J. S. (2009). Image pattern classification for the identification of disease causing agents in plants. *Computers and Electronics in Agriculture*, *66*(2), 121-125.

Carisse, O., & Bouchard, J. (2010). Age-related susceptibility of strawberry leaves and berries to infection by *Podosphaera aphanis*. *Crop Protection*, *29*(9), 969-978.

Carrara, M., Comparetti, A., Febo, P., & Orlando, S. (2004). Spatially variable rate herbicide application on durum wheat in Sicily. *Biosystems Engineering*, *87*(4), 387-392.

Chaerle, L., & Van Der Straeten, D. (2000). Imaging techniques and the early detection of plant stress. *Trends in plant science*, *5*(11), 495-501.

Chandler, R. C. (2003). Autonomous agent navigation based on textural analysis. *Doctoral dissertation, University of Florida*.

Chang, Y. K., Zaman, Q. U., Schumann, A. W., Percival, D. C., Esau, T. J., & Ayalew, G. (2012). Development of color co-occurrence matrix based machine vision algorithms for wild blueberry fields. *Applied Engineering in Agriculture*, *28*(3), 315-323.

Chattha, H. S., Zaman, Q. U., Chang, Y. K., Farooque, A. A., Schumann, A. W., & Brewster, G. R. (2015). Effect of lighting conditions and ground speed on performance of intelligent fertilizer spreader for spot-application in wild blueberry. *Precision agriculture*, *16*(6), 654-667.

Chaudhary, P., Chaudhari, A. K., Cheeran, A. N., & Godara, S. (2012). Color transform based approach for disease spot detection on plant leaf. *International Journal of Computer Science and Telecommunications*, *3*(6), 65-70.

Chen, K., Sun, X., Qin, C., & Tang, X. (2010). Color grading of beef fat by using computer vision and support vector machine. *Computers and Electronics in Agriculture*, *70*(1), 27-32.

Chen, Y. R., Chao, K., & Kim, M. S. (2002). Machine vision technology for agricultural applications. *Computers and electronics in Agriculture*, *36*(2), 173-191.

Choudhary, G. M., & Gulati, V. (2015). Advance in Image Processing for Detection of Plant Diseases‖. *International Journal of Advanced Research in Computer Science and Software Engineering*, *5*(7).

Clément, A., Verfaille, T., Lormel, C., & Jaloux, B. (2015). A new colour vision system to quantify automatically foliar discolouration caused by insect pests feeding on leaf cells. *Biosystems Engineering*, *133*, 128-140.

Cohen, F. S., Fan, Z., & Patel, M. A. (1991). Classification of rotated and scaled textured images using Gaussian Markov random field models. *IEEE Transactions on Pattern Analysis and Machine Intelligence*, *13*(2), 192-202.

Cristianini, N., & Shawe-Taylor, J. (2000). An introduction to support vector machines and other kernel-based learning methods. *Cambridge university press.*

Daley, W. D., Carey, R., & Thompson, C. (1993). Poultry grading/inspection using color imaging. In *Machine Vision Applications in Industrial Inspection*, *International Society for Optics and Photonics*, *1907,* 124-133.

Daley, W. D., Carey, R., & Thompson, C. (1995). Real-time color grading and defect detection of food products. In *Optics in Agriculture, Forestry, and Biological Processing, International Society for Optics and Photonics*, *2345,* 403-412.

Darling, E. M., & Joseph, R. D. (1968). Pattern recognition from satellite altitudes. *IEEE Transactions on Systems Science and Cybernetics*, *4*(1), 38-47.

de Castro, A. I., Torres-Sánchez, J., Peña, J. M., Jiménez-Brenes, F. M., Csillik, O., & López-Granados, F. (2018). An automatic random forest-obia algorithm for early weed mapping between and within crop rows using UAV imagery. *Remote Sensing*, *10*(2), 285.

Dodgson, J. L. A. (2007). Epidemiology and sustainable control of *Podosphaera aphanis* (strawberry powdery mildew). *PhD dissertation, University of Hertfordshire.*

Dorj, U. O., Lee, M., & Yun, S. S. (2017). An yield estimation in citrus orchards via fruit detection and counting using image processing. *Computers and Electronics in Agriculture*, *140*, 103-112.

Dryden, K. Mardia (1998). Statistical Shape Analysis. Wiley, London.

Ei-Helly, M., Rafea, A., Ei-Gamal, S., & Whab, R. A. E. (2004). Integrating diagnostic expert system with image processing via loosely coupled technique. *Central Laboratory for Agricultural Expert System (CLAES)*.

Elfadel, I. M., & Picard, R. W. (1994). Gibbs random fields, cooccurrences, and texture modeling. *IEEE Transactions on Pattern Analysis and Machine Intelligence*, *16*(1), 24-37.

Elmhirst J. (2015). Crop profile for strawberry in Canada. Report produced by Pesticide Risk Reduction Program, Pest Management Centre, Agriculture and Agri-Food Canada, Ottawa, Canada. [Internet]. [cited Dec 2015 02]. Document Retrieved from: http://publications.gc.ca/collections/collection_2015/aac-aafc/A118-10-17-2013-eng.pdf.

Esau, T. J., Zaman, Q. U., Chang, Y. K., Schumann, A. W., Percival, D. C., & Farooque, A. A. (2014). Spot-application of fungicide for wild blueberry using an automated prototype variable rate sprayer. *Precision agriculture*, *15*(2), 147-161.

Esau, T., Zaman, Q., Groulx, D., Chang, Y., Schumann, A., & Havard, P. (2017). Supplementary light source development for camera-based smart spraying in low light conditions. *Applied Engineering in Agriculture*, *33*(1), 5-14.

Esau, T., Zaman, Q., Groulx, D., Farooque, A., Schumann, A., & Chang, Y. (2018). Machine vision smart sprayer for spot-application of agrochemical in wild blueberry fields. *Precision Agriculture*, *19*(4), 770-788.

FAO, Food and Agriculture Organization of the United Nations. (2016). FAOSTAT agriculture data. http://faostat3.fao.org/download/Q/QC/E. Accessed May 2016.

Farooque, A. A., Zaman, Q. U., Nguyen-Quang, T., Groulx, D., Schumann, A. W., & Chang, Y. K. (2016). Development of a predictive model for wild blueberry harvester fruit losses during harvesting using artificial neural network. *Applied Engineering in Agriculture*, *32*(6), 725-738.

Fleming, K. L., Westfall, D. G., Wiens, D. W., & Brodahl, M. C. (2000). Evaluating farmer defined management zone maps for variable rate fertilizer application. *Precision Agriculture*, *2*(2), 201-215.

Font, D., Pallejà, T., Tresanchez, M., Teixidó, M., Martinez, D., Moreno, J., & Palacín, J. (2014). Counting red grapes in vineyards by detecting specular spherical reflection peaks in RGB images obtained at night with artificial illumination. *Computers and Electronics in Agriculture*, *108*, 105-111.

Giacomelli, G. A., Ling, P. P., & Morden, R. E. (1996). An automated plant monitoring system using machine vision. In *International Symposium on Plant Production in Closed Ecosystems 440*, 377-382.

Gonzalez, R.C., & Wood, R.E. (2018). Digital image processing (4th ed.). New York, NY, USA: Pearson, Inc.

Gorsevski, P. V., & Gessler, P. E. (2009). The design and the development of a hyperspectral and multispectral airborne mapping system. *ISPRS Journal of Photogrammetry and Remote Sensing*, *64*(2), 184-192.

Goyal, R. K., Goh, W. L., Mital, D. P., & Chan, K. L. (1994). A translation rotation and scale invariant texture analysis technique based on structural properties. In *Proceedings of the Third International Conference on Automation Technology (Automation, 1994), Taipei*.

Gunasekaran, S. (1996). Computer vision technology for food quality assurance. *Trends in Food Science & Technology*, *7*(8), 245-256.

Guo, W., Rage, U. K., & Ninomiya, S. (2013). Illumination invariant segmentation of vegetation for time series wheat images based on decision tree model. *Computers and Electronics in Agriculture*, *96*, 58-66.

Guyer, D. E., Miles, G. E., Gaultney, L. D., & Schreiber, M. M. (1993). Application of machine vision to shape analysis in leaf and plant identification. *Transactions of the ASAE*, *36*(1), 163-171.

Guyer, D. E., Miles, G. E., Schreiber, M. M., Mitchell, O. R., & Vanderbilt, V. C. (1986). Machine vision and image processing for plant identification. *Transactions of the ASAE*, *29*(6), 1500-1507.

Haboudane, D., Miller, J. R., Tremblay, N., Zarco-Tejada, P. J., & Dextraze, L. (2002). Integrated narrow-band vegetation indices for prediction of crop chlorophyll content for application to precision agriculture. *Remote sensing of environment*, *81*(2), 416-426.

Haralick, R. M. (1979). Statistical and structural approaches to texture. *Proceedings of the IEEE*, *67*(5), 786-804.

Haralick, R. M., Shanmugam, K., and Dinstein, I. H. (1973). Textural features for image classification. *IEEE Transactions on Systems, Man and Cybernetics. 3*(6), 610-621.

He, K., Zhang, X., Ren, S., & Sun, J. (2016). Deep residual learning for image recognition. In *Proceedings of the IEEE conference on computer vision and pattern recognition*, 770-778.

Hellebrand, H. J., Linke, M., Beuche, H., Herold, B., & Geyer, M. (2000). Horticultural products evaluated by thermography. *AgEng, Warwick*, 26-26.

Huang, K. Y. (2007). Application of artificial neural network for detecting Phalaenopsis seedling diseases using color and texture features. *Computers and Electronics in Agriculture*, *57*(1), 3-11.

Huang, Y., Reddy, K. N., Fletcher, R. S., & Pennington, D. (2017). UAV low-altitude remote sensing for precision weed management. *Weed Technology*, 1-5.

Huang, Y., Thomson, S. J., Lan, Y., & Maas, S. J. (2010). Multispectral imaging systems for airborne remote sensing to support agricultural production management. *International Journal of Agricultural and Biological Engineering, 3*(1), 50-62.

Islam, M., Dinh, A., Wahid, K., & Bhowmik, P. (2017). Detection of potato diseases using image segmentation and multiclass support vector machine. In *Electrical and Computer Engineering (CCECE), 2017 IEEE 30th Canadian Conference on IEEE*, 1-4.

Jafari, A., Mohtasebi, S. S., Jahromi, H. E., & Omid, M. (2006). Weed detection in sugar beet fields using machine vision. *Int. J. Agric. Biol*, *8*(5), 602-605.

Jafari-Khouzani, K., Soltanian-Zadeh, H., & Elisevich, K. (2006). Hippocampus volume and texture analysis for temporal lobe epilepsy. In *Electro/information Technology, 2006 IEEE International Conference on IEEE*, 394-397.

Jain, A. K., Murty, M. N., & Flynn, P. J. (1999). Data clustering: a review. *ACM computing surveys (CSUR)*, *31*(3), 264-323.

Jeon, H. Y., Tian, L. F., & Zhu, H. (2011). Robust crop and weed segmentation under uncontrolled outdoor illumination. *Sensors*, *11*(6), 6270-6283.

Jones, H. G. (1999a). Use of thermography for quantitative studies of spatial and temporal variation of stomatal conductance over leaf surfaces. *Plant, Cell & Environment*, *22*(9), 1043-1055.

Jones, H. G. (1999b). Use of infrared thermometry for estimation of stomatal conductance as a possible aid to irrigation scheduling. *Agricultural and forest meteorology*, *95*(3), 139-149.

Jones, H. G. (2004). Irrigation scheduling: advantages and pitfalls of plant-based methods. *Journal of experimental botany*, *55*(407), 2427-2436.

Jones, H. G., Stoll, M., Santos, T., Sousa, C. D., Chaves, M. M., & Grant, O. M. (2002). Use of infrared thermography for monitoring stomatal closure in the field: application to grapevine. *Journal of Experimental Botany*, *53*(378), 2249-2260.

Jordan, V. W. L., & Hunter, T. (1972). The effects of glass cloche and coloured polyethylene tunnels on microclimate, growth, yield and disease severity of strawberry plants. *Journal of horticultural science*, *47*(3), 419-426.

Julesz, B. (1962). Visual pattern discrimination. *IRE transactions on Information Theory*, *8*(2), 84-92.

Julesz, B. (1975). Experiments in the visual perception of texture. *Scientific American*, *232*(4), 34-43.

Julesz, B., & Caelli, T. (1979). On the limits of Fourier decompositions in visual texture perception. *Perception*, *8*(1), 69-73.

Kai, S., Zhikun, L., Hang, S., & Chunhong, G. (2011). A research of maize disease image recognition of corn based on BP networks. In *Measuring Technology and Mechatronics Automation (ICMTMA), 2011 Third International Conference on IEEE, 1,* 246-249.

Kebapci, H., Yanikoglu, B., & Unal, G. (2010). Plant image retrieval using color, shape and texture features. *The Computer Journal*, *54*(9), 1475-1490.

Kim, D. G., Burks, T. F., Qin, J., & Bulanon, D. M. (2009). Classification of grapefruit peel diseases using color texture feature analysis. *International Journal of Agricultural and Biological Engineering*, *2*(3), 41-50.

Kim, M. S., Lefcourt, A. M., Chao, K., Chen, Y. R., Kim, I., & Chan, D. E. (2002). Multispectral detection of fecal contamination on apples based on hyperspectral imagery: Part I. Application of visible and near–infrared reflectance imaging. *Transactions of the ASAE*, *45*(6), 2027.

Kobayashi, T., Kanda, E., Kitada, K., Ishiguro, K., & Torigoe, Y. (2001). Detection of rice panicle blast with multispectral radiometer and the potential of using airborne multispectral scanners. *Phytopathology*, *91*(3), 316-323.

Krizhevsky, A., Sutskever, I., & Hinton, G. E. (2012). Imagenet classification with deep convolutional neural networks. In *Advances in neural information processing systems*, 1097-1105.

Kulkarni, A. H., & Patil, R. A. (2012). Applying image processing technique to detect plant diseases. *International Journal of Modern Engineering Research (IJMER)*, *2*(5), 3661-3664.

Kumar, A., Bharti, V., Kumar, V. K. U., & Meena, P. D. (2016). Hyperspectral imaging: A potential tool for monitoring crop infestation, crop yield and macronutrient analysis, with special emphasis to Oilseed Brassica. *Journal of Oilseed Brassica*, *7*(2), 113-125.

Kurtulmus, F., Lee, W. S., & Vardar, A. (2011). Green citrus detection using 'eigenfruit', color and circular Gabor texture features under natural outdoor conditions. *Computers and Electronics in Agriculture*, *78*(2), 140-149.

Lee, S., Ryu, J. H., Won, J. S., & Park, H. J. (2004). Determination and application of the weights for landslide susceptibility mapping using an artificial neural network. *Engineering Geology*, *71*(3-4), 289-302.

Lee, W. S., Slaughter, D. C., & Giles, D. K. (1999). Robotic weed control system for tomatoes. *Precision Agriculture*, *1*(1), 95-113.

Leinonen, I., & Jones, H. G. (2004). Combining thermal and visible imagery for estimating canopy temperature and identifying plant stress. *Journal of experimental botany*, *55*(401), 1423-1431.

Levine, M. D. (1985). Vision in Man and Machine. McGraw-Hill, New York, NY, USA.

Li, D., Shen, M., Li, D., & Yu, X. (2017a). Green apple recognition method based on the combination of texture and shape features. In *Mechatronics and Automation (ICMA), 2017 IEEE International Conference on IEEE,* 264-269.

Li, D., Zhao, H., Zhao, X., Gao, Q., & Xu, L. (2017b). Cucumber detection based on texture and color in greenhouse. *International Journal of Pattern Recognition and Artificial Intelligence*, *31*(08), 1754016.

Liu, B. (2017). Sustainable strawberry production and management including control of strawberry powdery mildew. *PhD dissertation, University of Hertfordshire.*

Lleó, L., Barreiro, P., Ruiz-Altisent, M., & Herrero, A. (2009). Multispectral images of peach related to firmness and maturity at harvest. *Journal of Food Engineering*, *93*(2), 229-235.

Loncaric, S. (1998). A survey of shape analysis techniques. *Pattern recognition*, *31*(8), 983-1001.

López-Granados, F., Torres-Sánchez, J., Serrano-Pérez, A., de Castro, A. I., Mesas-Carrascosa, F. J., & Peña, J. M. (2016). Early season weed mapping in sunflower using UAV technology: variability of herbicide treatment maps against weed thresholds. *Precision Agriculture*, *17*(2), 183-199.

Lu, R., & Chen, Y. R. (1999). Hyperspectral imaging for safety inspection of food and agricultural products. In *Pathogen Detection and Remediation for Safe Eating, International Society for Optics and Photonics, 3544,* 121-134.

Maas, J. (1998). Compendium of Strawberry Diseases. *The American Phytopathological Society Press, St. Paul, Minnesota, USA,* 17–1835.

Madadlou, A., Emam-Djomeh, Z., Mousavi, M. E., Ehsani, M., Javanmard, M., & Sheehan, D. (2009). Response surface optimization of an artificial neural network for predicting the size of re-assembled casein micelles. *Computers and Electronics in Agriculture*, *68*(2), 216-221.

Mahendran, R., Jayashree, G. C., & Alagusundaram, K. (2012). Application of computer vision technique on sorting and grading of fruits and vegetables. *J Food Process Technol*, *10*, 2157-7110.

McCormick, B. H., & Jayaramamurthy, S. N. (1974). Time series model for texture synthesis. *International Journal of Parallel Programming*, *3*(4), 329-343.

Meade, N. (2000). Evidence for the selection of forecasting methods. *Journal of forecasting*, *19*(6), 515-535.

Mehl, P. M., Chao, K., Kim, M., & Chen, Y. R. (2002). Detection of defects on selected apple cultivars using hyperspectral and multispectral image analysis. *Applied Engineering in Agriculture*, *18*(2), 219.

Meng, Q., Qiu, R., He, J., Zhang, M., Ma, X., & Liu, G. (2015). Development of agricultural implement system based on machine vision and fuzzy control. *Computers and Electronics in Agriculture*, *112*, 128-138.

Meunkaewjinda, A., Kumsawat, P., Attakitmongcol, K., & Srikaew, A. (2008). Grape leaf disease detection from color imagery using hybrid intelligent system. In *Electrical Engineering/Electronics, Computer, Telecommunications and Information Technology, 2008. ECTI-CON 2008. 5th International Conference on IEEE, 1,* 513-516.

Meyer, G. E., Hindman, T. W., Jones, D. D., & Mortensen, D. A. (2004). Digital camera operation and fuzzy logic classification of uniform plant, soil, and residue color images. *Applied Engineering in Agriculture*, *20*(4), 519.

Miller, W. M., Schumann, A. W., & Whitney, J. D. (2004). Evaluating variable rate granular fertilizer technologies in Florida citrus. In *Proc. Fla. State Hort. Soc, 117*(1), 161-166.

Miller, W. M., Throop, J. A., & Upchurch, B. L. (1998). Pattern recognition models for spectral reflectance evaluation of apple blemishes. *Postharvest Biology and Technology*, *14*(1), 11-20.

Mohan, B. K., & Porwal, A. (2015). Hyperspectral image processing and analysis. *Curr. Sci*, *108*, 833-841.

Mohanty, S. P., Hughes, D. P., & Salathé, M. (2016). Using deep learning for image-based plant disease detection. *Frontiers in plant science*, *7*.

Moya, E. A., Barrales, L. R., & Apablaza, G. E. (2005). Assessment of the disease severity of squash powdery mildew through visual analysis, digital image analysis and validation of these methodologies. *Crop Protection*, *24*(9), 785-789.

Mucherino, A., Papajorgji, P., & Pardalos, P. M. (2009). A survey of data mining techniques applied to agriculture. *Operational Research*, *9*(2), 121-140.

Murthy, S. K. (1998). Automatic construction of decision trees from data: A multi-disciplinary survey. *Data mining and knowledge discovery*, *2*(4), 345-389.

National Climate Data and Information Archive (2018). Environment Canada. http://www.climate.weatheroffice.gc.ca.

Nelson, M. D., Gubler, W. D., & Shaw, D. V. (1995). Inheritance of powdery mildew resistance in greenhouse-grown versus field-grown California strawberry progenies. *Phytopathology*, *85*(4), 421-424.

Nelson, M. D., Gubler, W. D., & Shaw, D. V. (1996). Relative resistance of 47 strawberry cultivars to powdery mildew in California greenhouse and field environments. *Plant disease*, *80,* 326-328.

Neto, J. C., Meyer, G. E., Jones, D. D., & Samal, A. K. (2006). Plant species identification using Elliptic Fourier leaf shape analysis. *Computers and Electronics in Agriculture*, *50*(2), 121-134.

O'Shaughnessy, S. A., Evett, S. R., & Colaizzi, P. D. (2015). Dynamic prescription maps for site-specific variable rate irrigation of cotton. *Agricultural Water Management*, *159*, 123-138.

Ochoa, D., Cevallos, J., Vargas, G., Criollo, R., Romero, D., Castro, R., & Bayona, O. (2016). Hyperspectral imaging system for disease scanning on banana plants. In *SPIE Commercial+ Scientific Sensing and Imaging, International Society for Optics and Photonics,* 98640M-98640M.

Oerke, E. C., Steiner, U., Dehne, H. W., & Lindenthal, M. (2006). Thermal imaging of cucumber leaves affected by downy mildew and environmental conditions. *Journal of Experimental Botany*, *57*(9), 2121-2132.

Ohta, Y. I., Kanade, T., & Sakai, T. (1980). Color information for region segmentation. *Computer graphics and image processing*, *13*(3), 222-241.

Omrani, E., Khoshnevisan, B., Shamshirband, S., Saboohi, H., Anuar, N. B., & Nasir, M. H. N. M. (2014). Potential of radial basis function-based support vector regression for apple disease detection. *Measurement*, *55*, 512-519.

Pajares, G., García-Santillán, I., Campos, Y., Montalvo, M., Guerrero, J. M., Emmi, L., Romeo, J., Guijarro, M. & Gonzalez-de-Santos, P. (2016). Machine-vision systems selection for agricultural vehicles: A guide. *Journal of Imaging*, *2*(4), 34.

Palleja, T., & Landers, A. J. (2015). Real time canopy density estimation using ultrasonic envelope signals in the orchard and vineyard. *Computers and Electronics in Agriculture*, *115*, 108-117.

Payne, A. B., Walsh, K. B., Subedi, P. P., & Jarvis, D. (2013). Estimation of mango crop yield using image analysis–segmentation method. *Computers and Electronics in Agriculture*, *91*, 57-64.

Peng, Y., & Lu, R. (2007). Prediction of apple fruit firmness and soluble solids content using characteristics of multispectral scattering images. *Journal of Food Engineering*, *82*(2), 142-152.

Peressotti, E., Duchêne, E., Merdinoglu, D., & Mestre, P. (2011). A semi-automatic non-destructive method to quantify grapevine downy mildew sporulation. *Journal of microbiological methods*, *84*(2), 265-271.

Pertot, I., Zasso, R., Amsalem, L., Baldessari, M., Angeli, G., & Elad, Y. (2008). Integrating biocontrol agents in strawberry powdery mildew control strategies in high tunnel growing systems. *Crop protection*, *27*(3-5), 622-631.

Pineda, M., Pérez-Bueno, M. L., & Barón, M. (2018). Detection of bacterial infection in melon plants by classification methods based on imaging data. *Frontiers in plant science*, *9*, 164.

Polder, G., Van Der Heijden, G. W. A. M., Jalink, H., & Snel, J. F. H. (2007). Correcting and matching time sequence images of plant leaves using penalized likelihood warping and robust point matching. *Computers and Electronics in Agriculture*, *55*(1), 1-15.

Pydipati, R., Burks, T. F., & Lee, W. S. (2005). Statistical and neural network classifiers for citrus disease detection using machine vision. *Transactions of the ASAE*, *48*(5), 2007-2014.

Pydipati, R., Burks, T. F., & Lee, W. S. (2006). Identification of citrus disease using color texture features and discriminant analysis. *Computers and Electronics in Agriculture*, *52*(1), 49-59.

Rajkumar, P., Wang, N., EImasry, G., Raghavan, G. S. V., & Gariepy, Y. (2012). Studies on banana fruit quality and maturity stages using hyperspectral imaging. *Journal of Food Engineering*, *108*(1), 194-200.

Ramakrishnan, M. (2015). Groundnut leaf disease detection and classification by using back probagation algorithm. In *Communications and Signal Processing (ICCSP), 2015 International Conference on IEEE,* 0964-0968.

Rastogi, R., and Chadda, V. K. (1989). Applications of image processing in biology and agriculture J. K. Sainis, *Molecular Biology and Agriculture Division, BARC newsletter.*

Rehman, T. U., Zaman, Q. U., Chang, Y. K., Schumann, A. W., Corscadden, K. W., & Esau, T. J. (2018). Optimising the parameters influencing performance and weed (goldenrod) identification accuracy of colour co-occurrence matrices. *Biosystems Engineering*, *170*, 85-95.

Remagnino, P., Mayo, S., Wilkin, P., Cope, J., & Kirkup, D. (2017). Machine Learning for Plant Leaf Analysis. In *Computational Botany, Springer Berlin Heidelberg,* 57-79.

Rodriguez, D., Fitzgerald, G. J., Belford, R., & Christensen, L. K. (2006). Detection of nitrogen deficiency in wheat from spectral reflectance indices and basic crop eco-physiological concepts. *Australian Journal of Agricultural Research*, *57*(7), 781-789.

Rojas-Moraleda, R., Valous, N. A., Gowen, A., Esquerre, C., Härtel, S., Salinas, L., & O'Donnell, C. (2017). A frame-based ANN for classification of hyperspectral images: assessment of mechanical damage in mushrooms. *Neural Computing and Applications*, *28*(1), 969-981.

Romeo, J., Guerrero, J. M., Montalvo, M., Emmi, L., Guijarro, M., Gonzalez-de-Santos, P., & Pajares, G. (2013). Camera sensor arrangement for crop/weed detection accuracy in agronomic images. *Sensors*, *13*(4), 4348-4366.

Ropodi, A. I., Panagou, E. Z., & Nychas, G. J. (2016). Data mining derived from food analyses using non-invasive/non-destructive analytical techniques; determination of food authenticity, quality & safety in tandem with computer science disciplines. *Trends in Food Science & Technology*, *50*, 11-25.

Rosenfeld, A., & Thurston, M. (1971). Edge and curve detection for visual scene analysis. *IEEE Transactions on computers*, *100*(5), 562-569.

Rosenfeld, A., & Troy, E. B. (1970). Visual texture analysis (No. TR-70-116; ORO-3662-10). *Maryland Univ., College Park (USA). Computer Science Center.*

Rosenfeld, R. and Kak, A. (1982). Digital Picture Processing. Academic Press Orland, FL, USA.

Sabzi, S., Abbaspour-Gilandeh, Y., & Javadikia, H. (2017). Machine vision system for the automatic segmentation of plants under different lighting conditions. *Biosystems Engineering*, *161*, 157-173.

Safren, O., Alchanatis, V., Ostrovsky, V., & Levi, O. (2007). Detection of green apples in hyperspectral images of apple-tree foliage using machine vision. *Transactions of the ASABE, 50(6),* 2303-2313.

Saleem, S. R., Zaman, Q. U., Schumann, A. W., Madani, A., Farooque, A. A., & Percival, D. C. (2013). Impact of variable rate fertilization on subsurface water contamination in wild blueberry cropping system. *Applied Engineering in Agriculture*, *29*(2), 225-232.

Sankaran, S., Mishra, A., Ehsani, R., & Davis, C. (2010). A review of advanced techniques for detecting plant diseases. *Computers and Electronics in Agriculture*, *72*(1), 1-13.

Sankaran, S., Mishra, A., Maja, J. M., & Ehsani, R. (2011). Visible-near infrared spectroscopy for detection of Huanglongbing in citrus orchards. *Computers and Electronics in Agriculture*, *77*(2), 127-134.

Savakar, D. G., & Anami, B. S. (2015). Grading of bulk food grains and fruits using computer vision. *Journal of Agricultural Engineering and Biotechnology*, *3*(1), 1-10.

Schölkopf, B., & Smola, A. J. (2002). Learning with kernels: support vector machines, regularization, optimization, and beyond. *MIT press.*

Schor, N., Berman, S., Dombrovsky, A., Elad, Y., Ignat, T., & Bechar, A. (2017). Development of a robotic detection system for greenhouse pepper plant diseases. *Precision Agriculture*, *18*(3), 394-409.

Sela, E., Cohen, Y., Meron, M., Alchanatis, V., & Cohen, S. (2007). Use of thermal imaging for estimating and mapping crop water stress in cotton. In *Proceedings of 6th European Conference on Precision Agriculture*, 365-371.

Sena Jr, D. G., Pinto, F. A. C., Queiroz, D. M., & Viana, P. A. (2003). Fall armyworm damaged maize plant identification using digital images. *Biosystems Engineering, 85*(4), 449-454.

Shapiro, L. G., and Stockman, G. C. (2001). Computer Vision. *Upper Saddle River: Prentice–Hall.*

Shearer, S. A., & Holmes, R. G. (1990). Plant identification using color co-occurrence matrices. *Transactions of the ASAE*, *33*(6), 1237-1244.

Shrestha, D. S., & Steward, B. L. (2003). Automatic corn plant population measurement using machine vision. *Transactions of the ASAE*, *46*(2), 559.

Simonyan, K., & Zisserman, A. (2014). Very deep convolutional networks for large-scale image recognition. *arXiv preprint arXiv:1409.1556*.

Sladojevic, S., Arsenovic, M., Anderla, A., Culibrk, D., & Stefanovic, D. (2016). Deep neural networks based recognition of plant diseases by leaf image classification. *Computational intelligence and neuroscience*, *2016*.

Sonka, M., Hlavac, V., & Boyle, R. (2014). Image processing, analysis, and machine vision. *Chapter 14. PWS publishing, California.*

Spencer, DM. (1978). Powdery mildew of strawberries. *In:Spencer DM (ed) The Powdery Mildews (pp 355–358) Academic Press, NY, USA.*

Stajnko, D., Lakota, M., & Hočevar, M. (2004). Estimation of number and diameter of apple fruits in an orchard during the growing season by thermal imaging. *Computers and Electronics in Agriculture*, *42*(1), 31-42.

Statistics Canada. (2018a). Table 001-0009 [8]. Area, Production and Farm Gate Value of Fresh and Processed Fruits.

Statistics Canada. (2018b). Table 32-10-0364-01. Estimates, production and farm gate value of fresh and processed fruits.

Steward, B. L., & Tian, L. F. (1999). Machine-vision weed density estimation for real-time, outdoor lighting conditions. *Transactions of the ASAE*, *42*(6), 1897.

Stoll, M., & Jones, H. G. (2007). Thermal imaging as a viable tool for monitoring plant stress. *OENO One*, *41*(2), 77-84.

Story, D., Kacira, M., Kubota, C., Akoglu, A., & An, L. (2010). Lettuce calcium deficiency detection with machine vision computed plant features in controlled environments. *Computers and Electronics in Agriculture*, *74*(2), 238-243.

Sun, D. W. (2000). Inspecting pizza topping percentage and distribution by a computer vision method. *Journal of Food Engineering*, *44*(4), 245-249.

Sun, D. W. (Ed.). (2016). Computer vision technology for food quality evaluation. *Academic Press.*

Szegedy, C., Liu, W., Jia, Y., Sermanet, P., Reed, S., Anguelov, D., Erhan, D., Vanhoucke, V., & Rabinovich, A. (2015). Going deeper with convolutions. In *Proceedings of the IEEE conference on computer vision and pattern recognition*, 1-9.

Tang, L., Tian, L., & Steward, B. L. (2000). Color image segmentation with genetic algorithm for in-field weed sensing. *Transactions of the ASAE*, *43*(4), 1019.

Teuner, A., Pichler, O., & Hosticka, B. J. (1995). Unsupervised texture segmentation of images using tuned matched Gabor filters. *IEEE transactions on image processing*, *4*(6), 863-870.

Throop, J. A., Aneshansley, D. J., & Upchurch, B. L. (1993). Near-IR and color imaging for bruise detection on Golden Delicious apples. In *Optics in Agriculture and Forestry, International Society for Optics and Photonics, 1836,* 33-45.

Tian, L. (1995). Knowledge based machine vision system for outdoor plant identification. *PhD. dissertation. University of California Davis Library, Davis, California.*

Tian, L. (2002). Development of a sensor-based precision herbicide application system. *Computers and Electronics in Agriculture*, *36*(2-3), 133-149.

Tian, L. F., & Slaughter, D. C. (1998). Environmentally adaptive segmentation algorithm for outdoor image segmentation. *Computers and Electronics in Agriculture*, *21*(3), 153-168.

Tian, L. F., Slaughter, D. C., & Norris, R. F. (1997). Outdoor field machine vision identification of tomato seedlings for automated weed control. *Transactions of ASAE, 40*(6), 1761–1768.

Torrecilla, J. S., Otero, L., & Sanz, P. D. (2004). A neural network approach for thermal/pressure food processing. *J. Food Eng.,62*(1), 89-95.

Unay, D., & Gosselin, B. (2006). Automatic defect segmentation of 'Jonagold'apples on multi-spectral images: A comparative study. *Postharvest Biology and Technology*, *42*(3), 271-279.

Vadivambal, R., & Jayas, D. S. (2011). Applications of thermal imaging in agriculture and food industry-a review. *Food and Bioprocess Technology*, *4*(2), 186-199.

Velázquez-López, N., Sasaki, Y., Nakano, K., Mejía-Muñoz, J. M., & Romanchik, K. (2011). Detection of powdery mildew disease on rose using image processing with Open CV. *Revista Chapingo. Serie Horticultura*, *17*(2), 151-160.

VijayaLakshmi, B., & Mohan, V. (2016). Kernel-based PSO and FRVM: An automatic plant leaf type detection using texture, shape, and color features. *Computers and Electronics in Agriculture*, *125*, 99-112.

Wang, F., Song, L., Omasa, K., & Wang, J. (2017). Automatically diagnosing leaf scorching and disease symptoms in trees/shrubs by using RGB image computation with a common statistical algorithm. *Ecological Informatics*, *38*, 110-114.

Wang, Q., Nuske, S., Bergerman, M., & Singh, S. (2013). Automated crop yield estimation for apple orchards. In *Experimental robotics, Springer international publishing,* 745-758.

Wang, X., Zhang, M., Zhu, J., & Geng, S. (2008). Spectral prediction of Phytophthora infestans infection on tomatoes using artificial neural network (ANN). *International Journal of Remote Sensing*, *29*(6), 1693-1706.

Wei, W., Cui, M. Y., Hu, Y., Gao, K., Xie, Y. G., Jiang, Y., & Feng, J. Y. (2018). Ectopic expression of FvWRKY42, a WRKY transcription factor from the diploid woodland strawberry (Fragaria vesca), enhances resistance to powdery mildew, improves osmotic stress resistance, and increases abscisic acid sensitivity in Arabidopsis. *Plant Science*, *275*, 60-74.

Weizheng, S., Yachun, W., Zhanliang, C., & Hongda, W. (2008). Grading method of leaf spot disease based on image processing. In *Computer Science and Software Engineering, 2008 International Conference on IEEE, 6,* 491-494.

Weszka, J. S., Dyer, C. R., & Rosenfeld, A. (1976). A comparative study of texture measures for terrain classification. *IEEE Transactions on Systems, Man, and Cybernetics*, (4), 269-285.

Wettschereck, D., Aha, D. W., & Mohri, T. (1997). A review and empirical evaluation of feature weighting methods for a class of lazy learning algorithms. In *Lazy learning, Springer Netherlands,* 273-314.

Wijethunga, P., Samarasinghe, S., Kulasiri, D., & Woodhead, I. (2008). Digital image analysis based automated kiwifruit counting technique. In *Image and Vision Computing New Zealand, 2008. IVCNZ 2008. 23rd International Conference IEEE,* 1-6.

Wilhelm, S. (1961). Diseases of strawberry. A guide for the commercial grower. *Univ. Calif. Agr. Expt. Sta. Circ. 494.*

Woebbecke, D. M., Meyer, G. E., Von Bargen, K., & Mortensen, D. A. (1995). Shape features for identifying young weeds using image analysis. *Transactions of the ASAE*, *38*(1), 271-281.

Wspanialy, P. (2013). Early detection of powdery mildew in greenhouses. *Masters dissertation, University of Guelph.*

Wspanialy, P., & Moussa, M. (2016). Early powdery mildew detection system for application in greenhouse automation. *Computers and Electronics in Agriculture*, *127*, 487-494.

Xie, C., Shao, Y., Li, X., & He, Y. (2015). Detection of early blight and late blight diseases on tomato leaves using hyperspectral imaging. *Scientific reports*, *5*, 16564.

Xu, G., Zhang, F., Shah, S. G., Ye, Y., & Mao, H. (2011). Use of leaf color images to identify nitrogen and potassium deficient tomatoes. *Pattern Recognition Letters*, *32*(11), 1584-1590.

Yang, C., Lee, W. S., & Gader, P. (2014). Hyperspectral band selection for detecting different blueberry fruit maturity stages. *Computers and Electronics in Agriculture*, *109*, 23-31.

Yang, C., Lee, W. S., & Williamson, J. G. (2012). Classification of blueberry fruit and leaves based on spectral signatures. *Biosystems Engineering*, *113*(4), 351-362.

Yang, C., Odvody, G. N., Thomasson, J. A., Isakeit, T., & Nichols, R. L. (2016). Change detection of cotton root rot infection over 10-year intervals using airborne multispectral imagery. *Computers and Electronics in Agriculture*, *123*, 154-162.

Yang, J. D., Yang, T., Miao, T., Zhu, C., Shen, Q. C., Peng, Y. F., Mei, P. & Dang, Y. Q. (2018). Recognition of powdery mildew disease of strawberry leaves based on convolutional neural network. *Jiangsu Journal of Agricultural Sciences*, (3), 7.

Yano, I. H., Santiago, W. E., Alves, J. R., Toledo, L., Mota, M., & Teruel, B. (2017). Choosing classifier for weed identification in sugarcane fields through images taken by uav. *Bulgarian journal of agricultural science*, *23*(3), 491-497.

Ye, M., Cao, Z., Yu, Z., & Bai, X. (2015). Crop feature extraction from images with probabilistic superpixel Markov random field. *Computers and Electronics in Agriculture*, *114*, 247-260.

Yousefi, S., & Kehtarnavaz, N. (2011). A new stochastic image model based on Markov random fields and its application to texture modeling. In *Acoustics, Speech and Signal Processing (ICASSP), 2011 IEEE International Conference on IEEE,* 1285-1288.

Zaman, Q. U., Esau, T. J., Schumann, A. W., Percival, D. C., Chang, Y. K., Read, S. M., & Farooque, A. A. (2011). Development of prototype automated variable rate sprayer for real-time spot-application of agrochemicals in wild blueberry fields. *Computers and Electronics in Agriculture*, *76*(2), 175-182.

Zarco-Tejada, P. J., Berni, J. A., Suárez, L., Sepulcre-Cantó, G., Morales, F., & Miller, J. R. (2009). Imaging chlorophyll fluorescence with an airborne narrow-band multispectral camera for vegetation stress detection. *Remote Sensing of Environment*, *113*(6), 1262-1275.

Zeiler, M. D., & Fergus, R. (2014). Visualizing and understanding convolutional networks. In *European conference on computer vision, Springer, Cham,* 818-833.

Zhang, D., & Lu, G. (2004). Review of shape representation and description techniques. *Pattern recognition*, *37*(1), 1-19.

Zhang, F., Zaman, Q. U., Percival, D. C., & Schumann, A. W. (2010). Detecting bare spots in wild blueberry fields using digital color photography. *Applied Engineering in Agriculture*, *26*(5), 723-728.

Zhang, G. P. (2000). Neural networks for classification: a survey. *IEEE Transactions on Systems, Man, and Cybernetics, Part C (Applications and Reviews), 30*(4), 451-462.

Zhang, N. & Chaisattapagon, C. (1995). Effective criteria for weed identification in wheat fields using machine vision. *Transactions of the ASAE 38(3):* 965-974.

Zhang, J., & Tan, T. (2002a). Affine invariant texture analysis based on structural properties. In *Proceedings of the Fifth Asian Conference on Computer Vision (ACCV 2002)*, 216-221.

Zhang, J., & Tan, T. (2002b). Brief review of invariant texture analysis methods. *Pattern recognition*, *35*(3), 735-747.

Zhang, L., Yang, Q., Xun, Y., Chen, X., Ren, Y., Yuan, T., Tan, Y., & Li, W. (2007). Recognition of greenhouse cucumber fruit using computer vision. *New Zealand Journal of Agricultural Research*, *50*(5), 1293-1298.

Zhou, B., Xu, J., Zhao, J., Li, A., & Xia, Q. (2015). Research on cucumber downy mildew detection system based on SVM classification algorithm. In *3rd Int'l Conf on Mat, Mech and Manu Eng*.

Zhou, R., Damerow, L., Sun, Y., & Blanke, M. M. (2012). Using colour features of cv.'Gala'apple fruits in an orchard in image processing to predict yield. *Precision Agriculture*, *13*(5), 568-580.

Zucker, S. W. (1976). Toward a model of texture. *Computer Graphics and Image Processing*, *5*(2), 190-202.

APPENDIX

February 15, 2019

Journal Article
Computers and Electronics in Agriculture
ELSEVIER PUBLISHERS

Dear Sir/Madam

I am preparing my M. Sc thesis for submission to the Faculty of Graduate Studies at Dalhousie University, Halifax, Nova Scotia, Canada. I am seeking your permission to include a manuscript version of the following paper(s) as a chapter in the thesis:

Mahmud, M. S., Zaman, Q. U., Esau, T. J., Price, G. W., & Prithiviraj, B. (2019). Development of an artificial cloud lighting condition system using machine vision for strawberry powdery mildew disease detection. *Computers and Electronics in Agriculture, 158, 219-225.*

Canadian graduate theses are reproduced by the Library and Archives of Canada (formerly National Library of Canada) through a non-exclusive, world-wide license to reproduce, loan, distribute, or sell theses. I am also seeking your permission for the material described above to be reproduced and distributed by the LAC(NLC). Further details about the LAC(NLC) thesis program are available on the LAC(NLC) website (www.nlc-bnc.ca).

Full publication details and a copy of this permission letter will be included in the thesis.

Yours sincerely,

Md. Sultan Mahmud
M. Sc Candidate, Agriculture
Dalhousie University, Halifax, Canada

Permission is granted for:

a) the inclusion of the material described above in your thesis.

b) for the material described above to be included in the copy of your thesis that is sent to the Library and Archives of Canada (formerly National Library of Canada) for reproduction and distribution.

Name: John K. Schueller Title: Chair Editor-in-Chief

Signature: Date: 15 Feb 2019